Pharmacokinetic/Pharmacodynamic modelling with a stochastic perspective. Insulin secretion and Interleukin-21 development as case studies

Rune Viig Overgaard

Preface

This thesis was prepared at Informatics Mathematical Modelling, at the Technical University of Denmark in partial fulfillment of the requirements for acquiring the Ph.D. degree in engineering.

The topic of the Ph.D. thesis is Pharmacokinetic/Pharmacodynamic modelling with a particular focus on stochastic differential equations. Insulin secretion and Interleukin-21 development was used as case studies.

The thesis consists of a summary report and a collection of five research papers written during the Ph.D. study and published/submitted to international journals.

Lyngby, June 2006

Rune Viig Overgaard

Acknowledgements

Many people have been involved and contributed during the course of the present Ph.D. I wish to express my sincere gratitude to all of you. Thank you! In particular

- Many thanks to my excellent team of supervisors, Henrik Madsen, Carsten Knudsen, and Mats Karlsson.

- Thanks to my fellow Ph.D. students at DTU, Christoffer Tornøe, Kim Nolsøe, Lasse E. Christiansen, and Niels Sommer for good laughes, and for great discussions on statistics, drug development, and life in general.

- Warm thanks to the Uppsala group for always making me feel welcome in your excellent scientific environment.

- I wish to thank my long list of scientific collaborators. Nick Holford in particular, you have certainly enriched my insights to the world of PKPD and to new ways of living the good life.

- Many thanks goes to Steen H. Ingwersen and the Biomodelling group at Novo Nordisk for opening your doors, showing me the works, and continually providing new opportunities and challenges.

- And finally, a special thanks to friends, family, and my girlfriend Ida van der Blom, for support and encouragement when needed.

Abstract

Mathematical models are used for many different purposes during the development of new drugs. These models can for example help to figure out how much medicine should be given and how often it should be given in order to obtain the desired effect. In other words, the models can help to create the users manual for a new medicinal product. These models are called Pharmacokinetic/Pharmacodynamic (PK/PD) models, where the PK part typically describes the concentration of drug in the body, and the PD part describes the effect of the drug. If one, for example, develop a PK/PD model for aspirin, the PK part could describe the concentration of aspirin in the blood after you take the tablet. Initially the concentration will increase gradually, and at some point the concentration will begin to decline. The PD part could for example describe the level of pain that start of high, begin to decrease after you take the tablet, and presumably increase again when the amount of aspirin has been eliminated from the body. The typical PK/PD model can be created based on data from an existing experiment, e.g. measurements of concentration and pain relieve at various time points. These models can then simulate the results of new experiments and thereby quickly and inexpensively investigate, e.g. whether aspirin should be administered two or three times daily to obtain the desired effect. The results will naturally be tested in new experiments before the users manual can be accepted for a new medicinal product.

In the present project, new methods are investigated for the formulation and estimation of these mathematical PK/PD models. Specifically, it is investigated whether stochastic differential equations (SDEs) may improve PK/PD models and PK/PD model results. SDEs can be understood as differential equations where the solution is not completely predictable. This randomness could occur, e.g. if there are random variations in the speed with which the drug is removed

from the body. In our previous example, one could imagine that this would lead to small fluctuations in the concentration of aspirin in the blood. Biological systems in general are often composed of numerous sub-processes that cannot be expected to perform completely identical from occasion to occasion or from minute to minute. In this way random fluctuations can occur, also because of perturbations from processes that are not modelled, and it is argued that SDEs provide a more natural description of these systems than ordinary differential equations.

During the course of the present project, several models with many different purposes have been developed. These models are developed within two main subjects, insulin secretion and development of IL-21 as a new anti cancer drug. We find that SDEs are useful in many aspects of PK/PD modelling, both for insulin secretion modelling and for models used during the development of IL-21. Most importantly, SDEs could improve the models ability to execute their respective main purposes, to describe, predict, or increase the understanding of the system.

Resumé

Matematiske modeller bliver brugt på mange forskellige måder igennem udviklingen af nye lægemidler. Disse modeller kan for eksempel hjælpe med at finde ud af hvor meget medicin man skal give og hvor ofte det skal gives for at opnå den ønskede effekt. Med andre ord kan modellerne hjælpe til at udarbejde brugermanualen til et nyt lægemiddel. Disse modeller kaldes Farmakokinetik/Farmakodynamik (PK/PD) modeller, hvor PK delen typisk beskriver koncentrationen af lægemiddel i kroppen, og PD delen beskriver lægemidlets effekt. Hvis man for eksempel laver en PK/PD model for aspirin, kunne PK delen beskrive koncentrationen af aspirin i blodet efter man tager en tablet. Først vil koncentrationen stige gradueret, og lidt senere vil stigningen ophøre så koncentrationen falder igen. PD delen kunne for eksempel beskrive smerteniveauet som starter højt, falder lidt efter man har taget tabletten og formodentlig øges igen efter der ikke er mere aspirin tilbage i kroppen. En typisk PK/PD model kan laves på baggrund af data fra et eksisterende forsøg, fx målinger af koncentration og af den smertestillende effekt. Modellerne kan derefter simulere resultatet af nye forsøg, og på den måde kan man hurtigt og billigt undersøge, fx om aspirin skal gives to eller tre gange om dagen for at opnå den ønskede effekt. Disse resultater skal naturligvis testes i nye forsøg før man kan vedtage brugermanualen for et givet lægemiddel.

I dette projekt undersøges nye metoder til formulering og estimering af disse matematiske PK/PD modeller. Specifikt undersøges hvorvidt stokastiske differentialligninger (SDEer) kan forbedre PK/PD modellerne og deres resultater. SDEer kan forstås som differentialligninger hvor løsningen ikke er fuldstændig forudsigelig. Sådanne tilfældigheder kunne opstå, for eksempel hvis der er tilfældige variationer i den hastighed hvormed lægemidlet fjernes fra blodet. For vores tidligere eksempel kunne man forestille sig at dette vil give anledning til

små fluktuationer i koncentrationen af aspirin i blodet. For biologiske systemer generelt, indgår der oftest mange små delprocesser der ikke kan forventes at være nøjagtig ens fra gang til gang eller fra minut til minut. Der kan således opstå tilfældige fluktuationer, også på grund af perturbationer fra processer der ikke er modelleret, og vi vil argumentere for at SDEer giver en mere naturlig beskrivelse af disse systemer end normale differentialligninger. En del af dette projekt har bestået i at formulere, implementere, og teste en ny metode der tillader brug af SDEer uden at gå på kompromis med de traditionelle metoder der bliver brugt indenfor PK/PD modellering.

Undervejs i dette projekt er der udviklet mange forskellige modeller med flere forskellige metoder til mange forskellige formål. Disse modeller er udviklet indenfor to hovedområder, insulinsekretion, og udvikling af IL-21 som et nyt lægemiddel indenfor kræftbehandling. Vi finder at SDEer er nyttige i mange aspekter af PK/PD modellering, både for insulin sekretions modeller, og for modeller brugt i udviklingen af IL-21. Vigtigst er det at SDEer kunne forbedre modellernes evne til at udfører deres respektive hovedformål, at beskrive, forudsige, eller øge forståelsen af systemet.

List of publications

The thesis is based on the following five scientific reseach papers,

A R. V. Overgaard, J. E. Henriksen, and H. Madsen. Insights to the minimal model of insulin secretion through a mean-field beta cell model. *J.Theor.Biol.*,21;237(4):382-9, 2005.

B R. V. Overgaard, N. Jonsson, C. W. Tornoe, and H. Madsen. Nonlinear mixed-effects models with stochastic differential equations: implementation of an estimation algorithm. *J.Pharmacokinet.Pharmacodyn.*, 32(1):85–107, 2005.

C R. V. Overgaard, K. Jelic, M. O. Karlsson, J. E. Henriksen, and H. Madsen Mathematical Beta Cell Model for Insulin Secretion following IVGTT and OGTT. *Accepted for publication in Annals of Biomedical Engineering.* 2006.

D R. V. Overgaard, M. O. Karlsson, and S. H. Ingwersen Pharmacodynamic model of Interleukin-21 effects on Red Blood Cells in cynomolgus monkeys. *Submitted to Journal of Pharmacokinetics and Pharmacodynamics.* 2006.

E R. V. Overgaard, N. Holford, K. A. Rytved, and H. Madsen PKPD Model of Interleukin-21 Effects on Thermoregulation in Monkeys - Application and Evaluation of Stochastic Differential Equations. *Accepted for publication in Pharmaceutical Research.* 2006.

Collaboration with other researchers during the Ph.D. have resulted in the following list of research papers. The main contribution to these papers have been from other researchers, hence they will not be addressed in this thesis.

- C. W. Tornoe, R. V. Overgaard, H. Agerso, H. A. Nielsen, H. Madsen, and E. N. Jonsson. Stochastic differential equations in NONMEM: implementation, application, and comparison with ordinary differential equations. *Pharm.Res.*, 22(8):1247–1258, 2005.

- R. Vio, P. Andreani, R. V. Overgaard, and H. Madsen. Stochastic modelling of 3:2 resonance in kHz QPOs. *Accpeted for publication in Astronomy & Astrophysics.* 2006.

- K. Jelic, R. V. Overgaard, M. C. Jørgensen, P. Damsbo, S. H. Ingwersen, T. V. Korsgaard,S. D. Luzio, G. Dunseath, and D. R. Owens. A cross-sectional analysis of pancreatic beta cell responsiveness following a mixed meal in non-diabetic and newly-diagnosed diabetic persons with type 2 diabetes mellitus. *Planed submission to Diabetologia 2006.*

- S. B. Mortensen, S. Klim, B. Dammann, N. R. Kristensen, H. Madsen and R. V. Overgaard. A MATLAB framework for estimation of NLME Models using Stochastic Differential Equations Applications for estimation of insulin secretion rates. *Planed submission to Journal of Pharmacokinetics Pharmacodynamics 2006.*

List of Abbreviations

ACF, autocorrelation function; AR, autoregressive; ARMA, autoregressive moving average; HGC, hyperglycemic clamp; EKF, extended Kalman filter; GPS, global positioning system; IL, interleukin; IL-21, interleukin-21; IL-21R, interleukin-21 receptor; IIV, inter-individual variability; IOV, inter-occasion variability; IV, intravenous; IVGTT, intravenous glucose tolerance test; KF, Kalman filter; MA, moving average; MTT, meal tolerance test; NCA, non-compartmental analysis; NK, natural killer; OGTT, oral glucose tolerance test; ODE, ordinary differential equation; PD, pharmacodynamics; PK, pharmacokinetics; RRI, ready releasable insulin; RRP, ready releasable pool; SDE, stochastic differential equation;

Contents

Introduction

Pharmacokinetic/pharmacodynamic (PK/PD) modelling is a promising discipline within drug development that is hoped to increase speed and reduce cost of bringing new drugs to market, ultimately leading to faster and cheaper medicines for the consumer. PK/PD modelling techniques are used, not only for drug development, but also to increase knowledge within physiology, pathophysiology, and biosciences in general.

The present project explores the possibility to improve standard PK/PD modelling techniques by bridging data driven modelling with more theoretical techniques. PK/PD models are most often based on ordinary differential equations (ODEs), where theoretical modelling components such as physiological and biophysical mechanisms may be implemented to improve the model quality. In the present project we shall pursue a modelling approach where ODEs are extended to stochastic differential equations (SDEs), in order to approach data driven methods that are believed to enable a more rigorous framework for statistical inference and model building. A main effort has been to formulate and exemplify the effects of SDEs in PK/PD models in terms of actual model performance criteria such as simulation properties, specific predictive performance criteria, parameter estimates, and diagnostic plots.

Two major areas of application have been addressed, modelling of insulin secretion and modelling during interleukin-21 (IL-21) development. Insulin secretion models are based on biophysical as well as semi-empirical techniques, with applications that includes 1) an increased understanding of beta cell physiology, 2) a concise description of beta cell function e.g. for diagnosis, 3) control of

an artificial pancreas, and 4) development of anti-diabetic drugs. IL-21 is a recently discovered cytokine that is currently evaluated as an anti-cancer therapy in early clinical development. The fascinating biology of IL-21 includes several markers that with benefit can be analyzed using PK/PD models, and thereby provide a realistic scenario to test novel modelling techniques.

The specific contributions of the present report include,

1. A new model for insulin secretion is presented to bridge current biophysical and more empirical modelling techniques, and thereby contribute to the purposes of both model types.

2. Several models are developed to describe, predict, and understand the effects of IL-21, and thereby contribute to the drug development program.

3. A new estimation method for non-linear mixed-effects models based on SDEs is formulated, implemented, and investigated. This method provides a realistic setting for PK/PD models based on SDEs, which was required for further investigations.

4. A comparison of PK/PD models based on ODEs and SDEs is conducted. This included several different models that are based on different principles and built with different purposes.

The remaining thesis is structured as follows: Chapter 2 aim to explain and motivate PK/PD modelling as a new scientific discipline within drug development. Basic PK/PD concepts and methods are reviewed. Chapter 3 describes the present status of PK/PD modelling during IL-21 development by summarizing the different models and how they can be used. A brief introduction of IL-21 biology and the potential role of PK/PD modelling during development of cancer treatment is provided. Chapter 4 discuss the purpose of insulin secretion modelling, emphasizing the potential roles of the proposed new insulin secretion model. Relevant aspects of the beta-cell physiology and typical beta cell function tests are summarized. Chapter 5 introduces and discusses the proposed algorithm for mixed-effects models based on SDEs in relation to a few existing parameter estimation methods for 1) SDEs and 2) non-linear mixed-effects models. A short introduction to the interesting mathematical aspects of SDEs and their application in other areas of research, is provided. Chapter 6 aim to illustrate the specific benefits of SDEs in PK/PD models for 1) simulation properties, 2) specific predictive performance criteria, 3) parameter estimates, and 4) diagnostic plots. This is carried out through a series of comparisons between ODE and SDE models. A short review of the application of SDEs in PK/PD modelling and other biosciences is provided.

PK/PD modelling

Strictly speaking, the term PK/PD model refers to a mathematical model for the pharmacokinetic (PK) and pharmacodynamic (PD) properties of a drug, as well as a causal link from PK to PD. In the present thesis, however, we shall use the common and more loose definition that includes also models dealing only with PK or only PD, and even physiologic models that contain no drugs but uses PK/PD methodology. By this definition, all models treated in the present thesis can be considered PK/PD models, also models of insulin secretion where no drugs are included. The following chapter aim to elaborate on the PK/PD concepts, the PK/PD methodology, and the use of PK/PD models.

2.1 Pharmacokinetics

Pharmacokinetics describes the relationship between drug administration and drug concentrations at various sites in the body as a function of time. It is a scientific discipline concerned with the absorption, distribution, and elimination of drugs [105].

- **Absorption** describes the, most often irreversible, movement of drugs from the site of administration to the systemic circulation. Models typ-

ically use an absorption compartment representing for example the gastrointestinal tract for oral administration, or a subcutaneous depot for subcutaneous administration. The rate of absorption is typically described as either constant (zero'th order) or proportional (first order) to the amount in the absorption compartment, but more complicated models can and have been applied.

- **Distribution** is the reversible movement of drug from one location to another within the body. PK models typically use a central compartment to represent the systemic circulation and distribution compartments to represent, e.g. tissue or intracellular space. The distribution processes is frequently modelled by diffusion and convection principles that leads to linear rate constants between the different compartments, whereas more complicated distribution mechanisms could include for example target mediated PK [78], for which drugs may distribute onto the drug target, generally a saturable process.

- **Elimination** is the irreversible removal of drug from the body, either by excretion e.g. via the kidneys, or by metabolism e.g. by enzymes in the liver. Elimination, is typically modelled to be proportional to the concentration in the systemic circulation, or saturable via the Michaelis-Menton equation, corresponding to limited elimination pathways.

Paper B involves a simulation study of a one compartment model with first order elimination. The scientific contribution of this work, however, is not on the pharmacokinetics, but on the statistical methods to be explored in Chapter 5 and 6.

2.2   Pharmacodynamics

Pharmacodynamics concerns the effect of a drug on the body. Many drugs induce pleiotropic effects at a variety of sites in the body, where each effect could start a chain of pharmacodynamic activity or directly lead to physiological counter regulatory mechanisms, making PD modelling a potentially difficult task. In opposition to PK, the possible PD mechanisms are numerous, making classification according to mechanisms a strenuous task, and we shall simply refer to a classification according to physiological precision that is described in the following section.

The present thesis involves PD models for the effect of IL-21 on Red Blood Cells (Paper D) and on temperature regulation (Paper E). If glucose is seen as the

drug, the intravenous and the oral glucose tolerance tests can be seen as PK/PD experiments, and two papers consider the pharmacodynamic effects of glucose on insulin secretion (Paper A and Paper C).

2.3 PK/PD models

PK/PD models typically involve a description from dosing to exposure (e.g. plasma concentration) to clinically relevant effect, possibly with intermediate effect variables such as biomarkers to support the link between concentration and effect. They can usually be categorized according to the level of physiological detail needed for the chosen application, i.e. empirical, mechanistic, or physiological.

- **Empirical** models are exclusively based on data, and disregard the underlying physiology and mechanisms involved in the response. The effect compartment model, see e.g. [43], is most often used as an empirical model for the delay between dose or concentration to drug effect. Empirical models are simple and descriptive, but the failure to include knowledge about the system constitute a high risk for erroneous predictions when extrapolating beyond the data used for estimation.

- **Physiological** models aim to include a complete description of the physiological system where all parameter values and mechanisms are consistent with findings from basic experimental research. The main disadvantage is a high dependence upon knowledge of the drug and physiological mechanism, and that parameter estimation is usually made difficult by structural unidentifiable parameters and models with a high degree of complexity. This may limit the ability of the model to give a precise description of available experiments and to incorporate variability in the simulation of new trials. However, these models can with advantage be used to understand the system, and for simulation (biosimulation) in situations where no data is available, as e.g. for the first human trials or when evaluating new drug targets.

- **Mechanistic** or mechanism-based models, see, e.g. [79], aim to include the most significant physiological mechanisms, while not necessarily using parameter values that are identical to findings via basic experimental research. By this definition, physiological models are mechanistic, but not necessarily *vice verse*, and mechanistic models thereby constitute a compromise between the level of physiological precision in physiological and empirical models. Mechanistic models are most often simpler than

physiological models, containing a set of descriptive parameters that can be estimated. Since these models are based on previous data as well as the most important physiological mechanisms, mechanistic modelling has been the preferred approach to extrapolate beyond the data used for estimation and provide us with a hypothesis for the outcome of future trials [110]. The trend of PK/PD modelling seems to be towards more mechanistic models, e.g. by approaching physiological models that can answer questions with more certainty, also when no data is available.

For pharmacokinetics, the non-compartmental analysis (NCA) is empirical, the usual compartment models are more mechanistic, whereas some research is put into physiology based PK (see [12] and references therein), where the flow of drug through all organs is described in terms of physiologically known values.

2.4   The Population PK/PD method

Population PK/PD deals with models across different populations of individuals as defined by demographics (such as age, sex, and weight), biological information (such as the value of biological markers), genetic information, comedications, environmental factors, and disease states [110]. The purpose being to explain the variation between individuals, so that dosage can be appropriately modified if particular populations exhibit a shift in the PK or therapeutic index [129] [121].

The population model framework consist of the following three parts: 1) A model for individual parameters that may include relationships to covariates such as demographics, other population factors, or even study specific factors. The parameter model typically also uses unexplained variability, e.g. inter-individual variability (IIV) and inter-occasion variability (IOV). 2) A structural model that depend upon the individual parameters is usually formulated by a set of differential equations or the solution thereof. It could be empirical, mechanistic, or physiological as previously discussed. 3) A residual error model, which contain the differences between structural model predictions and actual observations, arising because of assay error, variability in parameters, unknown perturbations, and errors in the structural model.

A consensus is arising for non-linear mixed-effects modelling, see Section 5.6, as the preferred technique for population modelling. With this technique, all data is modelled simultaneously, which enables the inclusion of information from one individual to the next, and thereby also from one treatment regimen/dose level to the next. The accumulating information obtained by many subjects treated

in different ways enable more mechanisms to be elucidated allowing reliable mechanistic models to be developed. For empirical models the number of necessary parameters will increase, and mechanistic models will eventually become the most parsimonious. Whereas these obvious benefits make population modelling, mixed-effects techniques, and mechanistic modelling go hand in hand, also other techniques have been widely used to investigate population data, e.g. the standard two-stage method[1].

The vast interest towards the population approach is evident, not only from regulatory guidelines [129] [121] and position papers [110] [35] [36] [37], but also from world wide yearly conferences on this type of modelling, e.g. PAGE (Population Approach Group Europe), PAGANZ (Population Approach Group in Australia & New Zealand), and ECPAG (East Coast Population Analysis Group). One might say that the scope of population modelling with mixed-effects techniques has grown beyond the purpose of dose adjustment because the method lend itself naturally for modelling PK/PD data that most often includes several individuals, possibly from different studies, possibly sparsely sampled, and possibly with a range of different treatment schedules.

The population approach, in the form of mixed-effects modelling is used in Papers B, C, D, and E. Paper B presents the work toward an extension of the population model, by extending the structural model from an ordinary differential equation (ODE) to a stochastic differential equation (SDE), which will be discussed in detail in Chapter 5 and 6.

2.5 The Role of PK/PD modelling in pharmaceutical development

It is the aim of the drug development program, to turn chemicals into drugs; that is, to provide the 'user's manual' required for their safe and efficacious use [110]. PK/PD modelling can contribute to many aspects of this process, for example related to the combination of information to facilitate the transition between the different phases in development, i.e. preclinical, and clinical phase I-IV, as presented in Figure 2.1.

It has recently been identified by the Food and Drug Administration in the U.S. (FDA) that the pharmaceutical development process lacks behind basic biomedical scientific innovation in speed and effectiveness [130]. Consequently

---

[1]The first stage involves separate parameter estimation for each individual, while the second stage involves a model for these parameter estimates as a function of population covariate information.
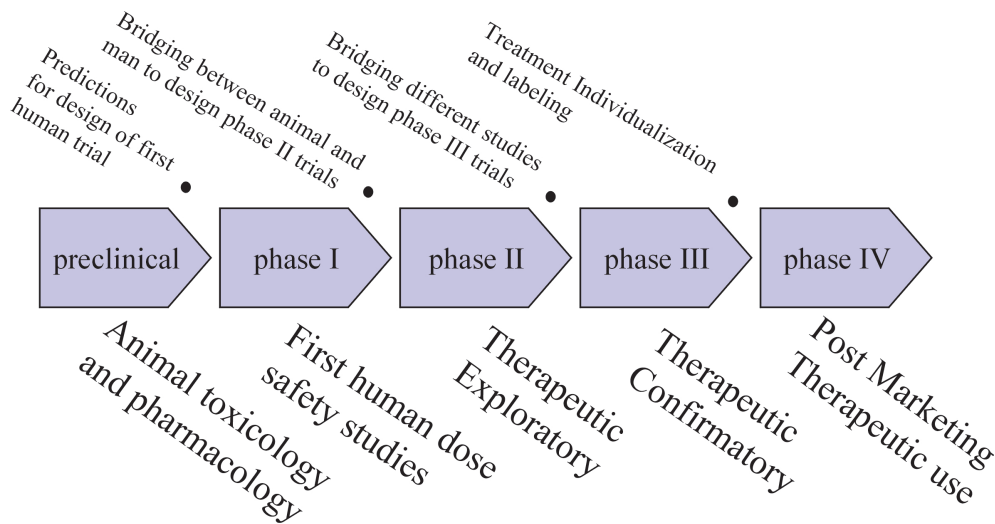
Figure 2.1: Diagram of the pharmaceutical development process. PK/PD modelling offers many contributions during this process, and some of these are concerned with combining information to support the transition between different phases, as marked with bullets.

development has increasingly contributed to the overall expenditure in time and money to carrying new drugs to market[2], ultimately having caused the observed slowdown in drugs reaching patients. Scientific research directed towards pharmaceutical development and information technology are foreseen to play a key role in strengthening pharmaceutical development [130] [98], and PK/PD modelling is identified directly to play a significant part in both of these directions.

Several initiatives have been taken to drive modelling forward to meet the needs of drug development: 1) Pharmacometrics was recognized as a scientific discipline of its own in 1982, with a special section in the journal of Pharmacokinetics and Biopharmaceutics. 2) Regulatory guidelines have been put forward to facilitate industrial use of modelling [129] and [121]. 3) The European Community has sponsored the COST B15 expert committee that addresses the role of PK/PD modelling [8], and [102]. 4) A number of independent position papers have been formulated to elaborate on the use of PK/PD modelling, see e.g. [110], [112], [44], and [28] that in essence all advocate increased knowledge based decisions in drug development as facilitated e.g. by PK/PD modelling. Whereas the practical goal of drug development is to demonstrate (confirm) efficacy, a paradigm shift has been suggested to focus more on science (learning)

---

[2]In 2001, a typical drug company spend $802 million during 10 to 15 years on bringing a new drug to market until approval by the FDA could be obtained [40].

during early drug development [111], which may partially be driven by PK/PD modelling.

The die is cast, and only the future will show whether drug development will make the necessary changes for PK/PD modelling to live up to its full potential.

Of the many ways to categorize the benefits of PK/PD modelling, the general division used e.g. in [44], is repeatedly referred to throughout this thesis. PK/PD models can be used to describe, predict, and understand the system under investigation.

- **Describe.** Mathematical models give a very concise and univocal summary of data, particularly useful when bridging knowledge from different studies.

- **Predict.** Models can be used to predict/simulate the outcome of new studies, e.g. with new dosing regimen or sampling schedules. Allometric scaling (see [101] and references therein) and physiology based PK (see [12] and references therein) are typically used to predict from animal to the first human studies, whereas complete trial simulations [52] can be used to predict the probability of success in statistically confirmatory trials by including between-subject variability, within-subject variability, compliance etc.

- **Understand.** PK/PD models can help to understand the fundamental mechanisms of the system, they being pharmacological, physiological, pathophysiological, biochemical or something else. In deed, modelling may help to test the consistency of competing theories for the observed effect, as used e.g. to resolve different mechanisms of drug action, which may be complicated by the presence of counter regulatory physiological effects.

The role of PK/PD modelling in IL-21 development shall be discussed in more detail in Section 3.3.

CHAPTER 3

PK/PD models of interleukin-21

Interleukin-21 (IL-21) is a recently discovered cytokine [90] with antitumor effects in preclinical and *in vitro* models, which is currently under clinical investigations as an immunotherapeutic anti-cancer drug. Several of the PK/PD models that were developed during the present project were motivated by the challenges of turning this biological molecule into a pharmaceutical compound. After a brief introduction of IL-21 biology and its potential role in cancer treatment, the present chapter will focus on these PK/PD models.

3.1 IL-21 Biology

It is six years since cloning of the interleukin-21 receptor (IL-21R) [88] and identification of IL-21 with a first analysis of its proliferative and functional effects on T, B, and natural killer (NK) cells [90]. Since then, IL-21 research has been progressing rapidly, now with more than 100 PubMed [5] publications. A detailed review is beyond the scope of the present section, but Figure 3.1 sketches a central part of the role of IL-21 in lymphocyte biology.

IL-21 has a protein structure that place it in the γ-chain family of cytokines,
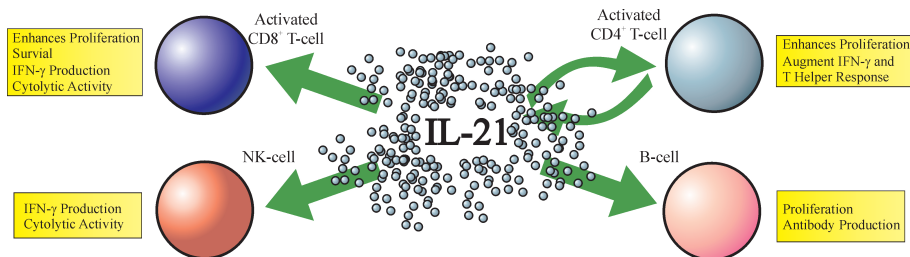
Figure 3.1: The biological effects of IL-21 on central lymphocytes, see [48] for a slightly more detailed version of this figure. IL-21 is produced by activated T-helper cells and has pleiotropic effects on T, B, and NK cells. The increased cytolytic activity and IFN-γ production from activated NK and T cells was one central motivation for the early suggestions of antitumor and immunotherapeutic effects in oncology. IL-21 is not only affecting lymphocytes, but also some myeloid cells and keratinocytes.

with greatest similarity to IL-2 and IL-15 [90], but the biological characteristics of IL-21 are distinct from other known cytokines. IL-21 is produced by activated T helper cells, and the IL-21R is expressed on T cells, B cells, NK cells, and some populations of myeloid cells and keratinocytes, consistent with cell types that respond to IL-21, see review [72]. From an oncology perspective, the most interesting immunomodulatory action of IL-21 is seen by activation and proliferation of lymphocytes, leading to increased cytolytic activity. Given these effects on lymphoid cell function, and the known effects of IL-2 and IL-15 on tumor regression *in vivo*, IL-21 has been anticipated also to have a role in tumor regression. Indeed, IL-21 has been shown to have potent antitumor activity in several experimental models [72]. The current status of the broad range of IL-21 effects on various cell lines, most recently reviewed in [72], is listed below:

- **T cells**. 1) Stimulation of T cell proliferation together with CD3-specific antibody. 2) Stimulation of cytotoxic T cell proliferation in synergy with IL-7 and IL-15, but not IL-2. 3) Induction of antitumor activity for cytotoxic T cells.

- **B cells**. 1) Cooperation with IL-4 to promote IgG antibody production. 2) Promotion of class switching to IgG1 and IgG3 antibodies. 3) Inhibition of transcription of part of IgE antibody constant region. 4) Induction of differentiation of B cells into plasma cells. 5) Pro-apoptotic effects on naive B cells, and B cells that are activated in the absence of T cells. 6) Stimulation of proliferation together with IgM or CD40 specific antibody.

- **NK cells**. 1) Induction of differentiation. 2) Induction of cytotoxic and apoptotic activity. 3) Induction of antitumor activity.

- **Myeloid cells**. Induction of monocyte-derived macrophages to secrete a potent neutrophil chemoattractant. 2) Inhibition of dendritic cell activation and maturation.

As outlined above, IL-21 has clear effects on lymphoid cells mediating anti-tumor activity, but evidence also points toward a role in inflammation [91]. For human diseases, IL-21 is speculated to play a role in autoimmunity, asthma and allergy, and oncology [72], where the present evidence is strongest for the latter. Although these observations motivate clinical studies, there is still a long way to go before this molecule can be used in an approved anti-cancer treatment strategy.

3.2   PK/PD in Early Anti-Cancer Development

The large medical need for new cancer therapy is evident. A recent global overview [89] of 26 cancers find 10.9 million new cases, 6.7 million deaths, and 24.6 million persons alive with cancer in 2002. In the US, cancer accounted for 23% of all deaths, ranking second only to heart disease [58]. Cancer cases are grouped into four stages denoted by Roman numerals I through IV, where the precise definition of the four stages vary among different cancers [4]. In general, stage I cancers are small localized cancers that are usually curable, while stage IV usually represents inoperable or metastatic cancer often associated with poor prognosis, sometime less than 5% probability of survival.

Conventional treatment includes surgery, radiotherapy, and chemotherapy. Although cytotoxic chemotherapy is a systemic treatment that can be used also against metastatic cancers, they lack selectivity leading to severe side effects and limited efficacy. Novel cancer therapies aim at targeted cancer treatment [108], e.g. by targeting specific cancer cell processes. Another strategy aim to modulate the immune system and thereby use the body's own defence mechanisms against the cancer cells. Experimental treatment with IL-21 pursues this latter strategy.

IL-21 is currently evaluated in early clinical development, and data used in the present thesis are from preclinical and phase I studies. For ethical reasons, new experimental cancer treatments in phase I studies are as a general rule conducted in patients with advanced disease (stage IV) and with no other treatment option. We should remember that these patients are severely ill, which influences their general state, their ability to recover from unwanted effects, and their ability to respond to immune modulation. Naturally, these circumstances will narrow the window of opportunity by reducing the drug efficacy and increasing the severity

of adverse events, complicating the development of new cancer treatments.

It has been argued that PK/PD modelling may be especially useful within oncology, where drugs tend to have a narrow therapeutic index [131]. In this setting, it is fruitful to consider both efficacy and safety markers, so that a two sided evaluation of the dosing regiments can be performed. Also the COST B15 experts have devoted special attention to modelling in the development of anti-cancer agents, advocating its use to integrate knowledge throughout the development process to reduce ethical concerns, uncertainty, risk, and resource costs [102].

3.3   PK/PD Modelling in IL-21 Development

Several models have been developed during the past years of pre-clinical and clinical testing of IL-21. In the following sections, we shall review some of these efforts with a focus on how the different models can and have been applied during development. The mathematical description and the scientific exploration of stochastic differential equations within some of these models, is given in Chapter 6.

3.3.1   IL-21 Effects on RBC

The effects of IL-21 on red blood cells (RBC) and haemoglobin concentration in the blood have been investigated with PK/PD modelling from preclinical studies, see Paper D, and modelling has continued up until the present stage in clinical development, see Section 6.5. Cynomolgus and Rhesus monkeys demonstrated a significant loss in RBC concentration following IL-21 administration, and anemia was at that stage judged as the most likely candidate to cause dose limiting toxicity in the clinic. Haemoglobin is no longer considered to be the most important toxicity marker, but it is dose dependent, and related to fatigue and quality of life of the patients [27], which could make it a relevant marker to aid dose and regimen selection.

PK/PD modelling of haemoglobin and RBC can and have been used to,

- **Give a univocal description of the observed effects.** 1) The effects of IL-21 is consistent among different trials, dosing regimens and species. 2) One way to describe the effects are: IL-21 treatment leads to a decrease in haemoglobin/RBC, which is considerably delayed compared to dosing

and IL-21 plasma concentration. 3) Besides the dose dependent drop, an additional drop in haemoglobin/RBC was found. This could be described as a placebo effect in the clinical studies, while for the monkey studies the drop in RBC concentration was found to be proportional to the amount of blood removed during the study. 4) A decrease in haemoglobin/RBC leads to an increased production of new red blood cells, which enters into the blood stream after a delay. 5) Haemoglobin/RBC is seen to recover, but the recovery is slow and is not seen to rebound above baseline levels.

- **Merge preclinical data with early clinical results.** The model for effects on RBC in monkeys was used during the clinical dose escalation, so that modelling could be used at a time point where clinical data was insufficient to identify the model structure and estimate all parameters. In other words, the monkey results were used as prior information for the clinical model, which became more and more "humanized" as more data became available. This was useful to describe current clinical data, give reasonable predictions for observed results at higher dose levels, and to give likely intervals for these predictions.

- **Demonstrate a clear dose response.** Due to differences in sampling schedules and starting haemoglobin/RBC level, it may be difficult to compare the the results from different studies and individuals. By modelling, the effect of IL-21 on the haemoglobin level could be summarized in one number, making it easier to identify the dose response curve.

- **Compare the observed effects for different treatment regimens.** Two treatment regimens were investigated in the phase I trials, 1) a cyclic regimen with 5 days of dosing followed by 9 days of rest, and 2) a continuous regimen with 3 times weekly dosing for six weeks. It is presently judged that the effect, e.g. the area under the baseline haemoglobin curve, will be similar in the two regimens if the same number of doses with identical amounts are administered in the two regimens, but slightly larger fluctuations are seen in the cyclic regimen.

- **Simulate predictions for anemia in other dosing regimens.** The model was used to simulate several different dose levels and dosing regimens to predict the probability for grade 3 anemia (haemoglobin concentration at 80-65g/L).

3.3.2   IL-21 Effects on platelet

Like the clear effects on RBC, IL-21 was observed to induce clear effects on platelets in preclinical studies. Modelling of the effects on platelet was initiated

during the clinical dose escalation study, and has subsequently been used to, 1) give a univocal description of the observed effects, 2) demonstrate dose response, 3) compare the observed effects for different treatment regimens, and 4) simulate predictions for thrombocytopenia in other dosing regimens, and thereby support dose selection in future studies.

PK/PD modelling of platelets was not performed during the present project, and will not be explored further in the present thesis.

3.3.3   IL-21 Effects on Temperature

Besides anemia, fever was considered the most clinically important toxicological finding in the preclinical studies of IL-21 in non-human primates. In the clinical study, fever is still a very frequent adverse event, but the rise in body temperature is easily normalized by the administration of paracetamol. A single PK/PD model for IL-21 effects on body temperature was developed using preclinical data, see Paper E and Section 6.3.

Modelling has been used to describe the complicated effects of IL-21 on the different mechanisms that regulate body temperature. One way to describe the effects is as follows: 1) A sufficiently high dose of IL-21 induces priming, i.e. no effect of IL-21 is seen until some priming has occurred. 2) Priming happens gradually and takes some time to occur, and this time may vary between individual monkeys. 3) After priming has occurred, circadian rhythm in metabolism vanish, and metabolism is kept at a daytime high value. 4) Further more, IL-21 administration will after priming induce a fast dose independent effect, i.e. a predetermined fixed size acute phase response, and a slow dose dependent effect. The fast and the slow effects are combined to give a saturable elevation of the set-point temperature. 5) This elevation cause a decrease in conductance, e.g. via vasoconstriction, leading to elevated core body temperature.

3.3.4   IL-21 Effects on Soluble CD25

The cell membrane molecule CD25 is the alpha subunit of the IL-2 receptor, which is shed e.g. from T-cells and NK cells during activation. High serum levels of soluble CD25 (sCD25) is considered a marker for general activation of the immune system[1], and sCD25 is presently used as a biomarker for the immunomodulatory activity of IL-21. Modelling of sCD25 was initiated during

---

[1]sCD25 is for example used as a diagnostic marker for chronic T-cell activation.

preclinical studies and is proceeding in the clinical phases, where it has been used to, 1) give a univocal description of the observed effects across different trials, dosing regimens, and species, 2) demonstrate a more clear dose response, 3) compare the observed effects for different treatment regimens and different patient populations, and 4) simulate effects on sCD25 to evaluate various treatment regimens that have not been tested experimentally. This evaluation has been compared to haemoglobin results, because it is necessary to include both efficacy and safety parameters in such an analysis.

PK/PD modelling of sCD25 has not been included as part of the present project, and will not be explored further in this thesis.

3.3.5   IL-21 Effects on Lymphocytes

As previously mentioned, IL-21 has various effects on the various lymphocyte cell lines. The observed total lymphocytes counts in plasma is seen to decrease immediately after dosing, and a rebound above baseline is seen after a few days. Although these effects do lead to short periods of lymphopenia, the effects on lymphocytes reflect the immunomodulatory mechanism of the drug that are believed to provide benefits to the patients. Modelling of lymphocytes were initiated during the phase 1 study, and has been used to 1) give a univocal description of the observed effects across different trials, dosing regimens, and species, and 2) simulate effects on lymphocytes and the probability of lymphopenia in various treatment regimens that has not been tested experimentally.

PK/PD modelling of lymphocytes has not been included as part of the present project, and will not be explored further in this thesis.

CHAPTER 4

PK/PD Modelling of Insulin secretion

Type 1 diabetes is characterized by complete beta cell function failure, whereas type 2 diabetes is a heterogeneous disorder characterized by a combination of impaired insulin secretion and insulin resistance [3], in which either factor can be dominant. Of these interrelated factors, the present thesis deals with insulin secretion, and we shall here review some relevant aspects of the beta-cell physiology, the typical tests used to assess glucose homeostasis and beta cell function, and how modelling is used within this field.

4.1   The physiology of biphasic insulin secretion

Insulin secretion in response to an abrupt increase in plasma glucose is known to be biphasic with a rapid peak at 2-4 min (first-phase), decrease to nadir at 10-15 min, and then gradually increase within the next couple of hours (second-phase)[1]. For both phases, it is observed that the amount of insulin released depend upon the level of the elevated glucose concentration. In physiologic

---

[1] *In vitro*, a third-phase of insulin secretion is observed [22] as desensitization of perfused beta cell islets, which is seen as a decline in secretion around 3 hours after the starting point of the hyperglycemic challenge [21].

situations, e.g. after the consumption of a meal, the glucose rises slowly and a first-phase peak is not seen, but there is still a significantly elevated early release that we shall refer to as first-phase release, since it is likely caused by the same mechanism.

The physiology behind the biphasic insulin secretion, as reviewed in [116], [117], and [103], entails a number of mechanisms that are not all fully understood:

- **Synthesis.** Glucose stimulates transcription as well as translation of proinsulin, but over short time periods proinsulin biosynthesis is mainly regulated by increasing the rate of translation of proinsulin mRNA. Evidence exist that newly synthesized secretory vesicles are secreted first [34], but for beta cells the current consensus is that upregulation of proinsulin contributes only partially to the gradual increase in second-phase response.

- **Granule pools.** After synthesis, proinsulin is split into insulin and C-peptide that are packed in equimolar amounts into granules by the golgi apparatus. Some granules move freely within the intracellular space while others are docked in the plasma membrane and only a fraction of the latter are ready to be released, thereby named the readily releasable pool (RRP), see review [104]. The RRP is believed to contain the granules contributing to the first phase secretion [87], while recent experiments with real-time imaging indicate that second phase secretion is due to granules that have just arrived at the plasma membrane [86].

  Insulin secretion following two sequential square-wave glucose stimuli will lead to two first-phase spikes. If the time between the two pulses is very short, the second first-phase release will be low, known as time dependent inhibition [80], which may be due to depletion of the RRP. On the other hand, a longer period of hyperglycemia is known to increase a subsequent first-phase response, called time dependent potentiation, which is likely due to an enlarged RRP associated with the elevated insulin release.

- **Exocytosis.** The release of insulin is tightly controlled by the electrical activity of the beta cell [103]. Intracellular glucose transforms into ATP, stopping the potassium efflux of the sodium-potassium pump, which depolarizes the cell. Depolarization opens the voltage gated calcium channels, and the rise of calcium activates certain proteins (e.g. SNARE proteins) that facilitate the exocytosis of insulin granules. A significant part of the insulin is secreted in small bursts that are synchronized among different beta cells, giving oscillations in plasma insulin concentration, see [96] and references therein[2].

---

[2]Rapid oscillations in insulin secretion have been reported with periods ranging from 5-15 min [96], whereas ultradian oscillations have been reported with periods 100-150 min [120].

- **Heterogeneity.** The heterogeneity between granules (being docked or not) can explain the existence of two phases, but the significance of heterogeneity among beta-cells is not fully recognized and understood. However, under the assumption that the RRP of a single beta-cell is emptied when it undergoes exocytosis, heterogeneity among beta-cells is needed to explain the increasing first-phase response to increasing glucose challenges, which is a promising hypothesis argued from experimental findings in [94], [95], and [107]. Indeed, individual beta-cells have been reported to differ in the glucose threshold levels for pro-insulin biosynthesis, glucose metabolism, calcium influx, and secretory activity, see [106] and references therein.

- **Incretin Effect.** The list of chemical, biological and pharmaceutical mediators that affect insulin secretion is long, and beyond the scope of this short summary. However, we wish to mention that oral ingestion of nutrients is known to enhance insulin secretion, the incretin effect, leading to higher insulin secretion during oral glucose challenge than from an experiment with matched glucose concentrations obtained by IV infusion of glucose, see e.g. [62]. The incretin effect is mediated by insulinotropic intestinal hormones, as e.g. glucagon-like peptide-1, which enhances both first and second phase release, see e.g. the experiments by Fritsche et al. [42]. Besides the effects of incretin hormones, we wish to list that 1) neuronal signals have been found to stimulate secretion prior to a meal [119], 2) the level of free-fatty-acid has been found to change the sensitivity of insulin secretion [15], and 3) that insulin may inhibit its own secretion [13].

Patients during the early stages of type 2 diabetes are most often subject to impaired or even lost first phase secretion, whereas the second phase and the baseline insulin level is frequently enhanced. The consequences of these changes may not be fully understood, but strong evidence indicates that early insulin release after glucose ingestion is a key determining factor for the subsequent glucose concentration [26]. Ultimately, these results indicate that a reduced first-phase may be a significant pathogenic factor, or even responsible for the development of impaired glucose tolerance [97].

4.2   Diagnostic tests

Diagnostic tests for the assessment of insulin secretion as well as insulin resistance for individual patients have great value for epidemiological and clinical studies. The most common oral administration tests are the oral glucose tolerance test (OGTT) and the meal tolerance test (MTT), but also the 24 hour

triple meal test has been used to more closely mimic a physiological relevant situation. The most common intravenous (IV) tests are the intravenous glucose tolerance test (IVGTT) and the clamp tests, e.g. the hyperglycemic clamp (HGC), where glucose is kept constant at an elevated level. Also other tests, such as the graded up&down glucose infusion test have been suggested [124], and less rigorous infusion tests are frequently used during the evaluation of new medicines.

4.3   Models of insulin secretion

Like other research of insulin secretion, modelling should more or less directly aim to ease the burden of diabetes. The two main directions for modelling insulin secretion is, 1) biophysical modelling to increase the understanding of the system, which resembles the "physiological" approach described above, and 2) by the "empirical" approach, to describe and summarize individual and population data.

Biophysical models that aim to increase knowledge and understanding of the basic physiology have contributed to many aspects of insulin secretion. Perhaps, the most comprehensive contribution are from models that describe the ion fluxes within single beta cells, see [41] and references therein. These models have enabled quantitative formulation of the processes that govern the oscillatory patterns of ions concentrations that are important e.g. for exocytosis.

For the whole body system, there has been two classical directions for biophysical models of insulin secretion, the "storage-limited model" [46] and the "signal-limited model" [51] that are compared in [85]. In the "storage-limited model", each phase of secretion corresponds to the release, by a constant signal, of a distinct pool of insulin granules, whereas in the "signal-limited model" a biphasic signal operates on one pool of granules. The distributed threshold hypothesis is a storage limited model that has been used to argue and derive many of the following more empirical models, see [73] and Paper A.

More empirical modelling of insulin secretion can be imagined within numerous areas to support a variety experiments. In the present context, we shall merely mention three applications of whole body models that are believed to be particular relevant for the present thesis, i.e. estimation of diagnostic indexes, controlling the artificial pancreas, and guiding pharmaceutical development of anti-diabetic drugs.

- **Metabolic Portrait.** Empirical insulin-glucose models have traditionally

been used with data from diagnostic tests, to estimate parameters that constitute a metabolic portrait. Thereby models have enabled diagnosis and tracking of the progression of diabetes. Such analysis can significantly benefit single subject investigations as well as large scale clinical and epidemiological studies to increase the knowledge of diabetes and the effects of treatment. This approach to modelling the insulin-glucose system typically follow the minimal model approach, where models are aimed to be as simple as possible, yet describing the most important features in data, see e.g. the original minimal model for glucose disposition [18]. Many models are very tightly linked to a particular diagnostic test, as e.g. minimal models for the IVGTT [123] and [125]. While these models exclusively aim to describe data from one test, a single approach is beginning to converge for diagnostic tests where the glucose concentration varies smoothly. The oral minimal model of insulin secretion, as it is frequently called, has been successfully used to model the OGTT [23], the graded up&down glucose infusion [124], and the MTT [29]. This approach makes use of a baseline (B), a static (k_s), and a dynamic (k_d) index, so that insulin secretion can be written,

$$
\begin{aligned}
\frac{dY}{dt} &= -\alpha Y - k_s[G - G_b] \\
SR &= B + Y + k_d\frac{dG}{dt}
\end{aligned}
\tag{4.1}
$$

where SR is the secretion rate, $[G - G_b]$ is the glucose above baseline, and α is a rate parameter. To some extent, the dynamic index corresponds to first-phase secretion and the static index corresponds to second-phase secretion.

- **Artificial pancreas.** The recent progress in glucose censoring devices makes the closed-loop artificial pancreas[3] within reach, leading to interest for insulin secretion models and algorithms to support this field [17], [115], and [114]. Very successful algorithms have been developed for the artificial pancreas, and one has been tested to outperform the real dog pancreas to keep a constant glucose concentration after a meal [99]. Constant low glucose concentration, however, has its price in terms of increased insulin delivery, which may cause weight gain, hypertension, or arteriosclerosis, and it has been argued that a more physiological insulin delivery may be preferable [114].

- **Anti-diabetic Drugs.** Modelling of insulin secretion to support the development of anti-diabetic drugs has not been significantly published, but

---

[3]The open-loop program deliver a predetermined amount of insulin to the patient, whereas the closed-loop artificial pancreas require continuous monitoring of blood glucose levels, see e.g. [39].

undoubtedly such efforts are beneficial. As previously discussed, modelling in pharmaceutical development is moving towards more mechanistic models. For insulin secretion, such models would improve the ability to incorporate drugs that target different mechanisms on the beta cell. It is also foreseen that mechanistic models would improve the prediction of different dose levels and administration schedules, via the inclusion of the relevant physiological regulatory mechanisms of the pancreas.

The two main contributions of the present project to modelling of insulin secretion are described in Paper A and Paper C. Paper A is primarily a theoretical paper that aim to illustrate how the two different minimal models for the IVGTT (published in [123] and [125]) are connected with different theoretical features in the distributed threshold model [46]. The hope is that these new insights to the minimal model of insulin secretion can lead to an understanding of the meaning of the estimated parameters, and aid in the pursuit of a more general and physiological correct model that can characterize the beta cell function, not only for the IVGTT, but also for other experiments. Paper C describes such an attempt, where data from the IVGTT and from the OGTT is modelled simultaneously. Modelling is performed via the population PK/PD method with a mixed-effects approach, which as previously discussed is well suited for modelling several individuals from different study designs. This mechanistic compromise between physiological and empirical modelling could potentially help to solve issues in the application of both types of models.

For physiological models, the model in Paper C may be regarded to improve knowledge of the system by providing a consistency check for the threshold distribution hypothesis as an explanation for the dose dependent first-phase secretion. In fact, an interesting conclusion was that threshold distribution as well as incretin effects for both first and second phase were necessary to describe differences between the IVGTT and the OGTT. All in all, the threshold distribution hypothesis was found to be consistent with the two experiments, with no physiological contradictions. In particular, I was pleased to find that for the IVGTT and the OGTT, the individually estimated sizes of the RRP were similar and exhibited a convincing correlation.

Paper C can be seen to aid all three previously mentioned application areas for empirical models, 1) the metabolic portrait, 2) the artificial pancreas, and 3) the development of anti-diabetic drugs. Each point is discussed in the following:

1. When the same individuals are subject to different diagnostic tests, one expect to get similar results, and at least a reasonable correlation should exist between indexes that describe the same physiology, e.g. the first-phase indexes should correlate. When different models are used for differ-

ent diagnostic tests, we must relax our requirement of similar indexes, but we should still expect a reasonable correlation. Indeed, a good correlation is seen for indexes from some diagnostic tests, but clear discrepancies have been found between the first-phase index from the HGC and the MTT, leading to the conclusion that further work is needed for these indexes to be routinely used in clinical and epidemiological studies [114]. The model described in Paper C aim to provide a higher degree of consistency to these indexes by providing a single model that can be used for parameter estimation in different tests, and thereby improving model based diagnosis and tracking of the progression of diabetes. Emphasis was devoted towards similarity, reproducibility, and prognostic relevance of individual parameters estimated in the IVGTT and the OGTT.

2. The oral minimal model for insulin secretion previously mentioned in (4.1) has been found to be a promising candidate for the artificial pancreas, both with subcutaneous glucose censoring and insulin delivery, and with IV glucose censoring and intraperitoneal insulin delivery [115]. A number of complications are involved in the implementation, e.g. that in the oral minimal model, 1) the parameters may differ according to the design of the diagnostic test, see [114], making it unclear which parameters to use, and 2) that the model lack a description of the RRP to explain time dependent inhibition and potentiation of the first phase of insulin secretion, which could be influential with the fluctuating glucose concentration found in every day living. The model described in Paper C is an attempt to overcome these problems. It provide a first step towards solving the consistency among indexes, and naturally incorporates time dependent inhibition as depletion of the RRP, and potentiation as an elevated RRP due to elevated glucose concentration.

3. The model described in Paper C provides a mechanistic description of the first and second phase of insulin secretion. Hereby, the model fill out an important gap in the list of modelling tools for development of anti-diabetic drugs. The model can be seen as a baseline model, which can be extended to include the action of different drugs, e.g. sulphonylureas acting on exocytosis, or incretin hormones that affect first-phase as well as second-phase.

Stochastic Differential Equations

- What happens if the parameters in a differential equation are randomly varying at all time points?

- How do we merge classical time-series modelling with the differential equations found in other sciences?

- How do we optimally filter away measurement noise in a system where the underlying theory is modelled with differential equations?

Stochastic differential equations (SDEs) provide the answer to these and many other questions. Similarly Øksendal [69] pose six fundamental questions to motivate the extension of ordinary differential equations (ODEs) to SDEs.

Parameter estimation, particularly in mixed-effects models based on SDEs, is an important topic of the present thesis that shall be touched upon in the present chapter. But first of all, we shall investigate the depth of the discipline by discussing some fundamental mathematical properties and fruitful applications of SDEs.

5.1   Mathematical Introduction

In the most common form[1], SDEs can be defined as,

$$d\boldsymbol{x} = \boldsymbol{g}(\boldsymbol{x})dt + \boldsymbol{\sigma}_w(\boldsymbol{x})d\boldsymbol{w}, \quad \boldsymbol{w}_{t_2} - \boldsymbol{w}_{t_1} \in N(0, |t_2 - t_1|I) \tag{5.1}$$

where $\boldsymbol{w}$ is a standard Wiener process, i.e. a continuous process where the increments $(\boldsymbol{w}_{t_2} - \boldsymbol{w}_{t_1})$ of non-overlapping time intervals are independent multivariate Gaussian with mean zero and a standardized variance-covariance. $\boldsymbol{g}(\boldsymbol{x})$ is called the drift term, and $\boldsymbol{\sigma}_w(\boldsymbol{x})d\boldsymbol{w}$ is the diffusion term giving rise to system noise. The diffusion term is called additive if $\boldsymbol{\sigma}_w$ is independent of $\boldsymbol{x}$ and multiplicative if $\boldsymbol{\sigma}_w(\boldsymbol{x})$ depend upon $\boldsymbol{x}$, such that multiplication of stochastic variables are involved in the term $\boldsymbol{\sigma}_w(\boldsymbol{x})d\boldsymbol{w}$. Most often, we refer to multiplicative diffusion in the proportional form that can be written $\boldsymbol{\sigma}_w\boldsymbol{x}d\boldsymbol{w}$.

SDEs are interesting objects that to fully understand require a substantial amount of university level mathematics, particular within the field of measure and integration theory [69]. In the interest of making the present thesis more accessible, the mathematical details will be skipped, and I shall merely mention two fundamental counterintuitive examples that illustrate the mathematical challenge of a rigorous consistent description.

1. SDEs cannot be defined in terms of the usual differential quotient $d\boldsymbol{x}/dt$, because the corresponding random term $d\boldsymbol{w}/dt$ is ill defined (not finite). An immediate consequence is seen by the notation used in (5.1), where the SDE is defined by $d\boldsymbol{x}$ rather than $d\boldsymbol{x}/dt$. A more peculiar consequence is that the Wiener process will cross zero an infinite number of times within any time interval that includes zero, possibly leading to strange behavior of the SDE solution.

2. Like for ODEs, the solution to an SDE (for a particular instance of the Wiener process) can be calculated by numerical integration, and the solution converge when the integration steps go to zero. However, unlike for ODEs, the SDE solution may depend upon the method of integration, making it important to state under which integration scheme the SDE should be understood. Itô and Stratonovich are two popular integration schemes that produce different solutions to the same SDE, see further discussion and Figure 5.1 in Section 5.3.

When starting to apply these objects without a complete understanding, it is comfortable to know that rigorous mathematics ensures us that SDEs, in spite of these counterintuitive properties, are in fact consistent objects.

---

[1]One can, and have imagined other forms of SDEs, e.g. with the more general Lévy processes that also include discrete jumps such as those originating from Poisson processes [70].

5.2 Applications of SDEs

Whereas the fundamental description of SDEs is a mathematical discipline, their application have been found useful in many areas of research. Specific areas of applications include finance, satellite navigation, theoretical physics, and modelling within various biosciences.

- Financial statistics dominates the applications of stochastic differential equation, where SDEs are used for estimation and simulation of e.g. the random fluctuations in stock price development, which is necessary for option pricing. Finance and SDEs are interconnected to an extent where SDEs are treated within standard course-work text books of finance [53], and so that financial applications are pushing forward the field of SDEs, as for example the connection between Lévy processes [70] and alternative option pricing strategies.

- Satellite navigation problems of reentry and orbit determination are classical applications of SDEs [55]. The use of stochastic processes have continued and they are now used to optimize satellite position estimates for the global positioning system (GPS). One example include a 56 state Kalman filter (to be discussed below) for the air force's most advanced navigation system [1].

- SDEs have been used to approximate the solution to the Schrödinger equation in quantum physics [64], which is only one possible interaction point between SDEs and theoretical physics. Please note the small contribution made during the present Ph.D. to SDEs within astrophysics, by stochastic simulations of the quasi periodic oscillations observed for neutron stars and black holes [132].

- Applications of SDEs in PK/PD and other biosciences shall be dealt with separately and in more depth in Chapter 6.

- Besides these concrete examples, SDEs makeup an important part of various engineering disciplines, e.g. control theory [118] system identification [109], and time series modelling [77].

Although most financial and theoretical research apply SDEs directly, most engineering applications, including GPS, use a continuous-discrete stochastic state-space model where the continuous SDE is observed at discrete time points with measurement error. Since PK/PD models are presently most often based on ODEs with measurement noise, it is obvious to use the stochastic state space formulation when ODEs are extended to SDEs. For this reason, the stochastic

state-space model play an important part of the present thesis. It can be written as,

$$dx = g(x, d, t, \phi)dt + \sigma_w dw, \quad w_{t_2} - w_{t_1} \in N(0, |t_2 - t_1|I)$$
$$y_i = f(x(t_i), d(t_i), \phi) + e_i, \qquad\qquad e_i \in N(0, \Sigma) \tag{5.2}$$

where x is a vector of the states, for example the amount of drug in the central compartment. g and f are vector functions, while σ_w is a matrix. d is the input, e.g. dose administration, t is time, ϕ is a vector of parameters, y_i is the i'th observation vector, and e_i is the associated measurement error with variance-covariance Σ. Again w is the standard multivariate Wiener process, which has independent increments.

The stochastic state-space model (5.2) has previously been used to define Grey-box models, see e.g. [126], where the grey in Grey-box is a mix between white (theoretical) and black (empirical). The theoretical part is implemented via differential equations, and the empirical part is fulfilled via system noise, which allow for a complete statistical description of data.

5.3   Physical Modelling

The view on physical modelling presented in [55] shall be reviewed and elaborated upon in the present section. This is meant to resolve the uncertainty associated with the different possible integration methods for practical applications, see Figure 5.1.

The nature of the mathematical challenges with SDEs lies in the microscopic or infinitesimal behavior. To understand how we should proceed, it is necessary to understand the microscopic behavior of the stochastic fluctuations in the physical system that we are modelling. Sometimes it is reasonable to say that the physical fluctuations are 1) differentiable, and sometimes it is reasonable to say that the infinitesimal increments (dw) are 2) truly independent making the stochastic noise non-differentiable. Let us elaborate on these two scenarios,

1. As argued in [55], the solutions to SDEs have no derivatives, and as a result of this erratic behavior may only be approximations of the physical process that we are modelling. We shall add that e.g. the true concentration of drug in the body will take a discrete jump whenever a single molecule is metabolized, making it non-differentiable, but only at separable points. Note also that the stochastic fluctuations in a model of concentration are likely originating from "under modelling" that could be improved by
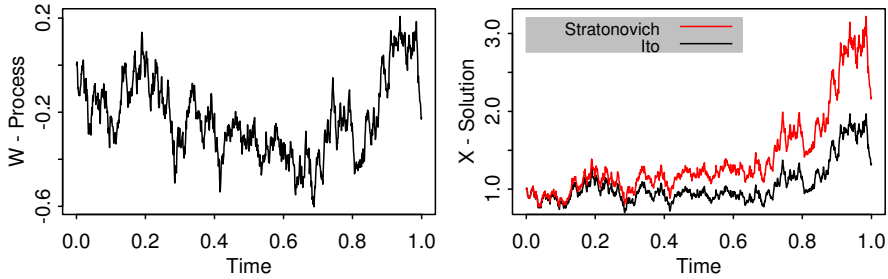
Figure 5.1: For one instance of the wiener process (left), the Itô and the Stratonovich integration scheme may yield different results (right). Both solutions are for the stochastic differential equation, $dX = X + dW$ with $X(0) = 1$.

extending the differential equations, and are thus differentiable in nature. If our SDEs should approximate a system with differentiable fluctuations, then it can be shown that the Stratonovich method of integration is the only appropriate one, see e.g. [55].

2. True independence of the stochastic infinitesimal increments is a common assumption for many models. For this scenario, the derivatives of the fluctuations will not be finite, and it can be shown that the Itô integration method is the only appropriate one, see e.g. [55].

For Itô integration, new rules of calculus (e.g. for change of variable) apply, while for Stratonovich integration the standard rules of calculus remain, making the latter easier to use. However, Itô integration has some useful statistical properties that make Itô the easy and preferred choice for development of many statistical estimation and filtering algorithms. Itô and Stratonovich integration give the same result when the diffusion term in (5.1) is additive, see e.g. [55] for more discussions on these two methods.

For PK/PD models, it is more common to use proportional than additive residual error models, making it likely that also multiplicative diffusion will become more common than additive diffusion. In many cases, one can do a transformation of the stochastic model into a model with additive diffusion [82]. I recommend to do this transformation before implementing system noise, so that only additive diffusion is needed. This line of approach, as undertaken e.g. in [11], is consistent with the Stratonovich method of integration.

5.4   Parameter Estimation of SDEs

The maximum likelihood approach was proposed by Fisher in 1922, and is still seen as the golden standard for parameter estimation in statistical models. The parameter estimates $\hat{\boldsymbol{\theta}}$ are given as,

$$\hat{\boldsymbol{\theta}} = \arg\max_{\boldsymbol{\theta}} L(\boldsymbol{\theta}, \mathcal{Y}) \tag{5.3}$$

where $\mathcal{Y} = [\boldsymbol{y}_1, ..., \boldsymbol{y}_N]$ is the observed data, and $L(\boldsymbol{\theta}, \mathcal{Y})$ is the likelihood function, given by the probability density function, $L(\boldsymbol{\theta}, \mathcal{Y}) = f_{\boldsymbol{\theta}}(\mathcal{Y}))$. For models based on SDEs it is convenient to formulate the likelihood function as the product of conditional densities,

$$L(\boldsymbol{\theta}, \mathcal{Y}) = \left(\prod_{i=2}^{N} p(\boldsymbol{y}_i | \mathcal{Y}_{i-1}) \right) p(\boldsymbol{y}_1) \tag{5.4}$$

where $\mathcal{Y}_i = [\boldsymbol{y}_1, ..., \boldsymbol{y}_i]$ represents all observations up to number i (typically, but not necessarily ordered in time), and $p(\boldsymbol{y}_i | \mathcal{Y}_{i-1})$ are the conditional densities. The fundamental problem for parameter estimation of the general SDE model given in (5.2), is that the conditional densities cannot be derived analytically[2]. The conditional densities also constitute a fundamental ingredient to estimate the true states of the system by optimally filtering away uncertainty due to measurement noise, i.e. solving the filtering problem [55].

5.4.1   The Extended Kalman Filter

The Kalman Filter (KF) [59] is the famous and extensively used analytical solution to the filtering problem for a linear discrete system with additive system noise and Gaussian measurement noise. The equivalent linear submodel of (5.2) can be written,

$$\begin{aligned} d\boldsymbol{x} &= (\boldsymbol{A}\boldsymbol{x} + \boldsymbol{B}\boldsymbol{d})dt + \boldsymbol{\sigma}_w d\boldsymbol{w} \\ \boldsymbol{y}_i &= \boldsymbol{C}\boldsymbol{x}(t_i) + \boldsymbol{D}\boldsymbol{d}(t_i) + \boldsymbol{e}_i \end{aligned} \tag{5.5}$$

where $\boldsymbol{A}$, $\boldsymbol{B}$, $\boldsymbol{C}$, $\boldsymbol{D}$ are matrices, while the remaining entities are identical to those used in (5.2).

---

[2]For models based on ODEs with uncorrelated measurement noise, the conditional densities collapse to unconditional densities that can be approximated arbitrarily well by a numerical integration of the differential equation. The counter part for SDEs would be to numerically solve the Fokker Planck Equations, which is generally considered too time consuming for estimation purposes.

For this model, the conditional densities will be Gaussian and therefore completely characterized by the mean and variance. The conditional densities describe the distribution of the following measurement conditioned on all the previous measurements, so that the mean of the distribution is identical to the prediction of the following measurement, i.e. the one-step prediction $\hat{\boldsymbol{y}}_{i|i-1}$. Likewise, the covariance of the conditional density will be the one-step prediction covariance $\boldsymbol{R}_{i|i-1}$. The KF is a recursive algorithm to calculate the analytical one-step predictions and the one-step prediction variances, see Table 5.1 for easy reference, and the appendix of Paper B for a more thorough description.

Table 5.1: The KF and the EKF are recursive algorithms to calculate the one-step predictions of the state $\hat{\boldsymbol{x}}_{i|i-1}$ and the one-step predictions for the observations $\hat{\boldsymbol{y}}_{i|i-1}$, and the associated variances $\boldsymbol{P}_{i|i-1}$ and $\boldsymbol{R}_{i|i-1}$ respectively. The KF gives the analytical solution for linear models with additive diffusion, while the EKF gives an approximate solution for non-linear models with additive diffusion.

Algorithm: The Kalman Filter	**Algorithm:** The Extended Kalman Filter
Given parameters and initial prediction $\boldsymbol{\phi}$, $\hat{\boldsymbol{x}}_{1|0}$ and $\boldsymbol{P}_{1|0}$	Given parameters and initial prediction $\boldsymbol{\phi}$, $\hat{\boldsymbol{x}}_{1|0}$ and $\boldsymbol{P}_{1|0}$
	$\boldsymbol{A} = (\frac{\partial \boldsymbol{g}}{\partial \boldsymbol{x}})_{\boldsymbol{x}=\hat{\boldsymbol{x}}}$ and $\boldsymbol{C} = (\frac{\partial \boldsymbol{f}}{\partial \boldsymbol{x}})_{\boldsymbol{x}=\hat{\boldsymbol{x}}}$
For $i = 1$ to N **do**	**For** $i = 1$ to N **do**
Output Prediction:	Output Prediction:
$\quad \hat{\boldsymbol{y}}_{i|i-1} = \boldsymbol{C}\hat{\boldsymbol{x}}_{i|i-1} + \boldsymbol{D}\boldsymbol{d}_i$	$\quad \hat{\boldsymbol{y}}_{i|i-1} = \boldsymbol{f}(\hat{\boldsymbol{x}}_{i|i-1}, \boldsymbol{d}_i, \boldsymbol{\phi})$
$\quad \boldsymbol{R}_{i|i-1} = \boldsymbol{C}\boldsymbol{P}_{i|i-1}\boldsymbol{C}^T + \boldsymbol{\Sigma}_{i|i-1}$	$\quad \boldsymbol{R}_{i|i-1} = \boldsymbol{C}\boldsymbol{P}_{i|i-1}\boldsymbol{C}^T + \boldsymbol{\Sigma}_{i|i-1}$
State Update:	State Update:
$\quad \boldsymbol{K}_i = \boldsymbol{P}_{i|i-1}\boldsymbol{C}^T\boldsymbol{R}_{i|i-1}^{-1}$	$\quad \boldsymbol{K}_i = \boldsymbol{P}_{i|i-1}\boldsymbol{C}^T\boldsymbol{R}_{i|i-1}^{-1}$
$\quad \hat{\boldsymbol{x}}_{i|i} = \hat{\boldsymbol{x}}_{i|i-1} + \boldsymbol{K}_i(\boldsymbol{y}_i - \hat{\boldsymbol{y}}_{i|i-1})$	$\quad \hat{\boldsymbol{x}}_{i|i} = \hat{\boldsymbol{x}}_{i|i-1} + \boldsymbol{K}_i(\boldsymbol{y}_i - \hat{\boldsymbol{y}}_{i|i-1})$
$\quad \boldsymbol{P}_{i|i} = \boldsymbol{P}_{i|i-1} - \boldsymbol{K}_i\boldsymbol{R}_{i|i-1}\boldsymbol{K}_i^T$	$\quad \boldsymbol{P}_{i|i} = \boldsymbol{P}_{i|i-1} - \boldsymbol{K}_i\boldsymbol{R}_{i|i-1}\boldsymbol{K}_i^T$
State Prediction:	State Prediction:
$\quad d\hat{\boldsymbol{x}}_{t|i}/dt = \boldsymbol{A}\hat{\boldsymbol{x}}_{t|i} + \boldsymbol{B}\boldsymbol{d}_t$	$\quad d\hat{\boldsymbol{x}}_{t|i}/dt = \boldsymbol{g}(\hat{\boldsymbol{x}}_{t|i}, \boldsymbol{d_t}, t, \boldsymbol{\phi})$
$\quad d\boldsymbol{P}_{t|i}/dt = \boldsymbol{A}_t\boldsymbol{P}_{t|i} + \boldsymbol{P}_{t|i}\boldsymbol{A}^T + \boldsymbol{\sigma}_w\boldsymbol{\sigma}_w^T$	$\quad d\boldsymbol{P}_{t|i}/dt = \boldsymbol{A}_t\boldsymbol{P}_{t|i} + \boldsymbol{P}_{t|i}\boldsymbol{A}^T + \boldsymbol{\sigma}_w\boldsymbol{\sigma}_w^T$
end for	**end for**

For the general system in (5.2), the matrices ($\boldsymbol{A}$, $\boldsymbol{B}$, $\boldsymbol{C}$, $\boldsymbol{D}$) will be replaced by non-linear functions, so the KF can no longer be used directly and the conditional densities will not necessarily be Gaussian. The extended Kalman filter (EKF) [55] refer to methods that apply a local linearisation of the model in order to use the KF equations [47] to give an approximate and Gaussian solution of the filtering problem. In principle, you can treat the general model by this method, but for multiplicative diffusion it is generally accepted that higher order filters should be applied [55], so the EKF presented in Table 5.1 assumes additive diffusion. As previously discussed, many models with multiplicative diffusion can be transformed into models with additive diffusion [82].

The KF and the EKF was in the preceding introduced as tools to derive or approximate the conditional densities, for use in maximum likelihood estimation of parameters. However, note that state estimation is perhaps the most common application of Kalman Filtering, which has been used e.g. to improve GPS position estimates and satellite navigation [55].

Further introductory reading on the KF and the EKF can be found in the recent document by Welch and Bishop [47], or the CTSM math guide [2].

5.4.1.1   Assumptions and Diagnostics for the EKF

Diagnostics enable model evaluation and comparison, and should be used to test the ability of the model to fulfil its objectives, and for assumption testing, e.g. by comparing diagnostics for two models based on different assumptions. However, when we choose to use an approximate solution to the model, it may be relevant to consider direct diagnostics for this approximation.

The basic assumptions of the EKF are that 1) the conditional densities are Gaussian, and 2) that the one step prediction mean and variance are well approximated by the prediction equations of the EKF. These assumptions can be tested by the distribution of the standardized one step prediction errors, which is supposed to be standard normal. One may use either simulated data or real data, and should remember that the distribution test for real data is simultaneously testing the assumptions of the EKF and the model fit to data.

When the basic assumptions of the EKF are broken, it could easily happen that parameters estimated by the EKF method would be different than the true parameters of a simulation study. In fact, the performance of different approximate methods are frequently assessed by the ability of the method to estimate the correct parameters in a simulation test. The parameter estimates from the presented KF and EKF based likelihood method are evaluated in [77], whereas [68] compares parameter estimates from the EKF based likelihood approach and a weighted least squares algorithm, and [84] compares parameter estimates from the EKF based likelihood approach with estimating functions to be discussed below. Paper B aim to test the parameter estimates for the EKF based likelihood approach when it is embedded in a mixed effects algorithm, see Section 5.6.

5.4.2 Other Parameter Estimation Methods

The EKF based likelihood approach is a well established method for parameter estimation in SDEs, but it is certainly not the only method, see review in [83]. Higher order filters constitute immediate extensions of the EKF [55], and below we shall briefly discuss two techniques that have been applied to PK/PD models, i.e. the general method of estimating functions and Markov chain Monte Carlo methods.

5.4.2.1 Estimating Functions

Estimating functions pursue parameter estimates via the solution to an estimating equation $\boldsymbol{f}(\mathcal{Y}, \boldsymbol{\theta}) = 0$, where $\boldsymbol{f}$ is the estimating function, $\mathcal{Y}$ is the data, and $\boldsymbol{\theta}$ is the parameter vector. By this definition, the Maximum Likelihood approach can be obtained via an estimating function, $\frac{d}{d\boldsymbol{\theta}} \log L(\mathcal{Y}, \boldsymbol{\theta}) = \mathcal{S}(\mathcal{Y}, \boldsymbol{\theta}) = 0$, where $\mathcal{S}(\mathcal{Y}, \boldsymbol{\theta})$ is the score function. See e.g. [100] for a review.

Estimating functions are most often seen as an alternative to the likelihood function when this cannot be obtained analytically. The goal is to derive estimating functions that within a given class of functions produce parameter estimates as close as possible to the maximum likelihood estimates. This can be done via optimality criteria, and one typical optimality criterion (F-optimality) ensures maximum correlation between the score function and the estimating function.

Estimating functions have been applied to the stochastic version of the linear compartment models that are typically applied within PK modelling [20], and to a two compartment model with additive measurement noise [19]. The main challenge for applying estimating functions to the models addressed in the present Ph.D. are viewed to be the following:

1. Whereas estimating functions could in principle be used for any model of the form presented in (5.2), there is to my knowledge no readily applicable strategy. They are most often used in the situation without measurement noise 5.1, for which a considerably larger class of models can be readily solved. A more general formulation is needed, where measurement noise can be combined with the typically very nonlinear situation of PK/PD, where not even ordinary differential equation can be solved analytically.

2. Implementation of estimating functions requires a good deal of time consuming mathematical derivations. A software implementation is needed that will enable the researcher to focus on different models rather than on the implementation thereof.

These challenges are far from trivial involving many potentially impossible steps, concluding estimation functions to be interesting, but beyond the scope of the present thesis.

5.4.2.2   Simulation based Techniques

The EKF and the estimating functions are both approximate techniques of the likelihood function for SDEs, while in fact simulation based techniques may converge towards the analytical solution. Markov chain Monte Carlo (MCMC), see e.g. [45], is a well established simulation based technique that can be applied in general, also for problems beyond those associated with SDEs. PKBUGS [75] is a software developed specifically for PK/PD modelling with MCMC, and a few examples have been published where MCMC is used to estimate SDEs in PK/PD, see [25], [10], and [11]. Also other simulations based methods have been used to estimate parameters for SDE based PK/PD models, see e.g. [30].

With MCMC you generate a series of parameter values so that after the series has converged, the distribution of parameter values will give the likelihood function and thereby the maximum likelihood estimate. Only the most recent parameter value is used to derive the next parameter value (Markov chain property), and this is derived by simulation (Monte Carlo property). The Metropolis-Hastings update [49] offer a two step strategy for generating a new parameter value, 1) simulate a new parameter from a proposal distribution that may depend on the old parameter value, 2) accept the proposed parameter with a probability that depend upon the likelihood ratio for the new and the old parameter and upon the symmetry of the proposal density. For the state-space model in (5.2) we must simulate both a new set of parameters and a set of states to find the likelihood function and use the Metropolis-Hastings update, see e.g. [11] for details.

Particle filtering methods provide a recent simulation based technique to solve the filtering problem for state estimation, which may also become useful for parameter estimation in the stochastic state-space model [33]. These methods use a particle representation of probability densities, so that Monte Carlo simulation can be used efficiently to propagate these densities forward in time, see [14] for a tutorial.

MCMC and other simulation based techniques are certainly potential alternatives for parameter estimation in PK/PD models based on SDEs. Compared to the EKF based likelihood approach, MCMC can be shown to converge to the true likelihood estimates, but may require many simulations until convergence and they are generally considered slow. Following the same line of thought,

MCMC methods are alternatives to the approximate first-order techniques of the non-linear mixed-effects problem to be discussed in the next section. Again, the tradeoff will be theoretically desirable parameter estimates versus speed, and the approximate likelihood techniques are the ones most widely used [7].

The two main reason for choosing the EKF and first-order techniques over MCMC and other simulation based techniques were that 1) EKF techniques is a field of special competencies at my department at DTU that we believe is efficient and practical, and 2) that the first-order approximations to the non-linear mixed-effects problem has proven useful for a substantially larger number of PK/PD models.

I do believe that the chosen technique was more productive than MCMC could have been, and further that it allowed comparison of ODE and SDE techniques for more advanced PK/PD models. However, it is certainly possible that MCMC and other simulation based techniques will have a larger rôle to play with the increasing computer power foreseen to come in the future.

5.5   Statistical Model Building

The Likelihood function is important, not only for parameter estimation, but also to perform tests that can be used during statistical model building. The Likelihood ratio is defined as,

$$\lambda = \max_{\boldsymbol{\theta} \in \Omega_0 \subset \Omega} L(\boldsymbol{\theta}, \mathcal{Y}) \bigg/ \max_{\boldsymbol{\theta} \in \Omega} L(\boldsymbol{\theta}, \mathcal{Y}) \tag{5.6}$$

λ is frequently used to test the null hypothesis, i.e. that the parameters belong to the parameter space Ω_0, which is a subset of the larger parameter space Ω. The difference between the simple model with parameter space Ω_0 and the expanded model with parameter space Ω could be a single covariate relationship to be estimated, but we shall refer to a more general model component. For simple Gaussian models, the distribution of λ can be found analytically, but for more complex models it is common to use the Wilk's Likelihood Ratio test. This is based on the asymptotic result that $-2\log(\lambda) \to \chi^2(\dim(\Omega \backslash \Omega_0))$ when the number of observations increases. By approximating the distribution of $-2\log(\lambda)$ with a χ^2 distribution, we can calculate the p-value for making type 1 errors, i.e. for rejecting a null hypothesis while the null hypothesis was actually true. In other words the risk that an error is made by keeping a model component, calculated under the assumption that the simple model is true.

The Likelihood ratio test is frequently used for statistical model building, also

for PK/PD models where it is the most common method for covariate selection. Several strategies have been suggested to select among model components that can be included or excluded independently of each other into a base model. Some examples are,

- **Forward Selection.** Start with the base model. At each step evaluate the p-value for all model components that are not yet included, and include the model component with the lowest p-value. Continue until no more model components meet the pre-specified limit for the p-value.

- **Backward Selection.** Start with a model that include all model components. At each step evaluate the p-value for all model components that are still in the model, and discard the model component with the highest p-value. Continue until all model components meet the pre-specified limit for the p-value.

- **Stepwise Selection.** A modification of the forward selection principle. Start with the base model. At each step evaluate the p-value for all model components in the model, and discard the model component with the highest p-value. If all model components in the model meet the pre-specified limit for the p value, you evaluate the p-value for all model components that are not yet included, and include the model component with the lowest p-value. Continue until all model components in the model meet the pre-specified limit for the p-value, and all model component that are not in the model do not.

The Backwards Selection adheres to the basic assumptions of the likelihood ratio test, which is in principle only valid if the true model is contained in the expanded model, whereas the other methods may be useful in practise. Further more, practical experience frequently demonstrates that the conclusion regarding a single model component depend upon the model used as a null hypothesis, making it important to use a null hypothesis as close as possible to the true model. System noise is one model component that can be tested via the Likelihood Ratio test, and it is frequently found to be quite significant with $-2\log(\lambda)$ values around 1000 for the temperature model and the insulin secretion model in Section 6. Since this model component can be extremely influential, it may be especially important for likelihood based statistical model building.

5.6 SDEs in Non-Linear Mixed-Effects modelling

In contrast to the exploratory field of SDEs in PK/PD, non-linear mixed-effects modelling is a well established and successful modelling technique for PK/PD models [7]. The complication of merging these two methods need to be addressed in order to test the applications of SDEs to PK/PD in a realistic setting. During the applications, we found that the sharing of information among subjects was quite useful to get robust parameter estimates, making the increased statistical complication worth while.

Non-linear mixed-effects models based on SDEs are investigated and advocated in the present thesis. These models can be written as an extension of the stochastic state-space model in (5.2) where the individual parameters ϕ are modelled with fixed effects θ that are identical for all individuals and random effects η that exhibit inter-individual variability with variance-covariance matrix Ω. The equations become,

$$
\begin{aligned}
\phi &= h(\theta, Z, \eta), & \eta &\in N(0, \Omega) \\
dx &= g(x, d, t, \phi)dt + \sigma_w dw, & w_{t_2} - w_{t_1} &\in N(0, |t_2 - t_1|I) \\
y_i &= f(x(t_i), d(t_i), \phi) + e_i, & e_i &\in N(0, \Sigma)
\end{aligned}
\tag{5.7}
$$

To simulate new data we first simulate a new set of individual parameters ϕ depending on the specific covariate information Z of the given individual. Second, we simulate one instance of the stochastic differential equation, and third we simulate random measurement noise to give us the observations. By this formulation, we have three sources of variability, inter-individual variability, system noise, and measurement noise, where all three random components, η, w, and e_i change between individuals. The first-stage model refer to the state-space model given by the two last equations, and the second-stage refer to the model for individual parameters, which often use a log-normal model, i.e. $h(\theta, Z) \exp(\eta)$.

5.6.1 Estimation in Non-Linear Mixed-Effects Models

Non-linear mixed-effects models are often based on ODEs, or the solution thereof, i.e. models where the SDE in (5.7) is replaced by an ordinary differential equation. We shall briefly leave the discussion of SDEs and mention the general challenge associated with the non-linear mixed-effects models.

For non-linear mixed-effects models, the predictions are non-linear functions of the random effects, making the likelihood function impossible to derive analytically for most models. Many techniques and algorithms have been developed

to solve this problem, and some of these have been implemented in ready to use software. These programs can be divided into three categories: 1) parametric approximate likelihood techniques, 2) nonparametric likelihood techniques, and 3) Bayesian methods [7]. Approximate likelihood techniques [92] [74] are the most common, implemented in e.g. NONMEM [16], Splus (called NLME [93]), and SAS (called NLINMIX). Nonparametric methods extend the model in (5.7) by loosening the assumption of Gaussian random effects to a nonparametric distribution, see e.g the USC*PACK program suite [57]. Bayesian MCMC methods are implemented in PKBUGS [75].

Presently, NONMEM is the most widely used PK/PD software for non-linear mixed-effects modelling, and in particular the first-order methods are widely applied. These methods use a linearisation of the model predictions with respect to the random effects, so that the likelihood function can be approximated by Gaussian densities. The first-order (FO) method linearizes around zero, while the first-order conditional estimation (FOCE) method linearizes around the conditional estimates of the random effects, see NONMEM user's guide [16] or Paper B for details. These techniques also form the basis for the estimation of mixed-effects modelling based on SDEs to be discussed in the following.

5.6.2 Estimation in Non-Linear Mixed-Effects Models based on SDEs

Table 5.2: Statistics of the estimation performance when simulating experiments with 100 individuals each sampled 3 times. The model is a one compartment model for an IV bolus experiment parameterized by clearance CL, and volume of distribution V, with coefficient of variation ω_{CL} and ω_V, system noise σ_w, and relative standard error on the measurement noise σ_e.

	V	CL	ω_V	ω_{CL}	σ_w	σ_e
Simulated value	10	0.5	0.2	0.2	0.2	0.1
Mean estimate	10.02	0.508	0.195	0.195	0.198	0.102
Std. Dev. of estimates	0.212	0.015	0.016	0.035	0.037	0.010
Mean estimated std. error	0.220	0.014	0.018	0.035	0.046	0.011

It is to be expected that many of the different parameter estimation methods for SDEs can be combined with many of the methods used for estimation in non-linear mixed-effects models. One approach is to estimate parameters via MCMC, as attempted in [11]. This is an appealing extension because it in principle gives us the exact maximum likelihood estimates, but it can be slow and thereby force us to make approximations that take us away from the true likelihood estimates.

Paper B describes the contribution of the present Ph.D. to parameter estimation in non-linear mixed-effects modelling based on SDEs. This article introduces the basic model framework in (5.7) and explains how the first-order method from NONMEM can be merged with the EKF. A series of simulation studies were used to demonstrate that system noise, measurement noise, and inter-individual variability can be estimated simultaneously, as is typically necessary for these models to be treated meaningfully. One example includes the statistics of the parameter estimates from 50 simulated trials, presented in Table 5.2. The simulation based conclusion were confirmed by a study in [31] that investigates simulations of a linear mixed-effects model based on SDEs that can be solved analytically.

The model framework of Paper B can be implemented in NONMEM version VI beta [127], which facilitate the speed and numerical performance necessary for practical applications of non-linear mixed-effects models based on SDEs. The following chapter is devoted to these applications, including stochastic modelling of core body temperature, haemoglobin, and insulin secretion.

CHAPTER 6

Applications of SDEs to PK/PD

Stochastic differential equations constitute a promising discipline with many possible applications within PK/PD modelling and biosciences in general. A relative large interest exists for new results within applications of SDEs to PK/PD with benefits including aspects of model development as well as model performance. However, the use of SDEs in PK/PD is complicated by software limitations and technical issues to an extent where progress is almost exclusively driven by statistical and technical universities with a prior knowledge about SDEs. Naturally, applications are appearing slowly compared to modelling techniques that are readily applicable for any bioscientist, and although the publication speed is picking up, the role of SDEs in PK/PD has not been resolved.

SDEs have been used within various biosciences such as physiology, biology, pharmacology, and pathophysiology as integral model component. Examples include realistic descriptions of fluctuations in HIV viral load and T-cell populations [128], [122], and [60], cortisol diurnal patterns [25], pulsatile secretion in the male hypothalamic-pituitary-Leydig cell axis [63], modelling of drug dissolution time [71], bacterial growth in a PK/PD model of bactericidal drugs [38], drug resistance during antineoplastic chemotherapy [9], for the rat nephron [32], for PK models [30], and for joint glucose-insulin models of the IVGTT [11]. Many

of these early contributions on SDEs in biosciences motivate the introduction of system noise by more realistic simulation properties and/or description of the system to be modelled. However, for a PK/PD modelling scientist who is not used to SDEs, it may take more than the possibility of a more realistic description to motivate learning the new and difficult skills necessary for implementing SDEs. Furthermore, inter-individual variability and measurement noise are well established ingredients to explain PK/PD data, making it difficult to foresee the virtually unexplored effects of a third level of variability on model development and modelling results. A main effort of the present work has been to formulate and exemplify the effects of system noise in PK/PD models in terms of actual model performance criteria such as simulation properties, specific predictive performance criteria, parameter estimates, and diagnostic plots.

In short, system noise has been proposed to aid, 1) diagnostics, 2) deconvolution, and 3) systematic model development, both in pursuit of models with system noise and in pursuit of those without. Compared to models based on ODEs, models based on SDEs may 4) give more realistic description of the fluctuations, 5) leading to better simulation properties, and 6) predictive performance. System noise was further seen to 7) increase stability of population parameters, and to 8) improve precision for the individual parameter estimates and their uncertainties. In the present chapter, we shall review some of these points, emphasizing the specific contributions made during the present thesis.

6.1   Diagnostics, Deconvolution, and Systematic Model Development

The introduction of system noise in classical engineering disciplines such as system identification [109] allow all model assumptions to be tested, also whether the residuals are independent or correlated. In the same line of thought, the continuous AR(1) autocorrelated processes has been implemented in NONMEM version V and advocated as a potential diagnostic for PK/PD models [61]. The autocorrelation function was found to be a useful tool, both to identify system noise when none is used, but also to locate model deficiencies when system noise has already been introduced, and it was used in all models presented in the present chapter. Note that the Lag Dependent Function [81] extend the autocorrelation to explore more general lag dependencies, which may be useful for nonlinear models.

Mathematically dynamic models can be understood as objects that take some input and produce some output. For linear models, deconvolution is a well established technique to calculate the input if you know the output and the pa-

rameters of the model. This technique has been used within PK/PD modelling for example to derive the rate of drug appearance and the secretion of endogenous hormones (e.g. insulin). In fact deconvolution methods are for example implemented in a standard PK/PD software WINNONLIN [6], and in a stand alone stochastic deconvolution program WINSTODEC [113]. For linear models, WINSTODEC has been seen to produce identical results as an SDE based deconvolution method, while the SDE setup offers a natural extension to treat also non-linear models [66].

The idea to use stochastic differential equations for diagnostics and deconvolution has been merged into a systematic tool for model development, as originally proposed in chemical engineering applications [68] and [65] and later adopted in PK/PD modelling [67] and [127]. The suggested procedure can be summarized as: 1) Start with and ODE, 2) Extent the model to an SDE, 3) Take significant system noise as an indicator for model deficiencies, 4) Let the structure of the estimated system noise inform or pinpoint you to the model deficiency, 5) Examine suggested misspecified parameters by parameter tracking, i.e. treating them as states that can be estimated (deconvoluted) via the EKF and the Kalman smoother. 6) Use non-parametric methods to locate functional relationships for the tracked parameters, 7) Extend the stochastic model with these functional relationships, 8) Continue with this procedure until no further improvements can be made.

As previously mentioned, diagnostics, deconvolution, and systematic model development can be used both in pursuit of models with system noise and in pursuit of those without. However, when system noise is to enter as a component in the final model, it may be worthwhile considering the connection between the cause of the fluctuations and the implementations of system noise, i.e. some of the mechanistic aspects.

6.2 Mechanistic Aspects of System Noise

Realizing that in many minds, the words mechanistic and mechanism based model are almost contradictory to stochastisity and random fluctuations - an explanation is needed. In the present thesis, mechanistic refer to the use of physiologic mechanisms in the model, see Section 2.3, and the mechanistic aspects of system noise involve the physiological cause of these fluctuations. Mechanistic modelling can be understood as a compromise in the level of physiological details included in empirical versus physiological models, but it is not necessarily a mix of these two modelling techniques. Grey-box modelling on the other hand, is understood as a mix between theoretical (white) and empirical (black)

modelling techniques. The present section investigate how random fluctuations can be implemented to comply with the physiological mechanisms, which is one aspect of Grey-box modelling.

The autocorrelation between residuals that is often observed for PK/PD models has motivated the introduction of the continuous first order autoregressive process (AR(1)) in NONMEM as an alternative residual error model [61]. The AR(1) process can be defined as a process P with a correlation decay rate ρ, i.e. $COV(P(t_1), P(t_2)) = V \exp(-\rho|t_1 - t_2|)$. Such a process could also be formulated as the steady state solution to a stochastic differential equation,

$$dP = -\rho P dt + \sigma dw \tag{6.1}$$

AR processes are usually exclusively motivated by data, and the implementation does not correspond to any explanatory mechanism for the observed fluctuations, making the AR process empirical in nature. On the other hand, SDEs can be implemented directly into the dynamical equations and thereby describe the cause of the observed fluctuations, making SDEs more mechanistic.

Let's consider an example with a one compartment PK model where fluctuations in clearance is known to cause random fluctuations in data. Within a given small time interval Δt, the fluctuations in clearance would lead to random variations in the eliminated amount during that period, e.g. $(CL/V)A\Delta t + \sigma \Delta w$, where A is the amount, CL is the clearance, V is the volume, and $\sigma \Delta w$ is the random deviation from the expected eliminated amount. This could be modelled with an SDE as,

$$dA = -(CL/V)A dt + \sigma dw \tag{6.2}$$

Exploring further into the origin of the random fluctuations in clearance, it is safe to assume that over any time interval, the eliminated amount will be positive definite. This is not inherent in the implementation above, but could be implemented e.g. by modelling the dynamic fluctuation in clearance as follows,

$$\begin{aligned} dA &= -(CL/V)A dt \\ dCL &= \sigma CL dw \end{aligned} \tag{6.3}$$

By introducing CL as a new state, the SDEs become non-linear, which is difficult to identify with many traditional statistical methods, but can be solved with the proposed EKF approach. Although we have assumed random fluctuations in clearance, the completely unbounded fluctuations in CL is unrealistic. This knowledge could be implemented by assuming that clearance varies around some value CL_0 with some correlation decay rate k, which may be written as,

$$\begin{aligned} dA &= -(CL/V)A dt \\ dCL &= -k(CL - CL_0)dt + \sigma CL dw \end{aligned} \tag{6.4}$$

As we see, the mechanistic knowledge about the fluctuation can be incorporated into models based on SDEs with varying levels of detail.

It is beyond the scope of the present thesis to discuss all possible mechanistic aspects of system noise and how they should be assessed. Instead, we shall introduce three real data cases that have been under investigation during the present project, and discuss the mechanistic aspects behind the stochastic implementation, how it was selected, and how modelling results was improved compared to the corresponding situation with ODEs.

6.3 Model of IL-21 Effects on Thermoregulation in Monkeys

This section summarizes some of the results in paper E.

Drugs may modify the regulation of body temperature by three fundamental mechanisms [76], either by 1) changing heat production i.e. increasing metabolism, 2) by changing heat loss e.g. by cutaneous vasoconstriction, or 3) indirectly by changing the regulation process i.e. by increasing the set-point temperature that may be associated with lowering the signaling of temperature sensitive neurons in the hypothalamus.

The problem of modelling regulation of core body temperature has been challenged with many different models. Physiology based models typically include a vast amount of mechanisms of heat regulation to produce fruitful simulation models, see [50] and references therein. More statistical models aim to precisely describe and help to identify the circadian rhythm of body temperature, see e.g. [24] and [54]. PK/PD models of temperature have successfully used complex feedback mechanisms in a set-point model to describe the observed oscillations in temperature after a pharmacodynamic challenge [135]. Further research has integrated the set-point model with an oscillator model for the circadian rhythm and handling effects to describe system effects together with drug induced hypothermia in rats [133].

The model presented in Paper E compliments existing models of thermoregulation on three points,

1. Provide a model framework for parameter estimation that include the fundamental mechanisms of drug action, i.e. heat production, heat loss, and set-point regulation. This model was formulated according to the basic
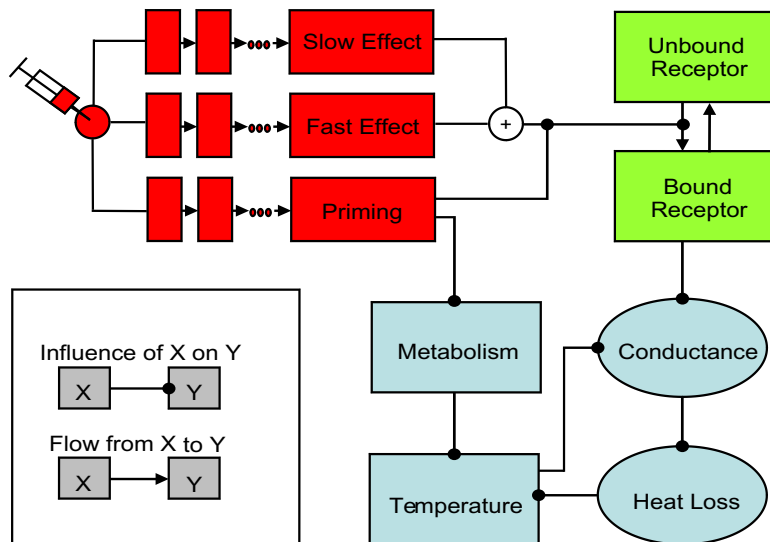
Figure 6.1: Model for IL-21 induced regulation of core body temperature in cynomolgus monkeys. The model includes a part that describes the general mechanisms for temperature regulation (blue), a part that describes how an intermediate receptor system is hypothesized to regulate the set-point temperature (green), and a part that empirically explains the relationship between administration of IL-21 and the effects (red). Each square box represents a compartment, i.e. a differential equation or the solution thereof, whereas each oval box represent an algebraic expression. A physical flow from one compartment to the next is depicted with an arrow, while a bullet is used to signify an influence of one model entity on another.

physiology of heat regulation [134], so that the circadian rhythm could be realistically described, and other external challenges may be incorporated.

2. It represents an attempt to bridge empirical modelling techniques with theory driven modelling, and thereby provide a Grey-box approach to modelling core body temperature. The theory of heat regulation is incorporated via differential equations, and the empirical model requirements were satisfied after implementation of system noise.

3. The model provides a quantitative description of the effects of IL-21 on thermoregulation in cynomolgus monkeys.

6.3.1   The Model

A detailed description of the model for IL-21 effects on thermoregulation is given in Paper E. For easy reference Figure 6.1 gives the structure of the model, and the equations below constitutes the fundamental stochastic differential equations.

$$
\begin{aligned}
dM &= -k_m(M - f_1(Drug, t))dt + \sigma_M dw_M \\
dT &= c^{-1}(M - k(T - T_a))dt \\
dBR &= (PD(t)(1 - BR) - k_R BR)dt + \sigma_{BR} dw_{BR} \\
k &= k_b + k_{inc}(T - T_z) \quad and \quad T_z = (1 + p_{tot}BR)T_b
\end{aligned}
\tag{6.5}
$$

M is the metabolic rate, which decays with a rate constant k_m towards the metabolism dictated by the circadian rhythm and the drug effect $f_1(Drug, t)$. T is core body temperature, c is the specific heat constant, T_a is the ambient temperature, k is the conductance of heat, which has the baseline value k_b, corresponding to a specific baseline temperature T_b, and k_{inc} gives how much k is upregulated if temperature increases above the set-point temperature. The steady state temperature can be understood to depend upon the metabolism, so that a fixed set-point value T_z can be defined corresponding to the baseline metabolic rate. The effects of IL-21 on the thermoregulatory set-point are modelled via a tolerance model that mimic a system of free and bound receptors BR, where k_R is the off rate for the bound receptor complex, PD is the drug effect, and p_{tot} is a parameter for the combined effect on the set-point temperature. IIV was implemented on the timing of the drug effect in $f_1(Drug, t)$ and $PD(t)$, see Paper E for details.

6.3.2   Aspects of the Stochastic Implementation

The model for IL-21 effects on thermoregulation includes three differential equations, one for each of metabolism, core body temperature, and fraction of bound receptors. Many possible mechanistic implementations of system noise could be imagined, but to avoid numerical difficulties it was decided to investigate system noise, only for these three fundamental equations. The following arguments can be given for the chosen implementation of system noise.

- Fluctuations in metabolism were motivated by the natural variations in movement and exercise patterns. Further investigations used the estimated parameters to simulate the metabolic rate in Figure 6.2, which exhibited reasonable stochastic and circadian fluctuations compared to another monkey species. Subsequently it was concluded that this proposed
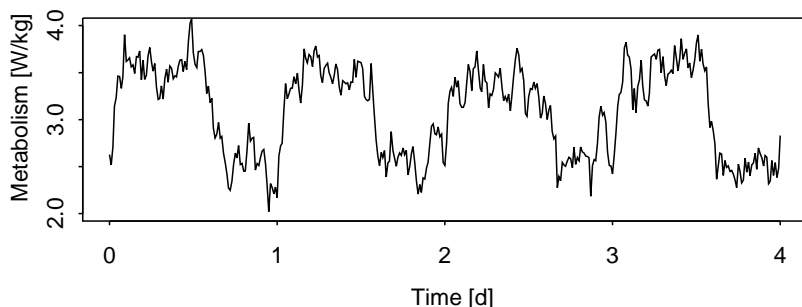
Figure 6.2: The simulated metabolism for cynomolgus monkeys demonstrate the circadian rhythm and stochastic fluctuations that were used to explain the observed fluctuations and circadian rhythm in core body temperature.

mechanism for temperature fluctuations could not be falsified. The simulations of metabolism were reasonable and far from zero, and it was not judged necessary to investigate a more complicated proportional model, which could ensure the metabolism to be strictly positive. Equivalent system noise for the temperature state could to a large extend compensate for variations in metabolism, and including both effects gave only modest improvement to the objective function value. System noise on metabolism was selected over direct effects on temperature because of an improved objective function value[1], more realistic simulations of metabolism, and since it enabled estimation of the rate constant k_m for stabilization of metabolism.

- System noise was also introduced for the receptor compartment. These fluctuations could reasonably account slow fluctuations, and were significant in a likelihood ratio test. The chosen stochastic implementation ensures that the total number of bound and unbound receptors remain constant. Further mechanistic considerations involved the need for strictly positive values in the receptor compartment, which could be ensured by system noise proportional to the fraction of bound (and unbound) receptors. A term with system noise proportional to the pharmacodynamic effect was tested and rejected.

It was not attempted to extend the model with stochastic fluctuations in other parameters or model components. However, the differential equations for metabolism and bound receptors may be seen as extensions that could be removed if an ODE model was pursued. In this case metabolism would simply be the $f_1(Drug, t)$

---

[1]These models were not nested, so the Likelihood ratio test could not be used.

function, and the bound receptor model would reduce to a simple E_{max} term in the equation for T_z.

6.3.3   Results

The inclusion of system noise had a number of positive effects on the model performance, which can be illustrated by a comparison between the mixed-effects model based on SDEs and the corresponding model based on ODEs. These include,

- The ODE model with uncorrelated residuals could be falsified by a simple statistical test of the autocorrelation function (ACF), whereas the SDE model was able to describe the correlation structure in the residuals. The ACF can be seen as a general model diagnostic, where an erroneous ACF will falsify the model, but the ACF may also be a more direct quality mark for model simulations. In particular, simulated data could be used to assess precision of parameter estimates for different sampling schedules. It is to be expected that the results would change if simulations are made with a model that produce a completely different residual error structure.

- The introduction of SDEs allows us to quantify and propose a mechanism for the fluctuations in temperature, i.e. random fluctuations in metabolic rate and in the fraction of bound receptors that affect the thermoregulatory set-point.

- The high measurement error estimated in the ODE model caused simulations to jump up and down erratically and unrealistically compared to simulations based on SDEs that realistically resembled the variations seen in data. This could become important, e.g. if one wish to predict the probability that treatment of a given individual causes temperature elevation above a certain level.

- IIV was reduced by the inclusion of system noise, and the simple predictive check demonstrated that the SDE model led to narrower confidence intervals, as is often seen with more accurate models for the variations.

- SDEs allowed us to simplify the model for inter-occasion variability on day and night time steady state temperature, which significantly improved the model speed.

6.4   A stochastic model for insulin secretion following an MTT

During the course of the present project a population covariate analysis for insulin secretion following a meal tolerance test (MTT) was performed and formulated as part of a larger analysis of 85 healthy and 417 patients with type 2 diabetes [56]. The main purpose of the modelling effort was to quantify insulin secretion as a function of glucose in terms of individual parameters, and to find the most important explanatory factors for these parameters. As a minor project, it was tested how the inclusion of stochastic differential equations would influence the individual parameter estimates.

6.4.1   The Model

The stochastic model for insulin secretion following an MTT can be written as,

$$
\begin{aligned}
dE &= -\frac{1}{\tau}(\beta G_{ab} - E)dt \\
dP &= -\rho P dt + \sigma dw \\
C_I &= (B_I + \alpha G_{ab} + E)\exp(P)\exp(\epsilon)
\end{aligned}
\tag{6.6}
$$

where E is proportional to the delayed glucose above baseline G_{ab}, with a time constant τ. C_I is the insulin concentration, and B_I is the baseline insulin level. Two proportional noise terms were used, ϵ is the usual uncorrelated measurement error, and P is the continuous AR(1) process that gives rise to stochastic fluctuations in the insulin concentration. IIV was implemented for α, β, and B_I, using a proportional model with a full variance-covariance matrix.

6.4.2   Aspects of the Stochastic Implementation

Prior to the implementation of system noise, the model contained only one differential equation, i.e. the equation for E. It was attempted to extend this equation to an SDE in various ways, 1) by additive system noise, 2) by additive system noise to the log-transformation of E, corresponding to proportional system noise, and 3) by using system noise proportional to the glucose concentration, but numerical stability remained a problem for all these models. The proportional AR(1) and measurement noise model given above provided a very stable alternative that is easy to apply for a wide variety of models. However, it
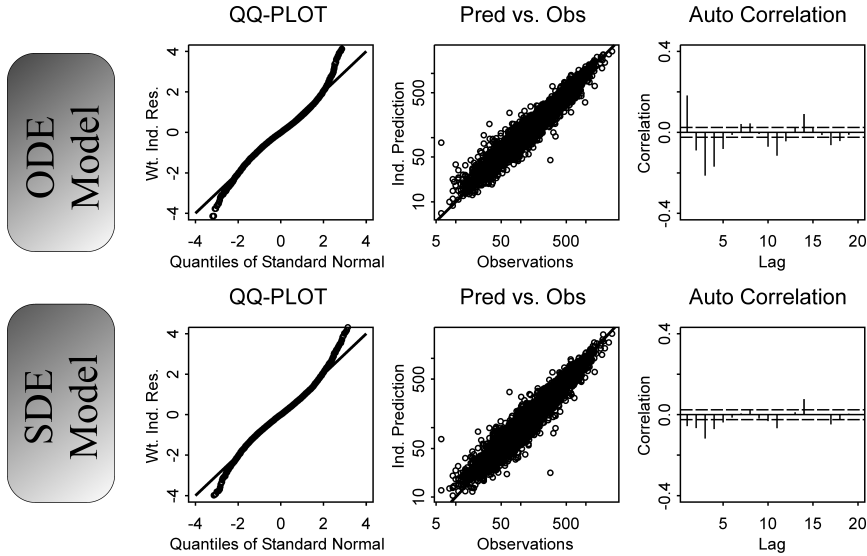
Figure 6.3: Diagnostic plots of the insulin secretion model. The mixed-effects model based on ODEs is placed in the top row, and the corresponding model based on SDEs is placed in the bottom row.

should be made clear that it is an empirical model, where the time scale of $1/\rho$ and τ are different. Interestingly, the time scale estimated for the stochastic fluctuations $\rho \approx 100min$ is close to the time scale estimated for the redistribution $k_{rd} \approx 115min$ in Paper C.

6.4.3   Results

The main results of the stochastic implementation are associated with the individual parameter estimates for α, β, and B_I. The precision of these parameter estimates can implicitly be investigated via the correlation between the parameter estimates and known covariates, where a lower correlation indicates more uncertainty in the estimates. The correlations for the SDE model and the corresponding ODE model are given in Table 6.1, leading to the following conclusions,

- By comparing ODE and SDE models with no covariates, we see that SDEs yield a slight improvement of the individual parameter estimates. The pairwise differences are not significant, but since the effect is seen consistently, also for other covariates, the difference is believable.

Table 6.1: Correlation between log-transformed parameter estimates and most important covariates, baseline glucose BG and the waist circumference WST.

Model \ Covariate	$\alpha \sim BG$	$\beta \sim BG$	$B_I \sim WST$
ODE model no covariates	-0.71	-0.77	0.52
SDE model no covariates	-0.76	-0.78	0.52
ODE model with covariates	-0.73	-0.81	0.56
SDE model with covariates	-0.79	-0.89	0.63

- From Table 6.1 we see that the introduction of covariates increases the correlation, both for the ODE model and the SDE model. This phenomena is caused by regression to the mean, where the *a posteriori* estimated parameter is a balance between the individual estimate obtained without prior information and the population mean given by the covariate relationship. We note that this effect is considerably larger for the SDE model than for the ODE model, which is probably due to an overestimated accuracy of the individual parameter estimates for the ODE model.

- The autocorrelation of the residuals was clearly reduced by the introduction of system noise, i.e. the ACF was improved, see Figure 6.3. But the improvement was insufficient, in the sense that the SDE model could also be falsified by the ACF. By comparing the present insulin secretion model with the model presented in Paper C, the present model is expected to be deficient, and hence it is satisfactory that this deficiency can be diagnosed by the ACF.

6.5 Model of IL-21 Effects on Haemoglobin

PK/PD models of the effects of IL-21 on haemoglobin were proposed already during preclinical studies (Paper D), and are presently used as part of the evaluation of IL-21 in the early stages of clinical development. These models have been used to predict the time course of haemoglobin for IL-21 administered in various treatment regimens, see also Section 3.3.1. Particular interest was devoted to the lowest haemoglobin concentration observed for each individual, where a haemoglobin level below 6.5g/dL is defined as a severe (grade 4) anemia, and below 8g/dL is defined as moderate (grade 3) anemia. In fact, the ability to simulate the lowest haemoglobin observation was taken as a predictive performance criteria to evaluate and compare models based on ODEs and SDEs.

6.5.1 The Model

The stochastic model for IL-21 effects on haemoglobin given in Figure 6.4 can be written as the following equations,

$$Input = k(E_{MAX}Dose/(ED_{50} + Dose) + E_0)$$
$$\frac{dA_1}{dt} = Input - k_t A_1$$
$$\frac{dA_2}{dt} = k_t A_1 - k_t A_2$$
$$\frac{dA_3}{dt} = k_t A_2 - k_t A_3 \tag{6.7}$$
$$dHMG_P = (k_b HMG_{BM} - A_3)dt + \sigma dw$$
$$dHMG_{BM} = (B_e(HMG_P - HMG_{Base}) - k_b HMG_{BM})dt - \sigma dw$$

where A_1, A_2, and A_3 are transit compartments, symbolizing the cascade of activity between dosing with IL-21 and effect. The rate constant k_t gives the total transit time as $3/k_t$. E_0 is the minimum effect, which is implemented as a placebo effect that enter at every dose, also when no drug is administered, whereas E_{MAX} and ED_{50} parameterize the dose related effect. When IL-21 acts, the plasma concentration of haemoglobin HMG_P will go below baseline HMG_{Base}. This drop increases the production rate of red blood cells and haemoglobin in the bone marrow HMG_{BM} with a rate that is proportional to the drop with a proportionality factor B_e. k_b is the transfer rate of haemoglobin from the bone marrow to the plasma compartment. σdw is the diffusion term, where the subtraction in the HMG_{BM} equation correspond to the addition in the HMG_P equation. This ensures that mass balance is conserved, i.e. if extra haemoglobin randomly appear in plasma, it is removed from the bone marrow compartment. IIV was implemented for $Input$ and HMG_{Base}, both via the proportional model.

6.5.2 Aspects of the Stochastic Implementation

There are two noteworthy aspects in the stochastic implementation of the haemoglobin model, 1) the link between dosing and effect is modelled exclusively with ODEs, and 2) system noise is implemented so that mass balance is conserved.

1. Simultaneous use of ODEs and SDEs may significantly reduce the complexity of the model, making it faster and numerically more robust. If the transit compartments were included as SDEs, the total number of states would be 5, and the number of independent elements in the full state
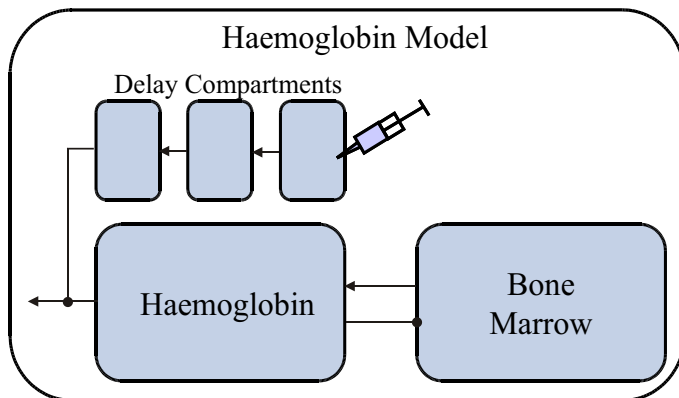
Figure 6.4: Model for IL-21 induced effects on haemoglobin.

covariance would increase from 3 to 15, so that the total number of differential equations in a NONMEM implementation of the Kalman Filter [127] would be 20, i.e. the maximum number for a default NONMEM installation. In theory, there should be no problems for large systems, but the practical situation may be quite different. A combination of ODEs and SDEs was not the only practical choice made for the present model. The original Red blood Cell (RBC) model for monkeys (Paper D) included a system of transit compartments between the bone marrow and plasma to mimic the maturation stages of RBCs. This system was removed in the stochastic model, in order to reduce the number of stochastic states and thereby also the size of the state covariance.

2. It was investigated whether to use additive system noise 1) as chosen, i.e. by restricting mass balance to be conserved, 2) only on the plasma compartment, 3) only on the bone marrow compartment, or combinations of the three possibilities. These options were associated with similar objective function values, and they could to a large extend replace each other. The first option was chosen because it was judged to be slightly more realistic than the other two, since it was associated with a lower variance of the individual residuals, and the predictive performance was slightly better.

6.5.3   Results

The inclusion of system noise for the present model had several positive effects. These include,
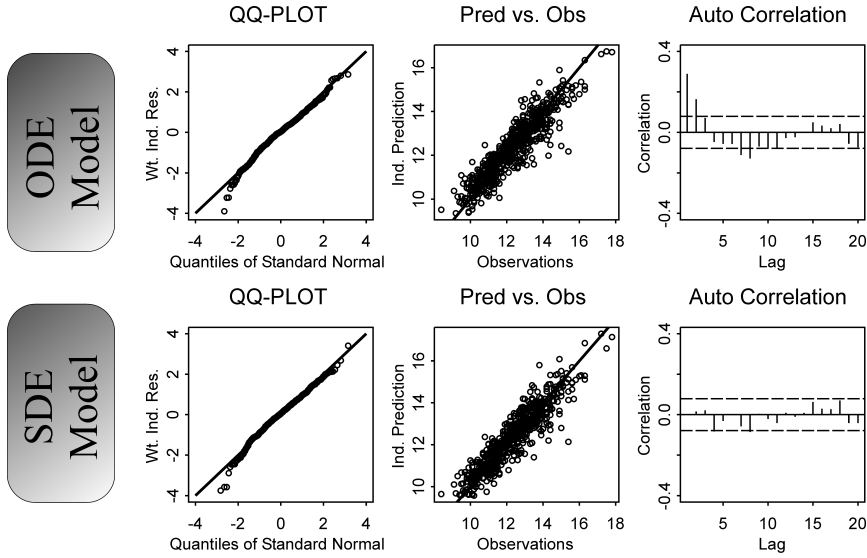
Figure 6.5: Diagnostic plots of the haemoglobin model. The mixed-effects model based on ODEs is placed in the top row, and the corresponding model based on SDEs is placed in the bottom row.

- The SDE model was able to describe the correlation structure in the residuals, whereas the ODE model with uncorrelated residuals could be falsified by a simple statistical test of the autocorrelation function.

- The introduction of SDEs allows us to propose and quantify a mechanism for the fluctuations in haemoglobin, i.e. a random release rate of haemoglobin from the bone marrow.

- The SDE model was found to yield more robust population parameters when small changes were made in the model. Five minor model changes were made, for which the SDE model consistently produced high ED_{50} estimates, and the ODE model estimates occasionally yielded very low values.

- The SDE model was found to yield a better predictive performance for the minimum level of haemoglobin. The predictive performance measure (PPM) for a given simulated trial was defined as,

$$PPM = \frac{1}{N} \sum_{individuals}^{N} \left(\min(HMG_{sim}) - \min(HMG_{obs}) \right) \qquad (6.8)$$

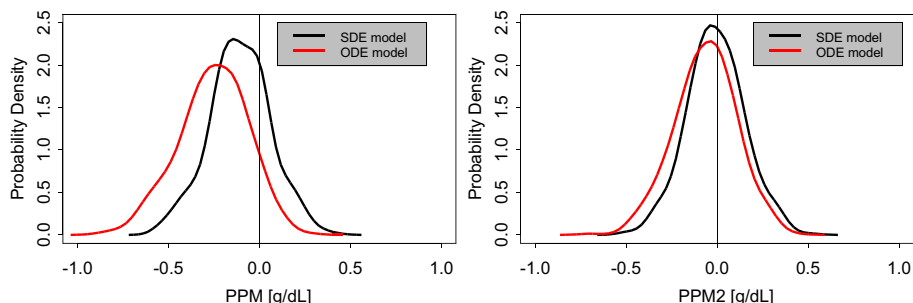where N is the number of individuals, HMG_{sim} is the simulated haemoglobin

Figure 6.6: Distribution of the Predictive Performance Measure (PPM) for the mixed-effects model based on SDEs and the corresponding model based on ODEs. PPM (left figure) is based on the minimum observed haemoglobin levels, and PPM2 (right figure) is based on the minimum of the moving average of the observed haemoglobin levels. For both measures, the preferred model would yield a narrow distribution around zero.

concentration for a given individual, with HMG_{obs} being the observed concentration. For a perfect model, the predictive performance measure (PPM) would always be close to zero, but for any real model some error is to be expected. The distribution of the PPM is compared for the ODE and the SDE model in Figure 6.6, where the ODE model is seen to be more biased than the SDE model. This bias for the ODE model may be caused by simulations with more erratic jumps, which increases the probability that one of the observations for a given individual will be extremely low. This hypothesis could be confirmed, since most bias was removed by using the moving average (MA) of two consecutive values to smooth out some of the erratic jumps, i.e. by using the following PPM,

$$PPM_2 = \frac{1}{N} \sum_{individuals}^{N} \left(\min(MA(HMG_{sim})) - \min(MA(HMG_{obs})) \right)$$

$$(6.9)$$

CHAPTER 7

Conclusion

During the past few decades Pharmacokinetic/pharmacodynamic (PK/PD) modelling has emerged as a promising discipline within drug development that is hoped to increase speed and reduce cost of bringing new drugs to market, ultimately leading to faster and cheaper medicines for the consumer. The primary goal of the present project was to explore the use of stochastic differential equations (SDEs) as a new statistical technique that could benefit this field. PK/PD models and modelling techniques are used, not only during drug development, but also for biosciences in general. Insulin secretion was selected as a case story that reflects biosciences in general, while development of IL-21 as a novel anticancer agent provided several different fascinating biological markers that with benefit could be analyzed using PK/PD models. A main effort has been to formulate and exemplify the effects of SDEs in PK/PD models in terms of actual model performance criteria such as simulation properties, specific predictive performance criteria, parameter estimates, and diagnostic plots.

Several achievements have been summarized in the present report and some are described in further detail in the series of papers presented in the appendices. These contributions include,

1. Paper A is primarily a theoretical paper that aim to illustrate how the two previously published minimal models for the IVGTT are associated with different theoretical features in the distributed threshold model.

2. Paper B presents a new estimation method for non-linear mixed-effects models based on SDEs, by merging the extended Kalman Filter used for SDEs with first-order methods used for non-linear mixed effects modelling. A series of simulation studies demonstrated that system noise, measurement noise, and inter-individual variability can be estimated simultaneously, as is typically necessary for these models to be treated meaningfully.

3. Paper C presents a new insulin secretion model and demonstrates its use for the IVGTT and the OGTT. Note that this model is likely to be applicable also for other experiments. The analysis provided a consistency check for the physiological understanding of the biophysical distributed threshold hypothesis, while simultaneously demonstrating the consistency of empirical parameters obtained from the two different diagnostic tests.

4. Section 3.3 summarizes several PK/PD models of the pleiotropic effects of IL-21. Among other things, these models have been used to 1) give a univocal description of the observed effects, including dose response relationships, 2) to bridge data from different species, treatment regimens, and patient populations, 3) to give predictions for new experiments, and 4) to increase understanding of the mechanisms of action for IL-21. Two of these models are described more thoroughly in Paper D and Paper E.

5. Chapter 6 summarizes several SDE based PK/PD models that have been developed during the present project, see also the more detailed description in Paper E. Several benefits of SDEs have been identified for each model. In particular, the three different overall purposes of the three different models was improved by SDEs, i.e. 1) individual parameters estimates were improved, 2) understanding of the system was increased, and 3) predictions and simulations were improved.

In summary, several different PK/PD modelling techniques have been used to develop many different models with a variety of purposes. We conclude that SDEs are useful in many aspects of PK/PD modelling, and may help modelers produce even better results.

Bibliography

[1] Air Force's Most Advanced Navigation System. *GPS World, http : //www.gpsworld.com/gpsworld/article/articleDetail.jsp?id = 53495,* 2003.

[2] Mathematics Guide, Continuous Time Stochastic Modelling. *http : //www2.imm.dtu.dk/ ∼ ctsm/,* 2003.

[3] Report of the expert committee on the diagnosis and classification of diabetes mellitus. *Diabetes Care,* 26 Suppl 1:S5–20, 2003.

[4] Cancer information by Type. *http : //www.cancer.gov/cancer_information/cancer_type/,* 2005.

[5] PubMed. *www.pubmed.gov,* 2006.

[6] WinNonlin. *http : //www.pharsight.com/products/prod_winnonlin_home.php,* 2006.

[7] L. Aarons. Software for population pharmacokinetics and pharmacodynamics. *Clin.Pharmacokinet.,* 36(4):255–264, 1999.

[8] L. Aarons, M. O. Karlsson, F. Mentre, F. Rombout, J. L. Steimer, and Peer A. van. Role of modelling and simulation in Phase I drug development. *Eur.J.Pharm.Sci.,* 13(2):115–122, 2001.

[9] M. Abundo, C. Rossi, M. Benassi, F. P. Gentile, and F. Mauro. A stochastic model of the acquisition of drug resistance during antineoplastic chemotherapy. *Health Phys.,* 57 Suppl 1:349–354, 1989.

[10] K. E. Andersen and M. Højbjerre. A Bayesian Approach to Bergman's Minimal Model. *Ninth International Workshop on Artificial Intelligence and Statistics*, 2003.

[11] K. E. Andersen and M. Højbjerre. A population-based Bayesian approach to the minimal model of glucose and insulin homeostasis. *Stat.Med.*, 24(15):2381–2400, 2005.

[12] M. E. Andersen. Development of physiologically based pharmacokinetic and physiologically based pharmacodynamic models for applications in toxicology and risk assessment. *Toxicol.Lett.*, 79(1-3):35–44, 1995.

[13] G. M. Argoud, D. S. Schade, and R. P. Eaton. Insulin suppresses its own secretion in vivo. *Diabetes*, 36(8):959–962, 1987.

[14] S. A. Arulampalam, S. Maskell, N. Gordon, and T. Clapp. A Tutorial on Particle Filters for Online Nonlinear/Non-Gaussian Bayesian Tracking. *IEEE Transaction on Signal Processing*, 50(2), 2002.

[15] E. O. Balasse and H. A. Ooms. Role of plasma free fatty acids in the control of insulin secretion in man. *Diabetologia*, 9(2):145–151, 1973.

[16] S. L. Beal and L. B. Sheiner. NONMEM User's Guides. *NONMEM Project Group, University of California, San Francisco*, 1994.

[17] B. W. Bequette. A critical assessment of algorithms and challenges in the development of a closed-loop artificial pancreas. *Diabetes Technol.Ther.*, 7(1):28–47, 2005.

[18] R. N. Bergman, Y. Z. Ider, C. R. Bowden, and C. Cobelli. Quantitative estimation of insulin sensitivity. *Am.J.Physiol*, 236(6):E667–E677, 1979.

[19] B. M. Bibby. A two-compartment model with additive white noise. *Department of theoretical statistics Aarhus University*, Research Report 290, 1994.

[20] B. M. Bibby. On estimation in compartmental diffusion models. *Department of theoretical statistics Aarhus University*, Research Report 305, 1995.

[21] J. L. Bolaffi, L. Bruno, A. Heldt, and G. M. Grodsky. Characteristics of desensitization of insulin secretion in fully in vitro systems. *Endocrinology*, 122(5):1801–1809, 1988.

[22] J. L. Bolaffi, A. Heldt, L. D. Lewis, and G. M. Grodsky. The third phase of in vitro insulin secretion. Evidence for glucose insensitivity. *Diabetes*, 35(3):370–373, 1986.

[23] E. Breda, M. K. Cavaghan, G. Toffolo, K. S. Polonsky, and C. Cobelli. Oral glucose tolerance test minimal model indexes of beta-cell function and insulin sensitivity. *Diabetes*, 50(1):150–158, 2001.

[24] E. N. Brown, Y. Choe, H. Luithardt, and C. A. Czeisler. A statistical model of the human core-temperature circadian rhythm. *Am.J.Physiol Endocrinol.Metab*, 279(3):E669–E683, 2000.

[25] E. N. Brown, P. M. Meehan, and A. P. Dempster. A stochastic differential equation model of diurnal cortisol patterns. *Am.J.Physiol Endocrinol.Metab*, 280(3):E450–E461, 2001.

[26] D. G. Bruce, D. J. Chisholm, L. H. Storlien, and E. W. Kraegen. Physiological importance of deficiency in early prandial insulin secretion in non-insulin-dependent diabetes. *Diabetes*, 37(6):736–744, 1988.

[27] D. Cella. Factors influencing quality of life in cancer patients: anemia and fatigue. *Semin.Oncol.*, 25(3 Suppl 7):43–46, 1998.

[28] W. A. Colburn and J. W. Lee. Biomarkers, validation and pharmacokinetic-pharmacodynamic modelling. *Clin.Pharmacokinet.*, 42(12):997–1022, 2003.

[29] Man C. Dalla, M. Campioni, K. S. Polonsky, R. Basu, R. A. Rizza, G. Toffolo, and C. Cobelli. Two-Hour Seven-Sample Oral Glucose Tolerance Test and Meal Protocol: Minimal Model Assessment of beta-Cell Responsivity and Insulin Sensitivity in Nondiabetic Individuals. *Diabetes*, 54(11):3265–3273, 2005.

[30] S. Ditlevsen and Gaetano A. De. Stochastic vs. deterministic uptake of dodecanedioic acid by isolated rat livers. *Bull.Math.Biol.*, 67(3):547–561, 2005.

[31] S. Ditlevsen and Gaetano A. De. Mixed effects in stochastic differential equation models. *Submitted*, 2006.

[32] S. Ditlevsen, K. P. Yip, and N. H. Holstein-Rathlou. Parameter estimation in a stochastic model of the tubuloglomerular feedback mechanism in a rat nephron. *Math.Biosci.*, 194(1):49–69, 2005.

[33] A. Doucet and V. Tadic. Parameter Estimation in General State-Space Models using Particle Methods. *Ann.Inst.Statist.Math.*, 55(2):409–422, 2003.

[34] R. R. Duncan, J. Greaves, U. K. Wiegand, I. Matskevich, G. Bodammer, D. K. Apps, M. J. Shipston, and R. H. Chow. Functional and spatial segregation of secretory vesicle pools according to vesicle age. *Nature*, 422(6928):176–180, 2003.

[35] E. I. Ette and P. J. Williams. Population pharmacokinetics I: background, concepts, and models. *Ann.Pharmacother.*, 38(10):1702–1706, 2004.

[36] E. I. Ette and P. J. Williams. Population pharmacokinetics II: estimation methods. *Ann.Pharmacother.*, 38(11):1907–1915, 2004.

[37] E. I. Ette, P. J. Williams, and J. R. Lane. Population pharmacokinetics III: design, analysis, and application of population pharmacokinetic Studies. *Ann.Pharmacother.*, 38(12):2136–2144, 2004.

[38] L. Ferrante, S. Bompadre, L. Leone, and M. P. Montanari. A stochastic formulation of the gompertzian growth model for in vitro bactericidal kinetics: parameter estimation and extinction probability. *Biom.J.*, 47(3):309–318, 2005.

[39] M. E. Fisher. A semiclosed-loop algorithm for the control of blood glucose levels in diabetics. *IEEE Trans.Biomed.Eng*, 38(1):57–61, 1991.

[40] Tufts Center for the Study of Drug Development. Backgrounder, How New Drugs Move Through the Development and Approval Process. *Boston*, 2001.

[41] L. E. Fridlyand, N. Tamarina, and L. H. Philipson. Modeling of Ca2+ flux in pancreatic beta-cells: role of the plasma membrane and intracellular stores. *Am.J.Physiol Endocrinol.Metab*, 285(1):E138–E154, 2003.

[42] A. Fritsche, N. Stefan, E. Hardt, H. Haring, and M. Stumvoll. Characterisation of beta-cell dysfunction of impaired glucose tolerance: evidence for impairment of incretin-induced insulin secretion. *Diabetologia*, 43(7):852–858, 2000.

[43] J. Gabrielsson and D. Weiner. *Pharmacokinetic and Pharmacodynamic data Analysis.* 1997.

[44] R. Gieschke and J. L. Steimer. Pharmacometrics: modelling and simulation tools to improve decision making in clinical drug development. *Eur.J.Drug Metab Pharmacokinet.*, 25(1):49–58, 2000.

[45] W. R Gilks, S. Richardson, and D. J. Spiegelhalter. *Markov Chain Monte Carlo in Practice.* Chapman and Hall, London, 1996.

[46] G. M. Grodsky. A threshold distribution hypothesis for packet storage of insulin and its mathematical modeling. *J.Clin.Invest*, 51(8):2047–2059, 1972.

[47] G.Welch and G.Bishop. An Introduction to the Kalman Filter. *Departmentof Computer Sciences, University of North Carolina, Chapel Hill*, 2004.

[48] T. Habib, A. Nelson, and K. Kaushansky. IL-21: a novel IL-2-family lymphokine that modulates B, T, and natural killer cell responses. *J.Allergy Clin.Immunol.*, 112(6):1033–1045, 2003.

[49] W. K. Hastings. Monte Carlo sampling-based methods using Markov chains and their applications. *Biometrika*, 57:97–109, 1970.

[50] G. Havenith. Individualized model of human thermoregulation for the simulation of heat stress response. *J.Appl.Physiol*, 90(5):1943–1954, 2001.

[51] J. C. Henquin, N. Ishiyama, M. Nenquin, M. A. Ravier, and J. C. Jonas. Signals and pools underlying biphasic insulin secretion. *Diabetes*, 51 Suppl 1:S60–S67, 2002.

[52] N. H. Holford, H. C. Kimko, J. P. Monteleone, and C. C. Peck. Simulation of clinical trials. *Annu.Rev.Pharmacol.Toxicol.*, 40:209–234, 2000.

[53] J. C. Hull. *Options, Futures and Other Derivatives*. Prentice Hall College Div, 2005.

[54] R. A. Irizarry, C. Tankersley, R. Frank, and S. Flanders. Assessing homeostasis through circadian patterns. *Biometrics*, 57(4):1228–1237, 2001.

[55] A. H. Jazwinsky. *Stochastic Process and Filtering Theory*. Academic Press, New York, USA, 1970.

[56] K. Jelic, R. V. Overgaard, M. C. Jørgensen, P. Damsbo, S. H. Ingwersen, S. D. Luzio, G. Dunseath, and D. R. Owens. A Cross-Sectional Analysis Of Beta-Cell Responsiveness after a Mixed Meal in Non-Diabetic and Type 2 Diabetics at Diagnosis. *Planned Submission*, 2006.

[57] R. W. Jelliffe. The USC*PACK PC programs for population pharmacokinetic modeling, modeling of large kinetic/dynamic systems, and adaptive control of drug dosage regimens. *Proc.Annu.Symp.Comput.Appl.Med.Care*, pages 922–924, 1991.

[58] A. Jemal, T. Murray, E. Ward, A. Samuels, R. C. Tiwari, A. Ghafoor, E. J. Feuer, and M. J. Thun. Cancer statistics, 2005. *CA Cancer J.Clin.*, 55(1):10–30, 2005.

[59] R. E. Kalman. A new approach to linear filtering and prediction problems. *J.Basic Eng.*, 82:35–45, 1960.

[60] A. Kamina, R. W. Makuch, and H. Zhao. A stochastic modeling of early HIV-1 population dynamics. *Math.Biosci.*, 170(2):187–198, 2001.

[61] M. O. Karlsson, S. L. Beal, and L. B. Sheiner. Three new residual error models for population PK/PD analyses. *J.Pharmacokinet.Biopharm.*, 23(6):651–672, 1995.

[62] F. Karpe, B. A. Fielding, J. L. Ardilouze, V. Ilic, I. A. Macdonald, and K. N. Frayn. Effects of insulin on adipose tissue blood flow in man. *J.Physiol*, 540(Pt 3):1087–1093, 2002.

[63] D. M. Keenan and J. D. Veldhuis. A biomathematical model of time-delayed feedback in the human male hypothalamic-pituitary-Leydig cell axis. *Am.J.Physiol*, 275(1 Pt 1):E157–E176, 1998.

[64] P. E. Kloeden and E. Platen. *Numerical Solution of Stochastic Differential Equations*. Springer-Verlag Berlin Heidelberg, 1992.

[65] N. R. Kristensen. Fed-Batch Process Modelling for State Estimation and Optimal Control. A Stochastic Grey-Box Modelling Framework. *PhD thesis, Department of Chemical Engineering, Technical University of Denmark,*, 2002.

[66] N. R. Kristensen, H. Madsen, and S. H. Ingwersen. A Deconvolution Method for Linear and Nonlinear Systems based on Stochastic Differential Equations. *PAGE poster presentation*, 2004.

[67] N. R. Kristensen, H. Madsen, and S. H. Ingwersen. Using stochastic differential equations for PK/PD model development. *J.Pharmacokinet.Pharmacodyn.*, 32(1):109–141, 2005.

[68] N. R. Kristensen, H. Madsen, and S. B. Jørgensen. Parameter estimation in stochastic grey-box models. *Automatica*, 40:225–237, 2004.

[69] B. Øksendal. *Stochastic Differential Equations - An introduction with applications*. Springer-Verlag, Berlin, Germany, 1998.

[70] B. Øksendal and A. Sulem. *Applied Stochastic Control of Jump Diffusions*. Springer-Verlag Berlin, Heidelberg New York, 2004.

[71] P. Lansky, V. Lanska, and M. Weiss. A stochastic differential equation model for drug dissolution and its parameters. *J.Control Release*, 100(2):267–274, 2004.

[72] W. J. Leonard and R. Spolski. Interleukin-21: a modulator of lymphoid proliferation, apoptosis and differentiation. *Nat.Rev.Immunol.*, 5(9):688–698, 2005.

[73] V. Licko and A. Silvers. Open-loop glucose-insulin control with threshold secretory mechanism: analysis of intravenous glucose tolerance tests in man. *Math.Biosci.*, 27:319–332, 1975.

[74] M. L. Lindstrom and D. M. Bates. Nonlinear mixed effects models for repeated measures data. *Biometrics*, 46(3):673–687, 1990.

[75] D. J. Lunn, J. Wakefield, A. Thomas, N. Best, and D. Spiegelhalter. PKBugs User Guide. *Dept.Epidemiology and Public Health, Imperial College School of Medicine, London.*, 1999.

[76] P. A. Mackowiak. *Drug Induced Fever. In Fever. Basic Mechanisms and Management.* Raven Pr, 1997.

[77] H. Madsen and J. Holst. *Modelling Non-Linear and Non-Stationary Time Series, IMM, Danish Technical University, Lyngby, Denmark, 2000.* IMM, Danish Technical University, Lyngby, Denmark, 2000.

[78] D. E. Mager and W. J. Jusko. General pharmacokinetic model for drugs exhibiting target-mediated drug disposition. *J.Pharmacokinet.Pharmacodyn.*, 28(6):507–532, 2001.

[79] D. E. Mager, E. Wyska, and W. J. Jusko. Diversity of mechanism-based pharmacodynamic models. *Drug Metab Dispos.*, 31(5):510–518, 2003.

[80] R. Nesher and E. Cerasi. Modeling phasic insulin release: immediate and time-dependent effects of glucose. *Diabetes*, 51 Suppl 1:S53–S59, 2002.

[81] H. A. Nielsen and H. Madsen. A generalization of some classical time series tools. *Computational Statistics and Data Analysis*, 37:13–31, 2001.

[82] J. N. Nielsen and H. Madsen. Applying the EKF to stochastic differential equations with level effects. *Automatica*, 37:107–112, 2001.

[83] J. N. Nielsen, H. Madsen, and P. C. Young. Parameter Estimation in Stochastic Differential Equations: An Overview. *Annual Reviews in Control*, 24:83–94, 2000.

[84] K. Nolsøe, J. N. Nielsen, and H. Madsen. Prediction-based estimating functions for diffusion processes with measurement noise . *Submitted*, 2006.

[85] M. D. O'Connor, H. Landahl, and G. M. Grodsky. Comparison of storage- and signal-limited models of pancreatic insulin secretion. *Am.J.Physiol*, 238(5):R378–R389, 1980.

[86] M. Ohara-Imaizumi, Y. Nakamichi, T. Tanaka, H. Ishida, and S. Nagamatsu. Imaging exocytosis of single insulin secretory granules with evanescent wave microscopy: distinct behavior of granule motion in biphasic insulin release. *J.Biol.Chem.*, 277(6):3805–3808, 2002.

[87] C. S. Olofsson, S. O. Gopel, S. Barg, J. Galvanovskis, X. Ma, A. Salehi, P. Rorsman, and L. Eliasson. Fast insulin secretion reflects exocytosis of docked granules in mouse pancreatic B-cells. *Pflugers Arch.*, 444(1-2):43–51, 2002.

[88] K. Ozaki, K. Kikly, D. Michalovich, P. R. Young, and W. J. Leonard. Cloning of a type I cytokine receptor most related to the IL-2 receptor beta chain. *Proc.Natl.Acad.Sci.U.S.A*, 97(21):11439–11444, 2000.

[89] D. M. Parkin, F. Bray, J. Ferlay, and P. Pisani. Global cancer statistics, 2002. *CA Cancer J.Clin.*, 55(2):74–108, 2005.

[90] J. Parrish-Novak, S. R. Dillon, A. Nelson, A. Hammond, C. Sprecher, J. A. Gross, J. Johnston, K. Madden, W. Xu, J. West, S. Schrader, S. Burkhead, M. Heipel, C. Brandt, J. L. Kuijper, J. Kramer, D. Conklin, S. R. Presnell, J. Berry, F. Shiota, S. Bort, K. Hambly, S. Mudri, C. Clegg, M. Moore, F. J. Grant, C. Lofton-Day, T. Gilbert, F. Rayond, A. Ching, L. Yao, D. Smith, P. Webster, T. Whitmore, M. Maurer, K. Kaushansky, R. D. Holly, and D. Foster. Interleukin 21 and its receptor are involved in NK cell expansion and regulation of lymphocyte function. *Nature*, 408(6808):57–63, 2000.

[91] M. Pelletier, A. Bouchard, and D. Girard. In vivo and in vitro roles of IL-21 in inflammation. *J.Immunol.*, 173(12):7521–7530, 2004.

[92] J. C. Pinheiro and D. M. Bates. Approximations to the Log-likelihood function in Nonlinear Mixed-Effects Models. *Journal of Computational and Graphical Statistics*, 4(1):12–35, 1995.

[93] J. C. Pinheiro and D. M. Bates. *Mixed-Effects Models in S and S-PLUS*. Springer, 2000.

[94] D. Pipeleers, R. Kiekens, Z. Ling, A. Wilikens, and F. Schuit. Physiologic relevance of heterogeneity in the pancreatic beta-cell population. *Diabetologia*, 37 Suppl 2:S57–S64, 1994.

[95] D. G. Pipeleers. Heterogeneity in pancreatic beta-cell population. *Diabetes*, 41(7):777–781, 1992.

[96] N. Porksen, M. Hollingdal, C. Juhl, P. Butler, J. D. Veldhuis, and O. Schmitz. Pulsatile insulin secretion: detection, regulation, and role in diabetes. *Diabetes*, 51 Suppl 1:S245–S254, 2002.

[97] S. Del Prato, P. Marchetti, and R. C. Bonadonna. Phasic insulin release and metabolic regulation in type 2 diabetes. *Diabetes*, 51 Suppl 1:S109–S116, 2002.

[98] PricewaterhouseCoopers. Pharma 2005 Silicon Rally: The Race to e-R&D. *Paraxal's Pharmaceutical RD Statistical Sourcebook 2002/2003*, 2005.

[99] K. Rebrin, U. Fischer, Woedtke T. von, P. Abel, and E. Brunstein. Automated feedback control of subcutaneous glucose concentration in diabetic dogs. *Diabetologia*, 32(8):573–576, 1989.

[100] M. Sørensen. *Estimating functions for discretely observed diusions: A review. In Selected Proceedings of the Symposium on Estimating Functions.* Hayward: Institute of Mathematical Statistics., 1997.

[101] J. E. Riviere, T. Martin-Jimenez, S. F. Sundlof, and A. L. Craigmill. Interspecies allometric analysis of the comparative pharmacokinetics of 44 drugs across veterinary and laboratory animal species. *J.Vet.Pharmacol.Ther.*, 20(6):453–463, 1997.

[102] F. Rombout, L. Aarons, M. O. Karlsson, A. Man, F. Mentre, P. Nygren, A. Racine, H. Schaeter, J. L. Steimer, I. Troconiz, and v A. Peer. Modelling and Simulation in the Development and use of Anti-Cancer Agents: An Underused Tool? *Journal of Pharmacokinetics and Pharmacodymics*, 31, No. 6, 2004.

[103] P. Rorsman, L. Eliasson, E. Renstrom, J. Gromada, S. Barg, and S. Gopel. The Cell Physiology of Biphasic Insulin Secretion. *News Physiol Sci.*, 15:72–77, 2000.

[104] P. Rorsman and E. Renstrom. Insulin granule dynamics in pancreatic beta cells. *Diabetologia*, 46(8):1029–1045, 2003.

[105] Malcom Rowland and Thomas N.Tozer. *Clinical Pharmacokinetics - Concepts and Applications.* 1995.

[106] A. P. Salgado, R. M. Santos, A. P. Fernandes, A. R. Tome, P. R. Flatt, and L. M. Rosario. Glucose-mediated $Ca(2+)$ signalling in single clonal insulin-secreting cells: evidence for a mixed model of cellular activation. *Int.J.Biochem.Cell Biol.*, 32(5):557–569, 2000.

[107] C. F. Van Schravendijk, R. Kiekens, and D. G. Pipeleers. Pancreatic beta cell heterogeneity in glucose-induced insulin secretion. *J.Biol.Chem.*, 267(30):21344–21348, 1992.

[108] R. M. Schultz. *Advances in Targeted Cancer Therapy.* 2005.

[109] T Söderström and P Stoica. *System Identification.* Prentice Hall International, 1989.

[110] L. Sheiner and J. Wakefield. Population modelling in drug development. *Stat.Methods Med.Res.*, 8(3):183–193, 1999.

[111] L. B. Sheiner. Learning versus confirming in clinical drug development. *Clin.Pharmacol.Ther.*, 61(3):275–291, 1997.

[112] L. B. Sheiner and J. L. Steimer. Pharmacokinetic/pharmacodynamic modeling in drug development. *Annu.Rev.Pharmacol.Toxicol.*, 40:67–95, 2000.

[113] G. Sparacino, G. Pillonetto, M. Capello, Nicolao G. De, and C. Cobelli. WINSTODEC: a stochastic deconvolution interactive program for physiological and pharmacokinetic systems. *Comput.Methods Programs Biomed.*, 67(1):67–77, 2002.

[114] G. M. Steil, A. E. Panteleon, and K. Rebrin. Closed-loop insulin delivery-the path to physiological glucose control. *Adv.Drug Deliv.Rev.*, 56(2):125–144, 2004.

[115] G. M. Steil and K. Rebrin. Closed-loop insulin delivery - what lies between where we are and where we are going? *Expert.Opin.Drug Deliv.*, 2(2):353–362, 2005.

[116] S. G. Straub and G. W. Sharp. Glucose-stimulated signaling pathways in biphasic insulin secretion. *Diabetes Metab Res.Rev.*, 18(6):451–463, 2002.

[117] S. G. Straub and G. W. Sharp. Hypothesis: one rate-limiting step controls the magnitude of both phases of glucose-stimulated insulin secretion. *Am.J.Physiol Cell Physiol*, 287(3):C565–C571, 2004.

[118] K. J. Åstrom. *Introduction to Stochastic Control Theory*. Academic Press, New Yourk, USA, 1970.

[119] J. H. Strubbe and A. B. Steffens. Neural control of insulin secretion. *Horm.Metab Res.*, 25(10):507–512, 1993.

[120] J. Sturis, K. S. Polonsky, E. Mosekilde, and Cauter E. Van. Computer model for mechanisms underlying ultradian oscillations of insulin and glucose. *Am.J.Physiol*, 260(5 Pt 1):E801–E809, 1991.

[121] H. Sun, E. O. Fadiran, C. D. Jones, L. Lesko, S. M. Huang, K. Higgins, C. Hu, S. Machado, S. Maldonado, R. Williams, M. Hossain, and E. I. Ette. Population pharmacokinetics. A regulatory perspective. *Clin.Pharmacokinet.*, 37(1):41–58, 1999.

[122] W. Y. Tan and H. Wu. Stochastic modeling of the dynamics of CD4+ T-cell infection by HIV and some Monte Carlo studies. *Math.Biosci.*, 147(2):173–205, 1998.

[123] G. Toffolo, R. N. Bergman, D. T. Finegood, C. R. Bowden, and C. Cobelli. Quantitative estimation of beta cell sensitivity to glucose in the intact organism: a minimal model of insulin kinetics in the dog. *Diabetes*, 29(12):979–990, 1980.

[124] G. Toffolo, E. Breda, M. K. Cavaghan, D. A. Ehrmann, K. S. Polonsky, and C. Cobelli. Quantitative indexes of beta-cell function during graded up&down glucose infusion from C-peptide minimal models. *Am.J.Physiol Endocrinol.Metab*, 280(1):E2–10, 2001.

[125] G. Toffolo, Grandi F. De, and C. Cobelli. Estimation of beta-cell sensitivity from intravenous glucose tolerance test C-peptide data. Knowledge of the kinetics avoids errors in modeling the secretion. *Diabetes*, 44(7):845–854, 1995.

[126] C. W. Tornøe, J. L. Jacobsen, O. Pedersen, T. Hansen, and H. Madsen. Grey-box modelling of pharmacokinetic/pharmacodynamic systems. *J.Pharmacokinet.Pharmacodyn.*, 31(5):401–417, 2004.

[127] C. W. Tornøe, R. V. Overgaard, H. Agersø, H. A. Nielsen, H. Madsen, and E. N. Jonsson. Stochastic differential equations in NONMEM: implementation, application, and comparison with ordinary differential equations. *Pharm.Res.*, 22(8):1247–1258, 2005.

[128] H. C. Tuckwell and Corfec E. Le. A stochastic model for early HIV-1 population dynamics. *J.Theor.Biol.*, 195(4):451–463, 1998.

[129] U.S.Food and Drug Administration. Guidance for Industry: Population Pharmacokinetics. *http://www.fda.gov*, 1999.

[130] U.S.Food and Drug Administration. Challenge and Opportunity on the Critical Path to New Medical Products. *http://www.fda.gov*, 2004.

[131] Ch van Kesteren, R. A. Mathot, J. H. Beijnen, and J. H. Schellens. Pharmacokinetic-pharmacodynamic guided trial design in oncology. *Invest New Drugs*, 21(2):225–241, 2003.

[132] R. Vio, P. Rebusco, P. Andreani, H. Madsen, and R. V. Overgaard. Stochastic Modelling of kHz QPO light curves. *Submitted*, 2006.

[133] S. A. Visser, B. Sallstrom, T. Forsberg, L. A. Peletier, and J. Gabrielsson. Modeling drug- and system-related changes in body temperature: Application to clomethiazole-induced hypothermia, long-lasting tolerance development, and circadian rhythm in rats. *J.Pharmacol.Exp.Ther.*, 2005.

[134] P. Webb. The physiology of heat regulation. *Am.J.Physiol*, 268(4 Pt 2):R838–R850, 1995.

[135] K. P. Zuideveld, H. J. Maas, N. Treijtel, J. Hulshof, P. H. van der Graaf, L. A. Peletier, and M. Danhof. A set-point model with oscillatory behavior predicts the time course of 8-OH-DPAT-induced hypothermia. *Am.J.Physiol Regul.Integr.Comp Physiol*, 281(6):R2059–R2071, 2001.

Paper A

Insights to the minimal model of insulin secretion through a mean-field beta cell model

Insights to the minimal model of insulin secretion through a mean-field beta cell model

R.V. Overgaard[a,*] , J.E. Henriksen[b], H. Madsen[a]

[a]*Informatics and Mathematical Modelling, Technical University of Denmark, Lyngby, Denmark*
[b]*Steno Diabetes Research Centre, Department of Endocrinology M, Odense University Hospital*

Abstract

The present work introduces an extension of the original minimal model of second phase insulin secretion during the intravenous glucose tolerance test (IVGTT), which can provide both physiological and mathematical insights to the minimal model. The extension is named the mean-field beta cell model since it returns the average response of a large number of nonlinear secretory entities. Several secretion models have been proposed for the IVGTT, and we shall identify two fundamentally different theoretical features of these models. Both features can play a central role during the IVGTT, including the one presented in the mean-field beta cell model.

© 2005 Elsevier Ltd. All rights reserved.

Keywords: Minimal model; Insulin secretion; Distributed threshold; Mean field

1. Introduction

The intravenous glucose tolerance test (IVGTT) is widely used in order to estimate parameters that constitute the so-called metabolic portrait of the test subject. The insulin sensitivity and glucose effectiveness provide the glucose kinetics part of the metabolic portrait, while the first- and second-phase insulin secretion indices are measures of pancreatic β-cell function. The parameters are embedded in two different minimal models, one describing the glucose kinetics (Bergman et al., 1979) while the other describes the insulin secretion (Toffolo et al., 1980). The minimal models are extensively used and implemented in published computer programs (Pacini and Bergman, 1986) and (Vega-Catalan, 1990). Here we shall concentrate upon the minimal model of insulin secretion (hereafter named MM), as applied e.g. in Pacini and Cobelli (1990), Marchesini et al. (1990), and Piccardo et al. (1994).

MM simply states that during an IVGTT, the second phase insulin secretion into plasma is proportional to the time since the glucose bolus was administrated and to the glucose concentration above some threshold value. MM is based on data, and does not provide any physiological arguments for why the secretion rate rises linearly in time, which subsequently might cast doubt on whether the physiology is satisfactory described by the model. Furthermore, the explicit time dependence causes mathematical problems, specifically when the two minimal models are unified (Gaetano and Arino, 2000).

Based on data analysis, other statistical models have been suggested to replace the minimal model of insulin secretion (Toffolo et al., 1995), (called M1 and M2 in the present paper, just as in the original paper). These models can be argued from theoretically more comprehensive models (Licko and Silvers, 1975), which make them physiologically and mathematically more

---

*Corresponding author. Tel.: +45 30 24 78 76; fax: +45 45 88 26 73.
E-mail address: rvo@imm.dtu.dk (R.V. Overgaard).

appealing. However, the physiologic assumptions and the theoretical feature behind these models are not the only reasonable ones, which is subject for further elaboration in the following.

The primary goal of the present paper is to introduce a theoretical and mathematical extension of the original MM that clarifies the physiologic background and describes the theoretical feature that has made MM a success. The added structure introduced to clarify the physiology solves the unboundedness of the secretion, which was the more crucial of the mathematical problems.

The theoretical idea behind the suggested model is to describe the collective secretory response of all the beta cells as a single object, a mean-field beta cell. The dynamics of the mean-field beta cell is different from the individual entities it is composed of, but we can give a physiological understanding of the mean-field model based on the behavior described by an appropriate model for the individual entities.

The secondary purpose of the present text is to compare M1 to the mean-field beta cell model in a theoretical context motivated by the distributed threshold model (Grodsky, 1972), which enables us to identify the two separate theoretical model features of the original MM and M1. Finally the models are compared in a short data analysis, to demonstrate that both theoretical features can be seen in the IVGTT experiment. This data analysis deals exclusively with the theoretical features, that could be identified only for a small number of subjects, whereas other complications of a full scale data analysis were completely ignored. The present model is thus not proposed as a competitive model for the IVGTT, but as a tool to illustrate the theoretical features that may be necessary to consider for new insulin secretion models. Especially when more mechanistic models are pursued for a coherent description of different challenges of the beta cell.

All models discussed in the present text are summarized in the appendix, for easy reference.

2. Insulin synthesis and release

Insulin secretion in response to an abrupt increase in blood glucose concentration can to a large extent be described by two phases, a rapid first phase followed by a slowly rising second phase. These phases are related to the pleiotropic effects that glucose induce on the beta cell, ranging over regulation of insulin biosynthesis, movement of insulin within the beta cell, and insulin release.

The duration of the IVGTT is only a few hours, which is a brief period when dealing with insulin synthesis. Over short periods (2 h or less) glucose regulates the proinsulin biosynthesis mainly by increasing the rate of translation of proinsulin mRNA. In vitro studies show that after an abrupt increase in plasma glucose concentration, the amount of translated proinsulin rises approximately linearly in time, see e.g. (Itoh et al., 1978), and approximately linearly with the glucose concentration (Welsh et al., 1986), for time periods and glucose concentrations comparable to the IVGTT. After synthesis, proinsulin is split into insulin and C-peptide, which are packed in equimolar amounts into granules.

The dynamics of intracellular granules, recently reviewed in Rorsman and Renstrom (2003), is an exploding area of research made available by new real-time imaging techniques. Among other things, these studies indicate heterogeneity of the intracellular insulin granules where some move freely within the intracellular space while others are docked in the plasma membrane and only a fraction of the latter are ready to be released, thereby named the readily releasable pool (RRP). Movement of granules from, e.g. the intracellular space to the RRP is included in the concept of redistribution that in the following mathematical models more generally covers changes in the level that insulin released is sensitive to glucose concentration. The RRP is believed to contain the granules contributing to the first phase secretion (Olofsson et al., 2002), while recent experiments with real-time imaging indicate that second phase secretion is due to granules that have just arrived at the plasma membrane (Ohara-Imaizumi et al., 2002). The second phase secretion is seen also when the synthesis of proinsulin is completely inhibited, indicating that recruitment of freely moving intracellular granules are responsible for the provision of new insulin to the membrane. However for other cell types, recent experiments using fluorescent cargo protein that changes color with time demonstrate that newly assembled secretory entities are secreted first (Duncan et al., 2003). For the beta cell, similar experiments might illuminate, whether upregulation of proinsulin does contribute to the second phase secretion after all.

The release of insulin is facilitated by glucose transforming into ATP, stopping the potassium efflux of the sodium–potassium pump, which depolarizes the cell. The depolarization opens voltage-gated calcium channels, and the rise of calcium leads to transport of insulin granules across the cell membrane. The insulin release, ranging over a few minutes, is very fast in the time frame of the IVGTT, and for this reason it is frequently modelled to be instantaneous, but it can also be identified dynamically as described later.

Heterogeneous response of insulin to glucose has been documented, not only at intra-cellular level, but also at the inter-cellular level. These differences exist both in the biosynthesis and in the secretory response, but also different beta cells have been seen to exhibit different thresholds for the glucose-induced insulin release

(Schravendijk et al., 1992). In the following mean-field beta cell model, we model the collective response of the many beta cells as one object, and thus lump together many forms of heterogeneities. The mathematical model will not depend on whether the inhomogeneity is at the level of beta cells or at the level of granules within the cell, and we shall thus simply refer to the secretory entities.

3. The mean-field beta cell model

The first mean-field beta cell model (MFM1 in the following) is a description of the above-basal second phase secretion during the IVGTT. The first phase secretion is not modelled, and could be included either by using a dirac delta function, or simply by letting the plasma insulin concentration start at the maximal insulin concentration I_{max}.

We shall quantify the physiological argument that the second phase secretion must be a combination of the provision of new insulin and the heterogeneity of the secretory entities. The ith entity is described by

$$dP/dt = -\alpha(P - H(G - h)),$$

$$SR_i = \beta H(G - h_i)P, \quad P(0) = 0,$$

where $H(\cdot)$ is the Heaviside (or step) function, h_i is the individual glucose threshold for the secretion entity, which gives us the heterogeneity in the individual above-basal second phase secretion rate, SR_i, P is the normalized rate of provision of new insulin, similar to what has been used e.g. in Grodsky (1972) and Toffolo et al. (1995), which in the present context is modelled identically for the individual entities. The provision is the combination of recruitment from intracellular granules and from newly synthesized insulin, and like proinsulin it rises slowly starting when glucose concentration rises above some global threshold h. $1/\alpha$ is the characteristic time-scale for the provisionary factor to approach its maximum level, and β is the proportionality factor between the normalized provision and the individual secretion rate.

MFM1 arises through the assumption that the number of secretory entities contributing to the total above-basal secretion is proportional to the glucose concentration above threshold, h. We have MFM1,

$$dP/dt = -\alpha(P - H(G - h)),$$

$$SR_{ab} = (\gamma/\alpha)[G - h]^+P, \quad P(0) = 0. \quad \text{(MFM1)}$$

$[G - h]^+$ is the positive part of $(G - h)$, which is modelled to be proportional to the number of contributing secretory entities. SR_{ab} is the total above-basal second phase secretion rate. The parameterization has been changed compared to the model of the individual

secretory entities, such that γ is the second phase secretion index (ϕ_2).

We remark that MFM1 respond differently than the individual secretory entities. The individual entities have a sharp threshold above which they begin to secrete, while the mean-field beta cell has a secretion proportional to the glucose concentration above some threshold. This threshold in MFM1 will not represent a typical threshold for the individual packets, but lie in the low end of the individual thresholds, which is in agreement with the typical MM estimation of a threshold near the basal glucose concentration.

Compared to MM, we have used an additional state variable and one extra parameter. The new state variable gives us an interpretation of the linear rise in time, and the extra parameter gives us a glucose-dependent upper bound on the secretion rate.

3.1. Deriving the minimal model from the mean-field beta cell model

In the typical IVGTT, the glucose concentration will not rise above threshold after the first time it has gone below. In this situation, we can derive MM from MFM1 in the limit $\alpha \to 0$. MFM1 can now be written,

$$P = \alpha t + O(\alpha^2) \text{ for } G > h,$$

$$SR_{ab} = (\gamma/\alpha)[G - h]^+P = \gamma[G - h]^+t \quad \text{(MM)}$$

which is the usual representation of the minimal model.

Since $(1/\alpha)$ is a characteristic time, we can understand the minimal model, as the limit where it takes an infinitely long time before the maximal provision is approached. In this limit the insulin secretion will rise unbounded, just as for the MM.

3.2. Including first phase secretion in the mean-field model

Up until now, we have assumed that the first phase secretion is instantaneous. This is obviously not true, and we might get a better description of the first few measurements by including a state representing the total amount of ready made insulin in the currently secreting entities. This state is named X in the following extended form of the mean-field beta cell model (MFM2 from this point). MFM2 is,

$$P = -\alpha(P - H(G - h)),$$

$$dX/dt = (\gamma/\alpha)[G - h]^+P - mH(G - h)X,$$

$$SR_{ab} = mH(G - h)X, \quad \text{(MFM2)}$$

where $1/m$ is the characteristic time for the first phase secretion, so by taking the limit $m \to \infty$ MFM1 is obtained. The first phase secretion index, ϕ_1 can be derived from the initial amount of readily releasable

insulin in all packets contributing to the first phase secretion.

4. Motivating models for the IVGTT from the distributed threshold hypothesis

The distributed threshold hypothesis (Grodsky, 1972) has played a central role in the development of a suitable model to estimate the secretion indices during an IVGTT. The original experiments on the perfused rat pancreas used to quantify the distributed threshold model was in fact used as motivation for MM (Toffolo et al., 1980). More directly the distributed threshold model has motivated another model for the IVGTT (Licko and Silvers, 1975), which in a slightly altered form has provided an alternative to MM (Toffolo et al., 1995). Also the mean-field beta cell model proposed in this paper can be motivated by the distributed threshold model. We shall present a summary of the distributed threshold model, and then demonstrate the two different approximations corresponding to the two model alternatives.

The fundamental hypothesis is that the readily releasable insulin is stored in small packets, where the different packets have different thresholds, secreting insulin into the plasma only when the glucose concentration has exceeded this threshold. The amount of readily releasable insulin in packets with threshold between θ and $\theta + \mathrm{d}\theta$ is given by $\xi(\theta, t)\,\mathrm{d}\theta$, so the threshold density distribution function ξ can be used to model the total secretion into plasma, i.e.

$$\mathrm{d}\xi(\theta, t)/\mathrm{d}t = -m\xi(\theta, t)H(G - \theta) + \gamma(\theta)P(G, t)$$
$$- \Gamma'\xi(\theta, t) + \gamma'(\theta)\int_0^\infty \xi(\theta', t)\,\mathrm{d}\theta',$$

$$\mathrm{d}P(G, t)/\mathrm{d}t = -\alpha[P(G, t) - P(G, \infty)],$$

$$SR_{tot} = m\int_0^G \xi(\theta, t)\,\mathrm{d}\theta. \qquad \text{(Dist-Thres)}$$

The secretion of insulin into the plasma is realized through the first term $-m\xi H(G - \theta)$, where $H(\cdot)$ is the Heaviside function, P is the provisionary factor, which asymptotically approaches the maximal provision $P(G, \infty)$ at a rate α. The last terms, $\Gamma'\xi$ and $\gamma' \int_0^\infty \xi\,\mathrm{d}\theta'$ are named redistribution terms corresponding to insulin exchange between the different packets, which can be understood as insulin changing its sensitivity to glucose, and not necessarily its spatial location. Redistribution is necessary in order to return to the initial insulin distribution in steady state after a glucose stimulation. Both γ and γ' are then assumed to be proportional to the threshold density distribution function at constant zero glucose concentration, $\xi(\theta, 0)$. SR_{tot} is the total secretion, $SR_{tot} = SR_b + SR_{ab}$, where SR_{ab} is the above-basal

secretion as modelled by the IVGTT models described in this paper, and SR_b is the basal secretion rate, which is assumed constant in models of the IVGTT.

Several experiments are needed to identify the different parameters in the distributed threshold model, so it cannot be used directly for the IVGTT. In order to see how the model can motivate MFM1, we present the following approximation of the distributed threshold model: (1) m is taken to infinity, corresponding to an instantaneous first phase secretion, (2) we model only the packets presently secreting, and disregard redistribution, also the important redistribution of insulin from packets not secreting. This approximation gives us,

$$\mathrm{d}P/\mathrm{d}t = -\alpha[P - P(G, \infty)],$$

$$SR_{tot} = fPX(G), \quad X(G) = \int_0^G \xi(\theta, 0)\,\mathrm{d}\theta,$$

where f is the proportionality factor between $\gamma(\theta)$ and $\xi(\theta, 0)$. The nonlinear functions for the accumulated initial insulin distribution (X) and the maximal provision ($P(G, \infty)$) have been fitted in the original work, see e.g. (O'Connor et al., 1980), to the functions presented in Fig. 1.

MFM1 corresponds to the further approximation,

$$X_{ab} \propto [G - h]^+, \quad P(G, \infty)_{ab} \propto H(G - h),$$

where X_{ab} and $P(G, \infty)_{ab}$ are the part of the functions contributing to the above-basal secretion.

This approximation of the distributed threshold model justifies that the number of secretory entities contributing to the above-basal secretion is proportional to the glucose concentration above threshold, as it is modelled in MFM1.
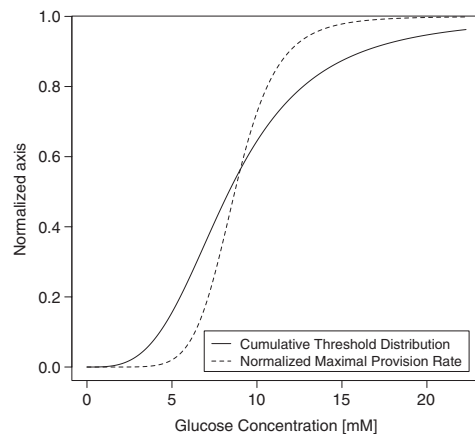

Fig. 1. The normalized cumulative distribution of thresholds, and the normalized maximal rate of provision, as estimated in e.g. O'Connor et al. (1980).

It was chosen to approximate the maximal provision with a piecewise constant function, because a linear approximation would produce a quadratic glucose dependence of the total secretion, while in the distributed threshold model the total glucose dependence of the above-basal secretion is approximately linear. The step function approximation of the maximal provision increases the secretion during the last part of the IVGTT where the glucose concentration is low but still above threshold, which to some extent counter effect that no redistribution has been modelled. This counter effect is perhaps the primary reason that one cannot include an improved description of the maximal provision without also including some form of redistribution.

One can argue that the maximal provision $P(G, \infty)_{ab}$ rather than the threshold distribution X_{ab} should be approximated with a step function. First of all the nonlinear function describing the maximal provision is steeper, hence closer to a step function than the cumulative distribution. Second, changes in the maximal provision influence the secretion only through the provision, while changes in the number of contributing secretory entities affect the secretion directly and immediately. During the IVGTT, the glucose concentration drops quickly, so it might be essential for the secretion model to respond correctly to an immediate decrease.

It is clear that the approximations lead to certain limitations of the model. Since we are modelling only the insulin content in packets presently secreting, the model does not take into account that insulin stored in other packets would secrete directly into plasma if the glucose concentration was to rise. During the IVGTT, this approximation is less important since after the administration of the glucose bolus the plasma glucose concentration is approximately monotonously decreasing. More important is the lack of redistribution that would facilitate an indirect contribution from packets not presently secreting. MFM1 has emphasized modelling of the immediate response of the beta cell, and not the precise form of the total provision, which might be more important for long slowly varying glucose stimulations, since all provisioned insulin is believed to be secreted at some point.

Another approximation of the distributed threshold model emphasizes modelling of the total provision and the total secretion. This approximation is called M1, which is a model for the above-basal second phase secretion. M1 is given by

$$\mathrm{d}P/\mathrm{d}t = -\alpha(P - \beta[G - h]^+),$$

$$SR_{ab} = P, \quad P(0) = 0 \qquad \mathrm{(M1)}$$

β is the second phase secretion index, and $1/\alpha$ can again be interpreted as a characteristic time for P to approach the glucose-dependent maximum provision. M1 is a slight variation of the model presented in Licko and Silvers (1975) previously compared to the minimal model in Toffolo et al. (1995). We shall here present the following argument for the model.

For the distributed threshold model, the total provision to all packets is proportional to P, and the redistribution terms makes sure that it will also be secreted at some point. Specifically in steady state, the secretion will be identical to the provision. M1 emphasizes the approximation of the maximal provision in order to precisely account for the total provision, which is then used to approximate the secretion. This approximation is expected to work best for slowly varying glucose stimulations, where the effect of inhomogeneous response from the different secretory entities is diminished by the redistribution of thresholds. The original mathematical approximation in Licko and Silvers (1975) was to disregard the part of the secretion, which is dependent upon variations in glucose concentration. This approximation will thus be exact for a constant glucose stimulation, i.e. the glucose step, and M1 will be very close to the distributed threshold model.

Just as MFM1 was extended to include first phase secretion, a similar extension could be formulated for M1 called M2 (Toffolo et al., 1995), but this provides no further insight in the present context.

5. Analysis

It is important to note that a regular performance comparison of the presented models is not provided and believed to be out of the scope of the present paper. Data has been included merely to illustrate the theoretical point that the inhomogeneity of the individual secretory entities may be an important interpretation for the plasma insulin profiles for some individuals following the IVGTT. As a tool to demonstrate this interpretation, we have provided the least-squares fit of the relevant models to data.

Six out of a group of 30 healthy volunteers completing an IVGTT were selected for the present analysis from a previously published data set (Henriksen et al., 2000). A bolus of 300 mg glucose per kg body weight (up to a maximum of 25 g) was administrated at $t = 0$, and blood samples were collected for measurement of plasma glucose and plasma insulin concentration at times: $-30, -20, -10, -1, 2, 3, 4, 5, 6, 8, 10, 12, 14, 16, 19, 22, 26, 30, 40, 50, 60, 70, 80, 90, 100, 110, 120, 140, 160, 180$ min relative to the time of injection. Plasma glucose was measured at the bedside on a Beckman Glucose Analyser (Beckman Instruments, Fullerton, CA, USA) by the glucose oxidase method. Plasma insulin blood samples were immediately centrifuged at $4\,^\circ$C and stored at $-20\,^\circ$C for later analysis by two-site, time-resolved
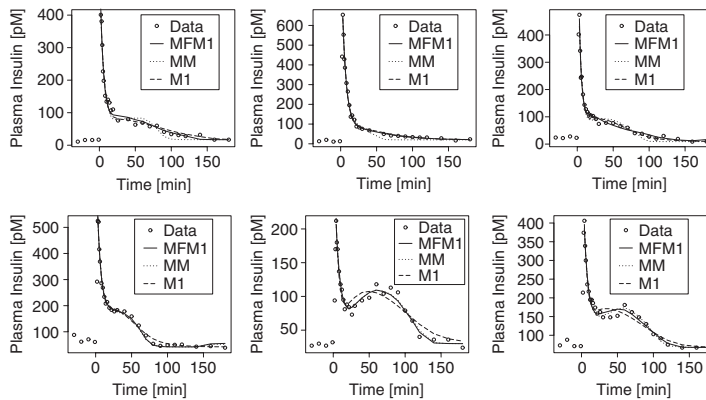
Fig. 2. Plasma insulin concentration and model predictions during an IVGTT for 6 different individuals, where 3 individuals exhibit a vague elongated second phase (top) while the remaining 3 have a more clear and short second phase insulin profile (bottom). The top plots demonstrate similar good predictions of M1 and MFM1, but problems of MM, in the case of elongated second phase where insulin concentrations are elevated also after the glucose concentration has returned towards baseline. In the bottom plots with more clear and short secretion profiles M1 has problems to account for the fast decrease in insulin level when the glucose concentration goes down, while in this case MM and MFM1 give similar good predictions.

immunofluorometric assay (DELFIA) (Hemmila et al., 1984).

The models for second phase secretion were assumed to describe the post-hepatic insulin delivery, and we used the standard first-order elimination

$$dI/dt = SR_{ab} - n(I - I_b),$$

where n is the elimination rate and I is the plasma insulin concentration with a basal value I_b.

Parameter estimates and model predictions were obtained by a least-squares fit of the different models to the plasma insulin concentration, assuming a known glucose concentration calculated as the linear interpolation of the measured glucose concentrations. All computations were performed in R.

5.1. Comparison of the one compartment models

Of the 6 subjects in the present analysis, 3 individuals were selected for their vague elongated second phase, and the remaining 3 because they exhibit a more clear second phase insulin profile. Many of the remaining unselected individuals, exhibited a more noisy insulin profile, or were in some other way more difficult to characterize into the two types of profiles. An elongated profile is consistent with secretion due to continued provision and redistribution after glucose has returned towards baseline as modelled in the distributed threshold model, but it might also be interpreted as biphasic disposition of insulin. A short second phase profile may indicate inhomogeneity of the secretory entities, where different entities stop secretion

at different glucose concentrations during the decrease of glucose in plasma. Here it is investigated to what extent the second phase secretion models MFM1, M1, and MM are able to describe these two fundamentally different features observed in data during an IVGTT.

All models were started at $t = 0$, while the first predictions were at the point of the highest measured insulin concentration where the modelled plasma insulin concentration was set to the parameter I_{max}. It was chosen to estimate all parameters except I_b, which was fixed to the average value of the insulin concentrations measured at 160 and 180 min. For MFM1 the parameters $(\alpha, \gamma, h, I_{max}, n)$ were estimated. For M1 the parameters $(\alpha, \beta, h, I_{max}, n)$ were estimated. For MM the parameters (γ, h, I_{max}, n) were estimated.

The results presented in Fig. 2 demonstrate that for the subjects with a clear second phase both MM and MFM1 are able to describe the rapid decrease of plasma insulin concentration, while M1 gives a more elongated insulin profile. These results indicate that for some individuals the inhomogeneity of the secretory entities included in MM and MFM1 but not in M1, may be necessary to accurately describe the second phase secretion during the IVGTT.

For individuals with a clear second phase the time to reach maximal provision was estimated to be very high indicating that we are close to the MM limit. The higher insulin provision can through the approximation of the distributed threshold model be interpreted as a compensation for the missing redistribution contribution to the active insulin packets.
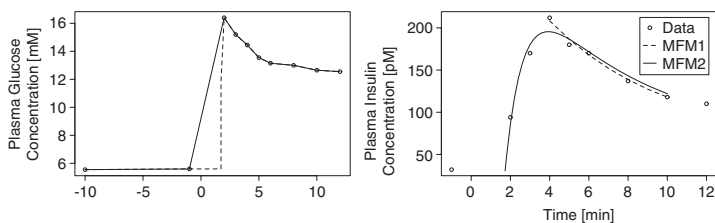
Fig. 3. Plasma glucose (left) and insulin (right) concentrations during the first minutes of the IVGTT. (left plot) A linear interpolation between glucose measurements (solid line) results in an unrealistic elevation of plasma glucose concentration before the IV glucose administration. Instead, it was chosen to estimate the starting point of the model, corresponding to using the glucose concentration profile given by the dashed line. (right plot) The predicted plasma insulin concentrations during first phase secretion are given for model MFM1 (dashed line) and MFM2 (solid line).

Further results demonstrated in Fig. 2 show that M1 and MFM1 are both capable of describing subjects with an elongated insulin profile, while the MM predictions seems to be forced towards baseline when glucose goes down. In this case the estimated time to reach maximal provision was shorter constituting the difference between MM and MFM1.

5.2. Comparing models for the first phase secretion

Two versions of the mean-field beta cell model have been presented, MFM1 and the extension MFM2, which increases the physiological understanding of the secretion by introducing a compartment for the readily releasable insulin. Here we demonstrate that this can be seen in data from an IVGTT.

The initial condition for MFM2 need some attention. X represents the amount of readily releasable insulin in all contributing entities at a given time. So the initial value for X is the amount of readily releasable insulin in all entities contributing to the first phase secretion, namely the active entities during the high glucose concentration right after the glucose bolus is administrated. In principle it does not make sense to use the model to predict insulin secretion before the glucose administration, where a small fluctuation in glucose concentration could be slightly above threshold, which would trigger a first phase spike.

The exact time for the rise in plasma glucose concentration after bolus administration is not known, and the glucose measurements around $t = 0$ are too sparse to obtain a good estimate directly from the glucose concentration profile, see Fig. 3. For MFM2 it was chosen to estimate the optimal starting point along with the other parameters, $(\gamma, h, m, X(0), \alpha, n)$.

The results in Fig. 3 compare MFM1 and MFM2 to demonstrate that the extra compartment for readily releasable insulin included in MFM2 does in fact enable us to describe the first phase secretion.

6. Conclusion

We have presented a physiological interpretable mean-field beta cell model for insulin secretion during the IVGTT, and showed that this model is very close to the original MM. In fact, it was shown that the original MM reappears in some limit of the mean-field model and that we may be close to this limit for some subjects. The model was extended with an extra compartment of readily releasable insulin, which enabled us to understand and describe the first phase secretion.

Theoretical insights of the model was given through the distributed threshold hypothesis, and it is observed that the mean-field model does actually incorporate the inhomogeneity of the different secretory entities. We have further summarized the approximation of a previously published IVGTT secretion model. This enabled us to understand the two fundamentally different approximations of the model, where one crudely approximates the provision and redistribution of newly synthesized insulin, while the other crudely approximates the inhomogeneity of the secretory entities. Investigations shows that both of the theoretical features may be important for data analysis. For some test subjects, in particular those with a clear second phase secretion, the inhomogeneity in the secretory response is essential, while for other subjects, in particular those with a vague elongated secretion, the prolonged secretion along with the redistribution seemed to be superior compared to the minimal model. In both cases the mean-field beta cell model was able to describe the observed profiles.

A comparison between data and model fits was provided to demonstrate that the theoretical features of redistribution and threshold heterogeneity is present in reality. Since MFM1 was able to describe both of these phenomena, it is intriguing to propose MFM1 as the new model to estimate and characterize beta cell function from the IVGTT. However, during data analysis it was found that differences in performance

of the models could be seen clearly only for a small subset of the subjects, and subsequently it was judged that a test of the computational applicability of the model for the would clutter the theoretical findings. Since MFM1 as a model for the IVGTT can provide only a modest improvement if any, it was chosen to keep the focus on the insights provided by the model. These theoretical insights could become important in the pursuit of a more general and physiological correct model that can characterize the beta cell function, not only for the IVGTT, but also for other experiments.

Appendix

All models discussed in the main text are summarized in Table 1 given below.

Table 1
Summary of insulin secretion models

Model		Abbreviation
$d\xi(\theta, t)/dt$	$= -m\xi(\theta, t)H(G - \theta) + \gamma(\theta)P(G, t)$ $\quad - \Gamma'\xi(\theta, t) + \gamma'(\theta)\int_0^\infty \xi(\theta', t)\,d\theta'$	Dist-Thres
$dP(G, t)/dt$	$= -\alpha[P(G, t) - P(G, \infty)]$	
SR_{tot}	$= m\int_0^G \xi(\theta, t)\,d\theta$	
dP/dt	$= -\alpha(P - H(G - h))$	MFM1
SR_{ab}	$= (\gamma/\alpha)[G - h]^+ P, \quad P(0) = 0$	
P	$= -\alpha(P - H(G - h)),$	MFM2
dX/dt	$= (\gamma/\alpha)[G - h]^+ P - mH(G - h)X$	
SR_{ab}	$= mH(G - h)X$	
SR_{ab}	$= \gamma[G - h]^+ t$	MM
dP/dt	$= -\alpha(P - \beta[G - h]^+)$	M1
SR_{ab}	$= P, \quad P(0) = 0$	

References

Bergman, R.N., Ider, Y.Z., Bowden, C.R., Cobelli, C., 1979. Quantitative estimation of insulin sensitivity. Am. J. Physiol. 236 (6), E667–E677.

Duncan, R.R., Greaves, J., Wiegand, U.K., Matskevich, I., Bodammer, G., Apps, D.K., Shipston, M.J., Chow, R.H., 2003. Functional and spatial segregation of secretory vesicle pools according to vesicle age. Nature 422 (6928), 176–180.

Gaetano, A.D., Arino, O., 2000. Mathematical modelling of the intravenous glucose tolerance test. J. Math. Biol. 40 (2), 136–168.

Grodsky, G.M., 1972. A threshold distribution hypothesis for packet storage of insulin and its mathematical modeling. J. Clin. Invest. 51 (8), 2047–2059.

Hemmila, I., Dakubu, S., Mukkala, V.M., Siitari, H., Lovgren, T., 1984. Europium as a label in time-resolved immunofluorometric assays. Anal. Biochem. 137 (2), 335–343.

Henriksen, J.E., Levin, K., Thye-Ronn, P., Alford, F., Hother-Nielsen, O., Holst, J.J., Beck-Nielsen, H., 2000. Glucose-mediated glucose disposal in insulin-resistant normoglycemic relatives of type 2 diabetic patients. Diabetes 49 (7), 1209–1218.

Itoh, N., Sei, T., Nose, K., Okamoto, H., 1978. Glucose stimulation of the proinsulin synthesis in isolated pancreatic islets without increasing amount of proinsulin mRNA. FEBS Lett. 93 (2), 343–347.

Licko, V., Silvers, A., 1975. Open-loop glucose–insulin control with threshold secretory mechanism: analysis of intravenous glucose tolerance tests in man. Math. Biosci. 27, 319–332.

Marchesini, G., Pacini, G., Bianchi, G., Patrono, D., Cobelli, C., 1990. Glucose disposal, beta-cell secretion, and hepatic insulin extraction in cirrhosis: a minimal model assessment. Gastroenterology 99 (6), 1715–1722.

O'Connor, M.D., Landahl, H., Grodsky, G.M., 1980. Comparison of storage- and signal-limited models of pancreatic insulin secretion. Am. J. Physiol. 238 (5), R378–R389.

Ohara-Imaizumi, M., Nakamichi, Y., Tanaka, T., Ishida, H., Nagamatsu, S., 2002. Imaging exocytosis of single insulin secretory granules with evanescent wave microscopy: distinct behavior of granule motion in biphasic insulin release. J. Biol. Chem. 277 (6), 3805–3808.

Olofsson, C.S., Gopel, S.O., Barg, S., Galvanovskis, J., Ma, X., Salehi, A., Rorsman, P., Eliasson, L., 2002. Fast insulin secretion reflects exocytosis of docked granules in mouse pancreatic B-cells. Pflugers Arch. 444 (1–2), 43–51.

Pacini, G., Bergman, R.N., 1986. MINMOD: a computer program to calculate insulin sensitivity and pancreatic responsivity from the frequently sampled intravenous glucose tolerance test. Comput. Methods Programs Biomed. 23 (2), 113–122.

Pacini, G., Cobelli, C., 1990. Estimation of beta-cell secretion and insulin hepatic extraction by the minimal modelling technique. Comput. Methods Programs Biomed. 32 (3–4), 241–248.

Piccardo, M.G., Pacini, G., Nardi, E., Rosa, M.S., Vito, R.D., 1994. Beta-cell response and insulin hepatic extraction in noncirrhotic alcoholic patients soon after withdrawal. Metabolism 43 (3), 367–371.

Rorsman, P., Renstrom, E., 2003. Insulin granule dynamics in pancreatic beta cells. Diabetologia 46 (8), 1029–1045.

Schravendijk, C.F.V., Kiekens, R., Pipeleers, D.G., 1992. Pancreatic beta cell heterogeneity in glucose-induced insulin secretion. J. Biol. Chem. 267 (30), 21344–21348.

Toffolo, G., Bergman, R.N., Finegood, D.T., Bowden, C.R., Cobelli, C., 1980. Quantitative estimation of beta cell sensitivity to glucose in the intact organism: a minimal model of insulin kinetics in the dog. Diabetes 29 (12), 979–990.

Toffolo, G., Grandi, F.D., Cobelli, C., 1995. Estimation of beta-cell sensitivity from intravenous glucose tolerance test C-peptide data. Knowledge of the kinetics avoids errors in modeling the secretion. Diabetes 44 (7), 845–854.

Vega-Catalan, F.J., 1990. A program to estimate insulin sensitivity and pancreatic responsivity from an IVGTT using the minimal modeling technique. Comput. Biomed. Res. 23 (1), 1–9.

Welsh, M., Scherberg, N., Gilmore, R., Steiner, D.F., 1986. Translational control of insulin biosynthesis. Evidence for regulation of elongation, initiation and signal-recognition-particle-mediated translational arrest by glucose. Biochem. J. 235 (2), 459–467.

Paper B

Non-linear mixed-effects models with stochastic differential equations: implementation of an estimation algorithm

Non-Linear Mixed-Effects Models with Stochastic Differential Equations. Implementation of an Estimation Algorithm

Rune V. Overgaard[1,2,*], Niclas Jonsson[3], Christoffer W. Tornøe[1,3,4], Henrik Madsen[1]

[1]Informatics and Mathematical Modelling, Technical University of Denmark, Lyngby, Denmark

[2]Experimental Medicine, Novo Nordisk A/S, Bagsvaerd, Denmark

[3]Dept. of Pharmaceutical Biosciences, Uppsala University, Sweden

[4]Experimental Medicine, Ferring Pharmaceuticals A/S, Copenhagen, Denmark

[*]To whom correspondence should be addressed.

Suggested running head: Mixed-Effects Models with SDEs

Written for submission to:
Journal of Pharmacokinetics and Pharmacodynamics

ABSTRACT

Pharmacokinetic/pharmacodynamic modelling is most often performed using non-linear mixed-effects models based on ordinary differential equations with uncorrelated intra-individual residuals. More sophisticated residual error models as e.g. stochastic differential equations (SDEs) with measurement noise can in many cases provide a better description of the variations, which could be useful in various aspects of modelling. This general approach enables a decomposition of the intra-individual residual variation ϵ into system noise $\boldsymbol{w}$ and measurement noise $\boldsymbol{e}$.

The present work describes implementation of SDEs in a non-linear mixed-effects model, where parameter estimation was performed by a novel approximation of the likelihood function. This approximation is constructed by combining the First-Order Conditional Estimation (FOCE) method used in non-linear mixed-effects modelling with the Extended Kalman Filter used in models with SDEs. Fundamental issues concerning the proposed model and estimation algorithm are addressed by simulation studies, concluding that system noise can successfully be separated from measurement noise and inter-individual variability.

KEY WORDS: SDE, PK/PD, Kalman filter, population modelling, system noise, correlated residuals.

1   INTRODUCTION

Non-linear mixed effects modelling has proven to be a useful tool in the characterization of pharmacokinetic (PK) and pharmacodynamic (PD) properties of drugs (see [1] and [2]). The models used in this mode of analysis are most frequently based on ordinary differential equations (ODEs), or the solutions thereof, supplemented by a model for the inter-individual variations in the structural model parameters and a model for the variation of the residuals that assumes independence, so that the residuals are uncorrelated. However, correlations between residuals are not uncommon, and it is well known that a violation of this basic statistical assumption may lead to erroneous estimates, for example of the inter-individual variations as demonstrated in [3].

In NONMEM [4], which is the most commonly used software for PK/PD analysis using non-linear mixed-effects models, it is possible to handle correlated residual errors using an AR(1) model [3]. Simulations suggest that the introduction of a model for correlated residuals may lead to 1) better estimates of the inter-individual variation, 2) better estimates of the structural parameters, 3) and a diagnostic tool giving a measure of the model improvement.

An alternative approach to model correlated residuals is to use stochastic differential equations (SDEs). This model structure includes the statistical functionality of the continuous AR(1) model, but is more flexible with respect to specifying models for different residual error correlation patterns.

With SDEs, the differences between individual predictions and observations are explained by two fundamentally different types of noise: 1) the dynamic noise, which enters through the dynamics of the system and may originate from model deficiencies or true random fluctuations within the system, and 2) the measurement noise, which represents the uncorrelated part of the residual variability, may be due to assay error or if the sample concentration is not representative for the true concentration in plasma. This could e.g. occur for samples during the distribution phase of an intravenous (IV) bolus administrated drug. The difference between two measurements at the same time point will therefore only be due to measurement noise. In a recent book on PK/PD modelling, it is suggested that the intra-individual variations may be more appropriately modelled by using SDEs rather than ODEs [5].

In addition to separating the residual error into dynamic noise and measurement noise, SDEs also allow the dynamic noise to be attributed to different model components. For example, if the absorption process of an orally administered drug cannot be well described by the model, this may lead to correlated residuals. However, if an AR(1) model was used to account for this, the auto-correlation pattern would be assumed effective along the whole concentration time profile. With SDEs, the dynamic noise component could be put directly on the state equation for the absorption meaning that the auto-correlation pattern is only assumed effective as long as absorption occurs. Furthermore, SDEs could facilitate the estimation of the actual absorption profile in a way similar to deconvolution, and thus reveal the misspecifications of the model [6]. The same approach can be used for other model components as well, and SDEs therefore has the potential to be a useful model building tool, as well as a diagnostic tool [7].

Besides the increased functionality, SDEs may indeed offer practical benefits in terms of

3

easier PK/PD modelling, particularly when more complicated mechanistic models are used. In this case, the number and complexity of the mechanisms involved may be too great for inclusion in a model used for estimation. Here SDEs may be included to describe some of these mechanisms, while only the major mechanisms are treated by the parametric model.

SDEs have been used for individual non-linear analysis of PK/PD data and have proven to be useful, both with respect to parameter estimation, model building, and simulation, e.g. in [8] and [9].

Both non-linear mixed-effects models and SDEs are highly non-trivial statistical problems where an analytical likelihood function can rarely be found. The combination of the two should therefore be treated with care. The problem has previously been addressed by the Markov Chain Monte Carlo (MCMC) method [10] for a combined minimal model of glucose disposal and insulin secretion. In the present paper, we combine the Gaussian approximation of the non-linear mixed-effects models with the Gaussian approximation of SDEs with measurement noise. The approximations are facilitated by the Extended Kalman Filter (EKF) to approximate the intra-individual likelihood function [11] and the First-Order Conditional Estimation (FOCE) method to approximate the population likelihood function [12].

The focus of the present study is on two fundamental issues concerning the implementation of SDEs in non-linear mixed effects models. The first is how the likelihood function of non-linear mixed-effects models with SDEs can be approximated to facilitate estimation in these models. The second focus concerns identifiability: Can the inter-individual variability, the measurement- and the system noise be separated? Or in other words, will significant system noise be predicted by the algorithm when none is used in the simulations (Type I error), and will the algorithm fail to detect significant system noise when it is truly present in the data (Type II error).

2 THEORY

Non-linear mixed-effects models can be thought of as a hierarchical model structure where the variability in concentration/effect is split into intra-individual variability described by the first-stage distribution and inter-individual variability described by the second-stage distribution [13, 14]. While the introduction of SDEs do not change this fundamental hierarchical structure, they do change the entities in the first stage density and the construction thereof. This section describes the notation for non-linear mixed-effects models used in the present paper, and proceed with an explanation of the extensions needed to include SDEs.

2.1 Notation of Non-Linear Mixed-Effects Models

Non-linear mixed-effects models are used to describe, understand, and simulate data structured as

$$\boldsymbol{y}_{ij}, \quad i = 1, \ldots, N \quad j = 1, \ldots, n_i \tag{1}$$

where the observation $\boldsymbol{y}_{ij}$ in general is a vector of responses for the ith individual at the jth time point, N is the number of individuals and n_i is the number of measurements for the ith individual.

The structural model used to describe the intra-individual data typically consists of a set of ODEs or the solution thereof. These ODEs are supplemented by a model of the residual variation that describes the differences between the structural model and the observations. This gives rise to the following equations for the first stage model:

$$\frac{d\boldsymbol{x}_i}{dt} = \boldsymbol{g}(\boldsymbol{x}_i, \boldsymbol{d}_i, t, \boldsymbol{\phi}_i) \tag{2}$$

$$\boldsymbol{y}_{ij} = \boldsymbol{f}(\boldsymbol{x}_i(t_{ij}), \boldsymbol{d}_i(t_{ij}), \boldsymbol{\phi}_i) + \boldsymbol{\epsilon}_{ij} \tag{3}$$

where for the ith individual, $\boldsymbol{x}_i(t)$ is a vector of state variables, e.g. the amount of drug in a PK model, $\boldsymbol{d}_i$ is a vector of inputs, e.g. dose administration, t is time, t_{ij} is the jth measurement time, $\boldsymbol{\phi}_i$ is a vector of the individual parameters, and $\boldsymbol{\epsilon}_{ij}$ is the jth residual. The residuals are typically modelled as serial independent with covariance matrix $\boldsymbol{\Sigma}$, which may depend on the states, input, time, and/or individual parameters. $\boldsymbol{\Sigma}$ is most often a scalar, except in the general case of multidimensional measurements. $\boldsymbol{g}(\cdot)$ and $\boldsymbol{f}(\cdot)$ are non-linear vector functions describing the dynamics of the states and the relationship between the states and the observations, respectively.

The second-stage model describes the inter-individual variations, which in the present work is accomplished through the following model for the individual parameters

$$\boldsymbol{\phi}_i = \boldsymbol{h}(\boldsymbol{\theta}, \boldsymbol{Z}_i) \exp(\boldsymbol{\eta}_i) \tag{4}$$

where $\boldsymbol{h}(\cdot)$ denotes the structural type parameter model, which is a function of the fixed-effects parameters $\boldsymbol{\theta}$ and typically also some covariates $\boldsymbol{Z}_i$. The random-effects $\boldsymbol{\eta}_i$ are independent and multivariate normally distributed with zero mean and covariance matrix $\boldsymbol{\Omega}$, resulting in a multivariate log-normal distribution for the individual parameters.

The total set of population parameters to be estimated in the non-linear mixed effects model can now be summarized as intra-individual variability, inter-individual variability, and fixed-effects parameters, given by the set ($\boldsymbol{\Sigma}$, $\boldsymbol{\Omega}$, and $\boldsymbol{\theta}$).

2.2 Non-Linear Mixed-Effects Models with Stochastic Differential Equations

Non-linear mixed-effects models based on SDEs extend the usual non-linear mixed-effects models by including system noise as an additional source of variation in the first-stage model. This extended model describes the intra-individual variation in data through two sources of noise, which in the present work will be described as two different types of population parameters: 1) $\boldsymbol{\Sigma}$ describing the covariance matrix of the measurement noise rather than that of the residuals, 2) the new parameter matrix $\boldsymbol{\sigma}_w$ describing the magnitude of the system noise. By this extension, the complete set of population parameters in non-linear mixed-effects models based on SDEs becomes ($\boldsymbol{\Sigma}$, $\boldsymbol{\sigma}_w$, $\boldsymbol{\Omega}$, and $\boldsymbol{\theta}$).

The formulation of the first-stage model can be separated into the design of a structural model and the addition of variations. Designing the structural model is equivalent to selecting the model structure for conventional PK/PD modelling, which means that exploratory data analysis and physiological knowledge may be applied in the usual manner. This process

consists of formulating a set of ODEs as those given in (2). Once the structural part of the first-stage model has been formulated, we can add variations to account for the differences between the measured and the predicted values. When SDEs are involved, the usual residuals will no longer be independent, and we need to describe the underlying variations of ϵ by system noise w as well as measurement noise e. The system noise can be added directly to the differential equations allowing for some random variations in the evolution of the states, which may be appropriate whenever the modeler fear that the true evolution of the states does not comply strictly with the structural model. Measurement noise is added to the model in the usual measurement equation, such that a first-stage model with SDEs can be written as

$$
\begin{aligned}
d\boldsymbol{x}_i &= \boldsymbol{g}(\boldsymbol{x}_i, \boldsymbol{d}_i, t, \boldsymbol{\phi}_i)dt + \boldsymbol{\sigma}_w d\boldsymbol{w} \quad &(5)\\
\boldsymbol{y}_{ij} &= \boldsymbol{f}(\boldsymbol{x}_i(t_{ij}), \boldsymbol{d}_i(t_{ij}), \boldsymbol{\phi}_i) + \boldsymbol{e}_{ij} \quad &(6)
\end{aligned}
$$

where $\boldsymbol{x}_i(t)$, $\boldsymbol{d}_i$, t, t_{ij}, $\boldsymbol{\phi}_i$, $\boldsymbol{g}(\cdot)$ and $\boldsymbol{f}(\cdot)$ are identical to what has previously been defined for ODEs in (2) and (3). $\boldsymbol{e}_{ij}$ are the independent identically distributed Gaussian measurement errors with covariance matrix $\boldsymbol{\Sigma}$, and $\boldsymbol{\sigma}_w d\boldsymbol{w}$ gives the system noise, where both $\boldsymbol{\Sigma}$ and $\boldsymbol{\sigma}_w$ may depend on the states, input, time, and/or individual parameters. If the magnitude of the system noise $\boldsymbol{\sigma}_w$ is zero, then the entire system noise term will vanish and the remaining part of the SDE will simply be the differential form of the ODE given in equation (2). SDEs are usually written on the differential form given above, because the term $d\boldsymbol{w}$ has a mathematical interpretation as the infinitesimal increments in the noise process ($\boldsymbol{w}$), whereas the corresponding derivative $d\boldsymbol{w}/dt$ cannot be treated mathematically. The individual specific system noise $\boldsymbol{w}$ is a standard vector Wiener process, i.e. a continuous time Gaussian process where the mean and variance of the differences between two time points are

$$
\begin{aligned}
E[\boldsymbol{w}_{t_2} - \boldsymbol{w}_{t_1}] &= 0 \quad &(7)\\
V[\boldsymbol{w}_{t_2} - \boldsymbol{w}_{t_1}] &= |t_2 - t_1|I \quad &(8)
\end{aligned}
$$

where I is the identity matrix. The Gaussian process can be understood to originate from the sum of many identically distributed stochastic events giving rise to the difference between the true evolution of the state and the evolution described by the structural term $\boldsymbol{g}(\cdot)$. Furthermore, the variance of the Wiener process increases linearly in time, which can be interpreted as a linear increase in the number of stochastic events contributing to the dynamic noise. [11] and [15] provide an introduction to applied stochastic differential equations, and [16] gives a more thorough mathematical introduction.

3   The Likelihood Function for the Non-Linear Mixed-Effects Model with SDEs

When the first-stage model is extended to include SDEs rather than ODEs, the first-stage probability density function can no longer be computed analytically. In the present section, we shall describe how the likelihood function is now formulated, how it can be approximated,

and how it is combined with the second-stage density to form the population likelihood function. This is all summarized in Table I, presented at the end of the section.

When the intra-individual model contains correlations in the residuals, the first-stage distribution must be factorized as a product of conditional densities that are conditioned not only upon (ϕ_i, Σ, σ_w, and d_i), but also on all previous measurements. Conditioning on previous measurements is central for the present text, giving rise to the term conditional densities used in the following. To see how factorization of the first stage density comes about, start with the distribution for the initial observation and successively add one observation at a time by the use of a reformulation of Bayes rule $P(A \cap B) = P(B|A)P(A)$. This gives us the following first stage density for the ith individual

$$p_1(\mathcal{Y}_{in_i}|\phi_i, \Sigma, \sigma_w, d_i) = \left(\prod_{j=2}^{n_i} p(y_{ij}|\mathcal{Y}_{i(j-1)}, \cdot) \right) p(y_{i1}|\cdot) \tag{9}$$

The so called conditional densities are given on the right hand side, $\mathcal{Y}_{ij} = [y_{i1}, ..., y_{ij}]$ represents all observations of the ith individual up to time t_{ij}, and conditioning on ϕ_i, Σ, σ_w, and d_i is represented by " $\cdot$ ".

If the SDEs are reduced to ODEs, the residuals will be uncorrelated, and the conditional densities will be identical to the unconditional densities, such that the likelihood function will reduce to the product of unconditional densities, as known for ODEs.

An analytical determination of the conditional densities requires a solution of a so called general non-linear filtering problem. This entails to start with the initial distribution and then successively solving Kolmogorov's forward equation for the SDE and applying Bayes' rule [11]. In practice, this approach involves the numerical solution of a partial differential equation for each time increment, which is too time consuming, making it computational infeasible, and an alternative is needed. Various methods have been proposed and are still investigated for parameter estimation in the general setup, and a consensus of a preferred method has not yet been reached [17].

In the present work we shall use a quasi likelihood method, i.e. a method that uses the Gaussian approximation, so we assume that the conditional densities are well approximated by Gaussian densities. This is a particularly useful choice since filtering techniques used for SDEs with measurement noise rely on separability of the first and second order moment, and since Gaussian densities are easily combined with the methods usually used in non-linear mixed-effects modelling. The calculation of the conditional densities for the intra-individual model is facilitated by the Extended Kalman Filter (EKF) [11]. In the case where the differential equations are linear and both system noise and measurement noise are state independent, the EKF reduces to the ordinary Kalman Filter, which in this case gives the exact likelihood function. When proportional system noise or proportional measurement noise is needed, one can typically log-transform the states or the measurements to approach the Gaussian distribution. These transformations will most often give rise to more severe non-linearities in the functions for the structural model $g(\cdot)$ and the measurement equation $f(\cdot)$ in (5) and (6). However, it is our experience that the conditional densities are well described by Gaussian distributions, also for highly non-linear systems. The assumption

7

of Gaussian conditional densities is easily tested by the distribution of the standardized residuals, while also more advanced methods have been developed, see [18].

The EKF approximates the conditional densities with Gaussian distributions, which is described in detail in Appendix A. The conditional densities describe the distribution of the following measurement conditioned on all the previous measurements, so that the mean of the distribution is identical to the prediction of the following measurement, i.e. the one-step prediction $\hat{\boldsymbol{y}}_{i(j|j-1)}$. Likewise, the covariance of the conditional density will be the one-step prediction covariance $\boldsymbol{R}_{i(j|j-1)}$. We have thus completely described the approximate Gaussian conditional densities by the conditional mean and covariance, which are

$$\hat{\boldsymbol{y}}_{i(j|j-1)} = E(\boldsymbol{y}_{ij}|\mathcal{Y}_{i(j-1)}, \cdot) \tag{10}$$
$$\boldsymbol{R}_{i(j|j-1)} = V(\boldsymbol{y}_{ij}|\mathcal{Y}_{i(j-1)}, \cdot) \tag{11}$$

The notation above is also used for the mean and variance of the first prediction, such that $\hat{\boldsymbol{y}}_{i(1|0)}$ is the unconditioned model prediction of the first observation, and $\boldsymbol{R}_{i(1|0)}$ is the covariance of the first prediction error.

The one-step prediction error $\boldsymbol{\epsilon}_{ij}$ is given by

$$\boldsymbol{\epsilon}_{ij} = \boldsymbol{y}_{ij} - \hat{\boldsymbol{y}}_{i(j|j-1)} \in N(0, \boldsymbol{R}_{i(j|j-1)}) \tag{12}$$

Using the notation above, the Gaussian approximation of the first-stage distribution density function in (9) can be written as

$$p_1(\mathcal{Y}_{in_i}|\cdot) \approx \prod_{j=1}^{n_i} \frac{\exp\left(-\frac{1}{2}\boldsymbol{\epsilon}_{ij}^T \boldsymbol{R}_{i(j|j-1)}^{-1} \boldsymbol{\epsilon}_{ij}\right)}{\sqrt{|2\pi\boldsymbol{R}_{i(j|j-1)}|}} \tag{13}$$

The second-stage density (4) can be written as $p_2(\boldsymbol{\eta}_i|\boldsymbol{\Omega})$, which is included in the same way as for ordinary differential equations. This gives us the full non-linear mixed-effects likelihood function

$$L(\boldsymbol{\theta}, \boldsymbol{\Sigma}, \boldsymbol{\sigma}_w, \boldsymbol{\Omega}) \propto \prod_{i=1}^{N} \int p_1(\mathcal{Y}_{in_i}|\boldsymbol{\eta}_i, \boldsymbol{\theta}, \boldsymbol{\Sigma}, \boldsymbol{\sigma}_w, \boldsymbol{d})p_2(\boldsymbol{\eta}_i|\boldsymbol{\Omega})d\boldsymbol{\eta}_i$$
$$= \prod_{i=1}^{N} \int \exp(\boldsymbol{l}_i)d\boldsymbol{\eta}_i \tag{14}$$

where

$$\boldsymbol{l}_i = -\frac{1}{2}\sum_{j=1}^{n_i}\left(\boldsymbol{\epsilon}_{ij}^T \boldsymbol{R}_{i(j|j-1)}^{-1}\boldsymbol{\epsilon}_{ij} + \log|2\pi\boldsymbol{R}_{i(j|j-1)}|\right) - \frac{1}{2}\boldsymbol{\eta}_i^T\boldsymbol{\Omega}^{-1}\boldsymbol{\eta}_i - \frac{1}{2}\log|2\pi\boldsymbol{\Omega}| \tag{15}$$

is the approximate a posteriori log-likelihood function for the random effects of the ith individual. It is observed that the likelihood function is based on the one-step prediction error.

In the case of no system noise ($\boldsymbol{\sigma}_w = 0$) the SDE in the model reduces to the more familiar ODE, and the one-step prediction covariances will reduce to the residual covariance $\boldsymbol{R}_{i(j|j-1)} = \boldsymbol{\Sigma}$. The one-step prediction errors will be identical to the usual unconditioned prediction errors, such that the likelihood function above will reduce to the one known for non-linear mixed-effects models based on ODEs.

As usual for non-linear mixed-effects models, the likelihood function cannot be solved analytically. Approximations therefore have to be made in order to estimate the parameters, which will be considered in the following.

3.1   Approximations of the Population Likelihood Function

The Gaussian structure of the individual likelihood functions allows us to use the well known Laplacian approximation, as well as the other approximation schemes frequently used in non-linear mixed-effects modelling to obtain the population likelihood function. The entities within the likelihood function structure ($\boldsymbol{\epsilon}$ and $\boldsymbol{R}$) are however extended compared to the standard problem. In the following we shall discuss the approximation when applied to these extended entities.

For non-linear mixed-effects models, the likelihood function is usually approximated by performing a second-order Taylor series expansion of the *a posteriori* individual log-likelihood function $\boldsymbol{l}_i$ around some value of the random effects, e.g. zero or the value of $\boldsymbol{\eta}_i$ that minimizes $\boldsymbol{l}_i$. The same approach is taken for mixed-effects model with SDEs, so the Laplacian approximation of (14) becomes

$$L(\boldsymbol{\theta}, \boldsymbol{\Sigma}, \boldsymbol{\sigma}_w, \boldsymbol{\Omega}) \propto \prod_{i=1}^{N} \int \exp(\boldsymbol{l}_i) d\boldsymbol{\eta_i} \approx \prod_{i=1}^{N} |\triangle \boldsymbol{l}_i|^{-1/2} \exp\left[\boldsymbol{l}_i - \frac{1}{2}\nabla \boldsymbol{l}_i^T \triangle \boldsymbol{l}_i^{-1} \nabla \boldsymbol{l}_i\right] \quad (16)$$

The gradient $\nabla \boldsymbol{l}_i$ of the *a posteriori* individual log-likelihood with respect to the random effects will vanish when the expansion is made around the true minimum, but it has been included here to account for the more general case. The Hessian $\triangle \boldsymbol{l}_i$ is thus a key element in the evaluation of the population likelihood function.

The numerical evaluation of double derivatives to form the Hessian is usually quite sensitive leading to uncertainty in the objective function and optimization problems. Several approximations have been developed specifically to avoid numerical calculations of double derivatives related to this Hessian in non-linear mixed-effects models. In the present work, we have used the First-Order Conditional Estimation (FOCE) method [4].

3.2   First-Order Conditional Estimation method

The FOCE method uses only first-order derivatives in the evaluation of the population likelihood function where the derivatives are evaluated at the conditional estimates of the random effects $\hat{\boldsymbol{\eta}}_i$. The likelihood function can thus be written as

$$L(\boldsymbol{\theta}, \boldsymbol{\Sigma}, \boldsymbol{\sigma}_w, \boldsymbol{\Omega}) \approx \prod_{i=1}^{N} |\triangle \boldsymbol{l}_i|^{-1/2} \exp(\boldsymbol{l}_i)|_{\hat{\boldsymbol{\eta}}_i} \quad (17)$$

where the second-order derivatives are disregarded such that the individual *a posteriori* log-likelihood function and its Hessian can be written as

$$l_i = -\frac{1}{2}\sum_{j=1}^{n_i}\left(\boldsymbol{\epsilon}_{ij}^T \boldsymbol{R}_{i(j|j-1)}^{-1}\boldsymbol{\epsilon}_{ij} + \log|2\pi\boldsymbol{R}_{i(j|j-1)}|\right) - \frac{1}{2}\boldsymbol{\eta}_i^T\boldsymbol{\Omega}^{-1}\boldsymbol{\eta}_i - \frac{1}{2}\log|2\pi\boldsymbol{\Omega}| \quad (18)$$

$$\triangle l_i \approx -\sum_{j=1}^{n_i}\left(\nabla\boldsymbol{\epsilon}_{ij}^T \boldsymbol{R}_{i(j|j-1)}^{-1}\nabla\boldsymbol{\epsilon}_{ij}\right) - \boldsymbol{\Omega}^{-1} \quad (19)$$

We note that the variance of the one-step predictions $\boldsymbol{R}_{i(j|j-1)}$ is generated through the dynamics of the system and will thus depend inherently upon the parameters of the model. This dependence leads to interactions between the intra-individual residuals and the random effects even in models that are usually homoscedastic. In the FOCE approximation given above, we are disregarding first-order derivatives of $\boldsymbol{R}_{i(j|j-1)}$, which is an approximation in the case of interactions, and thus a more crude approximation when modelling with SDE's as compared to ODEs. This approximation would be worse if directly including interactions between the random effects and system noise, which has been avoided in the present study, but could be included if one feel that it is necessary.

Interactions were included in the FOCE method presented here, so both the predictions and the covariances are evaluated at the conditional estimate. One could also, as it is implemented in NONMEM version V, use the conditionally estimated predictions together with covariances computed by the population predictions, corresponding to having no interactions, or even expand the likelihood function around the population average, corresponding to the first-order (FO) method.

4 METHODS

Several simulation studies are used to test whether the likelihood function formulated above can be advocated for estimating parameters in a non-linear mixed-effects model based on SDEs. These simulation studies are based on the PK model and the numerical implementation described below.

4.1 Model used for Simulation

We shall simulate experiments using a one-compartment PK model with IV bolus dose with a constant coefficient of variation for the uncorrelated measurement error and additive Wiener noise such that the ith individual is modelled by

$$dA_i = -\frac{CL_i}{V_i}A_i dt + \sigma_w dw \quad (20)$$

$$y_{ij} = \log\frac{A(t_{ij})}{V_i} + e_{ij}, \qquad e_{ij} \in N(0, \sigma_e^2) \quad (21)$$

where A_i is the amount of drug in the central compartment, y_{ij} is the measurement at time t_{ij}, e_{ij} is the measurement error and σ_e is the coefficient of variation for the measurement

error, w is a standard Wiener process, and σ_w is the magnitude of the system noise. V_i and CL_i are the individual parameters for volume of distribution and clearance, respectively. These are composed of a fixed effect and a random effect, i.e.

$$
\begin{aligned}
V_i &= V \exp(\eta_i^V), & \eta_i^V &\in N(0, \omega_V^2) & (22)\\
CL_i &= CL \exp(\eta_i^{CL}), & \eta_i^{CL} &\in N(0, \omega_{CL}^2) & (23)
\end{aligned}
$$

Hence, the six population parameters to be estimated are (V, CL, ω_V, ω_{CL}, σ_w, and σ_e).

The model is used to simulate two different experimental setups. First, the type I and type II errors are investigated using a somewhat data rich situation with 25 individuals, where the plasma concentration are sampled 12 times at times 0, 0.5, 1, 2, 4, 6, 8, 10, 12, 16, 20, and 24 hours. In the second experimental setup, we simulate 100 individuals, where the plasma concentration is sampled 3 times at times 0, 6, and 24 hours. This second analysis is included to illustrate that parameters in models based on SDEs may also be successfully estimated when only a few samples per individual are taken.

All simulations are performed using the same structural parameter values ($V = 10$ and $CL = 0.5$), while the simulated values of the noise parameters (ω_V, ω_{CL}, σ_w, and σ_e) all varies between 0.01 and 0.4. Examples of simulated individual profiles for various levels and types of intra-individual noise are presented in Figure 1.

4.2   Numerical Implementation

Evaluation of the approximate likelihood function, the optimization, and the simulations of the mixed-effects models based on stochastic differential equations were performed in MATLAB.

As previously described, the population log-likelihood can be approximated using the individual *a posteriori* log-likelihood functions and the Hessian of each of these. The individual likelihood functions can be calculated from the one-step predictions and covariances given by the Extended Kalman Filter as described in Appendix A depending on the initialization of the covariance of the states. The covariance of the states at the first measurement was set to the amount of system noise accumulating in a time span equal to that between the first and second measurement. This particular choice has proven successful in other software implementations [19].

The Hessian of the individual *a posteriori* log-likelihood function can be approximated using the gradients of the one-step predictions as previously described. These gradients were calculated numerically by a central differencing algorithm given in [20]. We note that other methods such as automatic differentiation may be useful, especially in a more general software implementation.

In order to ensure stability in the calculation of the objective function, simple constraints were introduced on the parameters, i.e.

$$
\theta_{min} < \theta < \theta_{max} \tag{24}
$$

These constraints were satisfied by solving the optimization problem with respect to a transformation of the original parameters, i.e.

$$\tilde{\theta} = \ln \left(\frac{\theta - \theta_{min}}{\theta_{max} - \theta} \right) \qquad (25)$$

Regardless of the true parameter value, minimum and maximum allowed values were chosen to be 10^{-5} and 50 respectively.

Two different initial parameter values were used in the optimization, one at 0.8 times the simulated value and one at 1.2 times the simulated value. Experience with the present implementation of the optimization problem tells us that the initial values should not be too low, so the smallest allowable set was chosen to be 0.04 and 0.06. In the figures showing the results, the estimate is plotted for both of these initial values, but any difference can rarely be seen. This gives some assurance of the size of the region governed by the local- if not global minima reached by the estimation procedure.

The asymptotic standard errors of the estimates were computed through the Hessian of the population log-likelihood, which was approximated by a finite difference algorithm given in [20]. The algorithm depends on the accuracy in the numerical evaluation of the likelihood
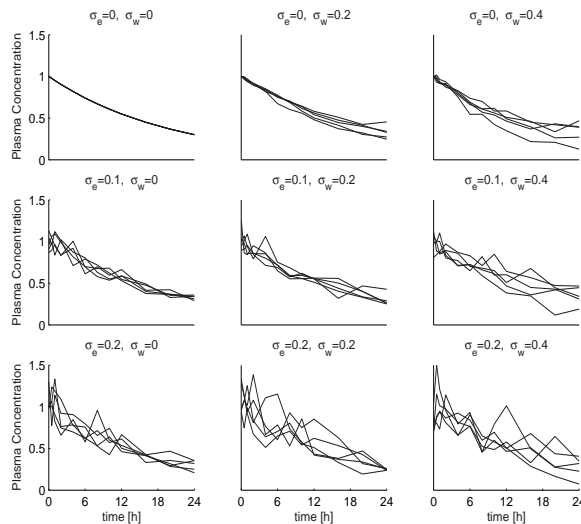
Figure 1: Simulated individual plasma concentration profiles for various levels and types of intra-individual noise. Simulations are made with no inter-individual variation, using $V = 10$ and $CL = 0.5$. Each individual was sampled 12 times, as in the somewhat frequently sampled experiment. The simulated measurements are connected with lines.

function. By graphical means, the number of significant digits in the likelihood function was found to be around 10, such that the number of significant digits in the Hessian should be around $10/3 \approx 3$, see [20].

The computation time on a standard laptop PC (1400 MHz Pentium IV processor) for one evaluation of the population likelihood function was between one and three seconds depending on the simulated example and a few minutes for a complete optimization. The relative swiftness compared to e.g. MCMC methods is a serious advantage of the presented algorithm, and this may enable estimation of SDEs in more general models for practical purposes.

5   Results

Successive simulation and estimation of many different experiments have been used to investigate the type I and type II error of the presented algorithm, and whether SDEs could be used in studies with only a few measurements per individual. In the present section we describe the results of these simulation studies.

5.1   System Noise is Separable From Other Sources of Variation

Any use of the presented algorithm is naturally dependent upon its ability to separate the three levels of noise proposed in the present paper. Separability should thus be among the fundamental issues to be addressed prior to investigation of real data or implementation in more general software. Since system noise is the central addition to the model setup, the central concern is towards separability of system noise e.g. whether system noise is detected when it is truly present in data (type II error).

Separability of system noise and type II errors were investigated in the first simulation study consisting of 40 simulated experiments with 25 individuals each sampled 12 times. Each simulated experiment was performed using a fixed level of inter-individual variation and measurement noise and with an increasing amount of system noise. The results presented in Figure 2 provides a visual confirmation that higher levels of system noise do not produce either additional measurement noise nor inter-individual variability, illustrating that system noise is in fact satisfactorily separable from the remaining noise parameters.

Furthermore, the variability and the standard error of the estimated values of inter-individual variation of the clearance is seen to increase when system noise increases. This indicates that the system noise does make estimation of this particular noise parameter more difficult, while the remaining noise parameters are not influenced to the same extent.

5.2   Insignificant Bias in the Estimated System Noise

A fundamental feature in maximum likelihood estimation of mixed-effects models is that the individual predictions are regressed towards the mean (the population prediction). This introduces manifest correlations in the intra-individual residuals, which in the present model

could be estimated as system noise introducing bias to the estimates. Bias in the estimated system noise could also originate in more general separability problems where inter-individual variation or intra-individual measurement noise is estimated as system noise. If a significant level of system noise is estimated when none is used in the simulation, then a type I error has occurred.

Bias in the system noise and type I errors were investigated in the second simulation study consisting of 40 simulated experiments with 25 individuals, each sampled 12 times. Each simulated experiment was performed using no system noise but with an increasing amount of inter-individual variation and measurement noise. This investigation might reveal a potential relationship between bias in the system noise and the level of the remaining noise parameters. The results presented in Figure 3 demonstrate that this relationship is small and that the existing bias is insignificant such that only few type I errors occur. The largest estimates of system noise was around 0.2, which in Figure 1 is seen to be a modest level of noise compared to the corresponding measurement noise.
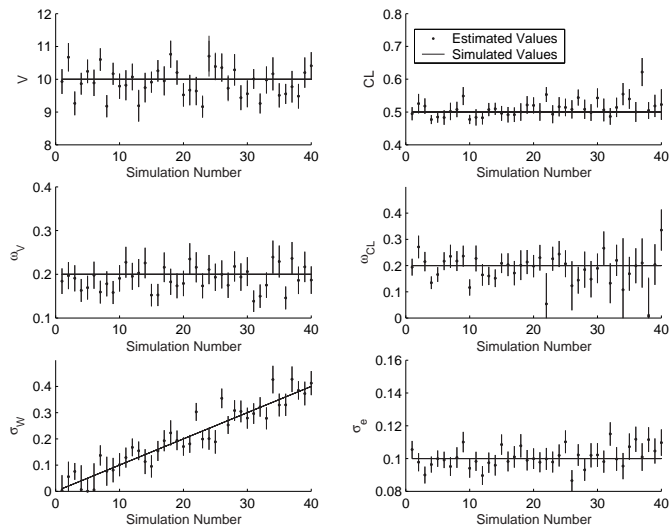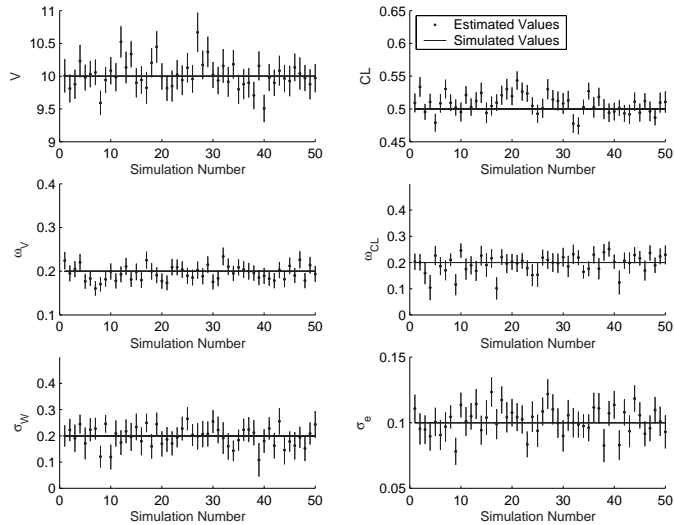

Figure 2: Simulated parameter values are given by the line and estimated parameters values are given by a dot supplemented by error bars representing plus/minus one standard error. The value of the system noise is satisfactorily inferred at increasing levels of system noise, and the bias introduced to the remaining parameters seems to remain small.

14

5.3   Estimation Based on Sparsely Sampled Individuals

A data set consisting of many sparsely sampled individuals is not uncommon within PK/PD modelling. However, parameter estimation in SDEs based on sparsely sampled individuals has previously been complicated by the need of rich sampling to separate system noise from measurement noise and the limitations of single subject estimation algorithms. Mixed-effects modelling has in this situation enabled parameter estimation of ODEs, making it interesting whether also SDEs can be successfully treated.

50 experiments with 100 individuals each sampled 3 times has been simulated and subsequently estimated. The results presented in Figure 4 demonstrate that estimation can be performed successfully with sparsely sampled individuals in the chosen model. We note that estimation based on 2 samples per individual failed to yield the same level of success, so 3 samples per individual may indeed be the lower limit when system noise is included simultaneously with measurement noise and inter-individual variability.

Statistics of the estimation results from Figure 4 are given in Table II, which demonstrates that the mean values of the estimated parameters are close to the true values used in the
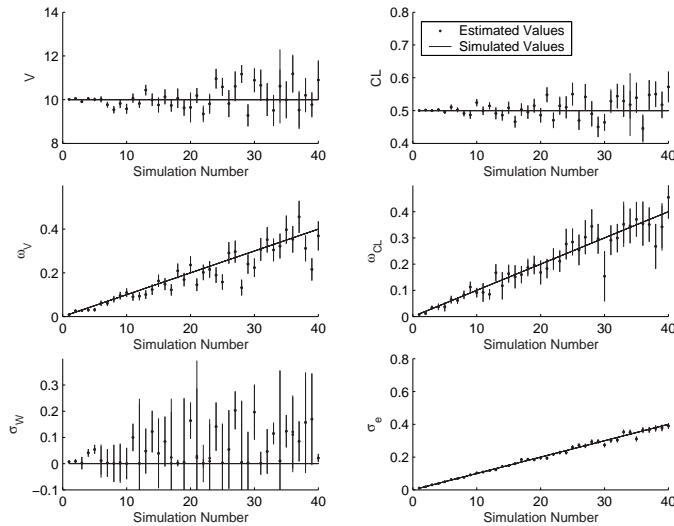
Figure 3: Simulated parameter values are given by the solid line and estimated parameters values are given by a dot supplemented by error bars representing plus/minus one standard error. The estimated system noise is insignificant in most of the simulated experiments, also when the other noise levels increase dramatically. Each simulation was estimated with two sets of initial conditions, which in a few cases gave two slightly different parameter estimates, such that two dots are seen for the same simulation number.

15

simulations and that the standard deviations of the estimates are relatively close to the mean of the standard error estimates. It should be mentioned that due to the relatively high number of simulated experiments, one is able to demonstrate bias in the estimated clearance values on a 95% confidence level. Note that bias exists in practically any algorithm for parameter estimation in complicated systems. This entails that bias in all parameter estimates will be found if the number of simulated experiments is increased sufficiently.

Figure 4: Simulated parameter values are given by the solid line and estimated parameters values are given by a dot supplemented by error bars representing plus/minus one standard error. Each simulated experiment consists of 100 individuals sampled 3 times.

6   Discussion

SDEs offer a general intra-individual error structure where the evolution of the states is allowed to deviate from the structural model. This work presented a novel approximation of the likelihood function for non-linear mixed-effects models based on SDEs and addresses some fundamental issues regarding parameter estimation in this new type of model.

When SDEs are implemented, one-step predictions and their variances were seen to take up the role of the usual unconditioned predictions and intra-individual variance in many ways. In the theory section, it was emphasized that these objects reduce to the usual predictions and variances when the system noise vanishes, and that they can be used to construct the

16

likelihood function. The fundamental model assumption of uncorrelated prediction errors is converted into the assumption of uncorrelated one-step prediction errors, such that diagnostic plots should be slightly changed. Predicted versus previous prediction should be replaced by one-step prediction versus previous one-step prediction. Furthermore, weighted residuals versus time or covariates or similar diagnostic plots should be replaced by corresponding plots of the one-step prediction error weighted by the one-step prediction variance.

Stochastic differential equations are complicated mathematical entities with peculiarities such as dependence in the solution upon the chosen interpretation of the infinitesimal correlation structure, or equivalently on the selected interpretation of the integral part of the SDE. The system noise is called multiplicative or additive when the diffusion term is dependent or independent of the state variable ($\boldsymbol{x}$), respectively. In the multiplicative case, the SDE proposed in equation (5) will be dependent upon the chosen interpretation of the infinitesimal correlation structure, and special attention is needed. In the present work, we restrict ourselves to the additive case where the solutions are independent of the interpretation, since for this case the EKF is recognized to work best. However, situations may arise where multiplicative noise is necessary, as already seen for PK/PD modelling in e.g. [10]. Luckily, a large class of SDEs with multiplicative diffusion can be transformed into SDEs with additive diffusion [21]. One may choose to do this transformation before implementing the diffusion, such that only additive diffusion is needed. This line of approach, as undertaken e.g. in [10], is consistent with the Stratonovich interpretation of the infinitesimal correlations, which is recommended for physical modelling [11].

The presented combination of SDEs and measurement noise constitute a general framework to describe the intra-individual variations, which includes many previous implementations of statistically sophisticated intra-individual models. Motivated by these efforts, we try to identify some of the potential benefits that the literature indicates SDEs can offer nonlinear mixed-effects models of PK/PD: 1) improve estimates of inter-individual variability, 2) improve structural parameter estimates, 3) give a diagnostic test of the model, 4) pinpoint model defects to be used in successive model improvement 5) improve simulation properties of the model, 6) provide a more realistic description of the observed variations, 7) allow fluctuations in physiological parameters, 8) enable deconvolution, 9) extend deconvolution to nonlinear PK/PD models, 10) improve estimation of the states in the system.

Points 1-3 were argued based on a simulation study including the AR(1) in mixed-effects modelling [3]. Points 3 and 4 were also demonstrated by SDEs with measurement noise for single subject PK/PD data in a work in progress using ready available software [19]. Points 5-7 were demonstrated by various case-by-case implementations of SDEs to PK/PD data, see e.g. [8], [9], and [10]. Point 8 was demonstrated for PK/PD models in [22], where deconvolution was facilitated by a random walk, which is a discrete version of a SDE. Since the SDE setup includes non-linear models, point 9 gives itself. Point 10 was demonstrated using a mixed-effects setup of random walks to improve estimation of the AUC [23].

The focus of the present investigation was implementation of SDEs in non-linear mixed-effects models, which could potentially boost the use of SDEs within PK/PD. Fundamental issues concerning the implementation was addressed by simulation and successive estimation of a non-linear mixed-effects model based on SDEs corresponding to a one-compartment

17

model. Three specific concerns were addressed: 1) Will bias in the estimated parameter values lead to significant estimates of system noise when none is used in the simulations (type I errors)? 2) will the system noise be separable from the remaining noise parameters? and 3) can the parameters in the proposed model also be determined with sparsely sampled individuals? The relationship between bias in the system noise and the level of the remaining noise parameters was found to be small and only few type I errors occurred. It was demonstrated that a significant level of system noise can be detected when it is truly present in data (no type II errors). Successful estimation was performed with population data including only 3 samples per individual, which may indeed be the lower limit, when three different types of noise are used.

In conclusion, it is confirmed that inter-individual variability, measurement- and system noise can be separated for the chosen model, which is necessary for non-linear mixed-effects models based on SDEs to be treated meaningfully. However, the presented model and study setup were quite simple, and the routines used in the numerical implementation were not state of the art. So the present investigation should be seen as a pilot study preceding a more general implementation, which more easily allows SDEs in non-linear mixed-effects models. A work in progress demonstrates how the EKF can be implemented in the control stream of NONMEM Version VI beta.

APPENDIX A: THE EXTENDED KALMAN FILTER

The Extended Kalman filter can be used to calculate the one-step predictions and the one-step prediction variances for a stochastic differential equation with additive diffusion and measurement noise. The algebra presented in the following appendix is all performed on the individual level, so to ease the notation, the i index referring to the individual has been dropped. The general intra-individual model treated here can be written as

$$
\begin{aligned}
d\boldsymbol{x} &= \boldsymbol{g}(\boldsymbol{x}, \boldsymbol{d}, t, \boldsymbol{\phi})dt + \boldsymbol{\sigma}_w d\boldsymbol{w} & (26) \\
\boldsymbol{y}_j &= \boldsymbol{f}(\boldsymbol{x}(t_j), \boldsymbol{d}(t_j), \boldsymbol{\phi}) + \boldsymbol{e}_j & (27)
\end{aligned}
$$

where $\boldsymbol{x}$ is the vector of state variables, $\boldsymbol{y}_j$ is the vector of measurements at time t_j, $\boldsymbol{e}_j$ are the associated normally distributed measurement errors with covariance matrix $\boldsymbol{\Sigma}$, and $\boldsymbol{\sigma}_w d\boldsymbol{w}$ is the system noise, where both $\boldsymbol{\Sigma}$ and $\boldsymbol{\sigma}_w$ may depend on input $\boldsymbol{d}$, time t and/or individual parameters $\boldsymbol{\phi}$.

The following notation for the derivatives is applied

$$
\boldsymbol{A}_t = \frac{\partial \boldsymbol{g}}{\partial \boldsymbol{x}}\bigg|_{\boldsymbol{x}=\hat{\boldsymbol{x}}_{t|j-1}}, \qquad \boldsymbol{C}_j = \frac{\partial \boldsymbol{f}}{\partial \boldsymbol{x}}\bigg|_{\boldsymbol{x}=\hat{\boldsymbol{x}}_{j|j-1}} \tag{28}
$$

One needs to initiate the EKF with a prediction of the initial state $\hat{\boldsymbol{x}}_{1|0}$ and a prediction of the covariance of the initial state $\boldsymbol{P}_{1|0}$. From this point, the EKF is a recursive algorithm starting with the calculation of the one step prediction of the measurement and its associated covariance matrix. This is achieved by

$$
\begin{aligned}
\hat{\boldsymbol{y}}_{j|j-1} &= \boldsymbol{f}(\boldsymbol{x}_{j|j-1}, \boldsymbol{d}_j, \boldsymbol{\phi}) & (29) \\
\boldsymbol{R}_{j|j-1} &= \boldsymbol{C}_j \boldsymbol{P}_{j|j-1} \boldsymbol{C}_j^T + \boldsymbol{\Sigma}_{j|j-1} & (30)
\end{aligned}
$$

Given the actual measurement, we can update our state prediction and variance to be predictions conditioned also on the jth measurement. This is performed by the update equations, i.e.

$$
\begin{aligned}
\hat{\boldsymbol{x}}_{j|j} &= \hat{\boldsymbol{x}}_{j|j-1} + \boldsymbol{K}_j(\boldsymbol{y}_j - \hat{\boldsymbol{y}}_{j|j-1}) & (31) \\
\boldsymbol{P}_{j|j} &= \boldsymbol{P}_{j|j-1} - \boldsymbol{K}_j\boldsymbol{R}_{j|j-1}\boldsymbol{K}_j^T & (32) \\
\boldsymbol{K}_j &= \boldsymbol{P}_{j|j-1}\boldsymbol{C}^T\boldsymbol{R}_{j|j-1}^{-1} & (33)
\end{aligned}
$$

where $\boldsymbol{K}_j$ is the Kalman gain.

The final step in the recursive algorithm is to predict the state and the state variance at the time of the following measurement. This is performed by solving the prediction equations, i.e.

$$
\begin{aligned}
d\hat{\boldsymbol{x}}_{t|j}/dt &= \boldsymbol{g}(\boldsymbol{x}_{t|j}, \boldsymbol{d}, t, \boldsymbol{\phi}) & (34) \\
d\boldsymbol{P}_{t|j}/dt &= \boldsymbol{A}_t\boldsymbol{P}_{t|j} + \boldsymbol{P}_{t|j}\boldsymbol{A}_t^T + \boldsymbol{\sigma}_w\boldsymbol{\sigma}_w^T & (35)
\end{aligned}
$$

After the prediction of the state value at the following measurement, we start again with predictions of the actual measurements until all the one-step predictions $\hat{\boldsymbol{y}}_{j|j-1}$ and all the one-step prediction variances $\boldsymbol{R}_{j|j-1}$ have been calculated. The algorithm is summarized in table III.

References

[1] L. Aarons. Pharmacokinetic and pharmacodynamic modelling in drug development. *Stat.Methods Med.Res.*, 8(3):181–182, 1999.

[2] L. B. Sheiner and J. L. Steimer. Pharmacokinetic/pharmacodynamic modeling in drug development. *Annu.Rev.Pharmacol.Toxicol.*, 40:67–95, 2000.

[3] M. O. Karlsson, S. L. Beal, and L. B. Sheiner. Three new residual error models for population PK/PD analyses. *J.Pharmacokinet.Biopharm.*, 23(6):651–672, 1995.

[4] S.L.Beal and L.B.Sheiner. *NONMEM User's Guides.* NONMEM Project Group, University of California, San Francisco, 1994.

[5] Rajesh Krishna (Ed.). *Applications of pharmacokinetic principles in drug development.* New York: Kluwer Academic/Plenum Publishers, 2004.

[6] N. R. Kristensen. A Method for Systematic Improvemenr of Stochastic Grey-Box Models. *Computers and Chemical Engineering*, 28(8):1431–1439, 2004.

[7] C. W. Tornøe *et al*. Grey-box modelling of pharmacokinetic/pharmacodynamic systems. *J.Pharmacokinet.Pharmacodyn.*, 31(5):401–417, 2004.

[8] Tornøe C. W., Jacobsen J. L., and H. Madsen. Grey-box pharmacokinetic/pharmacodynamic modelling of a euglycaemic clamp study. *Journal of Mathematical Biology*, 48(6):591–604, 2004.

[9] P. Sen, D. Bell, and D. Mohr. A calcium model with random absorption: a stochastic approach. *J.Theor.Biol.*, 154(4):485–493, 1992.

[10] K. E Andersen and M. Højbjerre. A Population-based Bayesian Approach to the Minimal Model of Glucose and Insulin Homeostasis. *Technical Report R-2003-25, Aalborg University*, 2003.

[11] A. H. Jazwinski. *Stochastic Processes and Filtering Theory.* Academic Press. New York, 1970.

[12] M. L. Lindstrom and D. M. Bates. Nonlinear mixed effects models for repeated measures data. *Biometrics*, 46(3):673–687, 1990.

[13] A. Racine-Poon and J. Wakefield. Statistical methods for population pharmacokinetic modelling. *Stat.Methods Med.Res.*, 7(1):63–84, 1998.

[14] L. Sheiner and J. Wakefield. Population modelling in drug development. *Stat.Methods Med.Res.*, 8(3):183–193, 1999.

[15] P. E. Kloeden and E. Platen. *Numerical Solutions of Stochastic Differential Equations, Second Edition.* Springer-Verlag. Heidelberg, 1995.

[16] B. Øksendal. *Stochastic Differential Equations, 4th Edition.* Springer-Verlag. Heidelberg, 1995.

[17] J. N. Nielsen, H. Madsen, and P. C. Young. Parameter Estimation in Stochastic Differential Equations: An Overview. *Annual Reviews in Control*, 24:83–94, 2000.

[18] J. Bak, H. A. Nielsen, and H. Madsen. Goodness of fit of stochastic differential equations. *21. Symp. Applied Statistics, ISBN 87-90117-24-7*, 1999.

[19] N. R. Kristensen, H. Madsen, and S. B. Jørgensen. Parameter Estimation in Stochastic Grey-Box Models. *Automatica*, 40:225–237, 2004.

[20] J. E. Dennis and R. B. Schnabel. *Numerical Methods for Unconstrained Optimization and Nonlinear Equations.* Prentice-Hall, NJ, 1983.

[21] J. N. Nielsen and H. Madsen. Applying the EKF to stochastic differential equations with level efects. *Automatica*, 37:107–112, 2001.

[22] A. Capderou, D. Douguet, T. Similowski, A. Aurengo, and M. Zelter. Non-invasive assessment of technetium-99m albumin transit time distribution in the pulmonary circulation by first-pass angiocardiography. *Eur.J.Nucl.Med.*, 24(7):745–753, 1997.

[23] P. Magni, R. Bellazzi, G. De Nicolao, I. Poggesi, and M. Rocchetti. Nonparametric AUC estimation in population studies with incomplete sampling: a Bayesian approach. *J.Pharmacokinet.Pharmacodyn.*, 29(5-6):445–471, 2002.

Table I: Summary of the Likelihood Evaluation Algorithm

Function: Approximate Individual *a posteriori* Log-Likelihood (l_i)	
$1:$	Function of $\boldsymbol{\eta}_i$ given ($\boldsymbol{\Sigma}$, $\boldsymbol{\sigma}_w$, $\boldsymbol{\Omega}$, $\boldsymbol{\theta}$, $\boldsymbol{Z}_i$, $\boldsymbol{d}_i$, and $\mathcal{Y}_{in_i}$)
$2:$	Use (4) to compute $\boldsymbol{\phi}_i$
$3:$	Initialize the state prediction and state covariance.
	See the numerical implementation below.
$4:$	Use EKF in Appendix A to compute $\boldsymbol{\epsilon}_{ij}$ and $\boldsymbol{R}_{i(j|j-1)}$
$5:$	**Return** l_i as computed in (15)

Function: Approximate Population Likelihood (L)	
$1:$	Function of ($\boldsymbol{\Sigma}$, $\boldsymbol{\sigma}_w$, $\boldsymbol{\Omega}$, and $\boldsymbol{\theta}$) given $\boldsymbol{Z}_i$, $\boldsymbol{d}_i$, and all observations
$2:$	**For** $i = 1$ to N **do**
$3:$	$\hat{\boldsymbol{\eta}}_i = \arg\min(\boldsymbol{l}_i)$
$4:$	Use EKF in Appendix A to compute $\boldsymbol{\epsilon}_{ij}|_{\hat{\boldsymbol{\eta}}_i}$, $\nabla\boldsymbol{\epsilon}_{ij}|_{\hat{\boldsymbol{\eta}}_i}$, and $\boldsymbol{R}_{i(j|j-1)}|_{\hat{\boldsymbol{\eta}}_i}$
$5:$	Use (18) and (19) to compute $\boldsymbol{l}_i|_{\hat{\boldsymbol{\eta}}_i}$ and $\triangle\boldsymbol{l}_i|_{\hat{\boldsymbol{\eta}}_i}$
$6:$	**end for**
$7:$	**Return** $L(\boldsymbol{\theta}, \boldsymbol{\Sigma}, \boldsymbol{\sigma}_w, \boldsymbol{\Omega})$ as computed in (17)

22

Table II: Statistics of the estimation performance when simulating experiments with 100 individuals each sampled 3 times.

	V	CL	ω_V	ω_{CL}	σ_w	σ_e
Simulated value	10	0.5	0.2	0.2	0.2	0.1
Mean of estimates	10.02	0.508	0.195	0.195	0.198	0.102
Standard deviation of estimates	0.212	0.015	0.016	0.035	0.037	0.010
Mean of standard error estimates	0.220	0.014	0.018	0.035	0.046	0.011

Table III: Algorithm for the Extended Kalman Filter

Algorithm: Kalman Filtering
1: Given parameters and initial prediction $\boldsymbol{\phi}$, $\hat{\boldsymbol{x}}_{1\|0}$ and $\boldsymbol{P}_{1\|0}$
2: **For** $j = 1$ to n_i **do**
3:     Use (29) and (30) to compute, $\hat{\boldsymbol{y}}_{j\|j-1}$ and $\hat{\boldsymbol{R}}_{j\|j-1}$.
4:     Use (33) to compute the Kalman Gain, $\boldsymbol{K}_j$
5:     Use (31) and (32) to compute updates, $\hat{\boldsymbol{x}}_{j\|j}$ and $\boldsymbol{P}_{j\|j}$
6:     Use (34) and (35) to compute $\hat{\boldsymbol{x}}_{(j+1)\|j}$ and $\boldsymbol{P}_{(j+1)\|j}$
7: **end for**
8: **Return** (for all j) $\boldsymbol{\epsilon}_j = \boldsymbol{y}_j - \hat{\boldsymbol{y}}_{j\|j-1}$ and $\boldsymbol{R}_{j\|j-1}$

24

Paper C

Mathematical Beta Cell Model for Insulin Secretion following IVGTT and OGTT

Mathematical Beta Cell Model for Insulin Secretion following IVGTT and OGTT

Rune V. Overgaard[1,2,3], Katarina Jelic[2], Mats Karlsson[3], Jan Erik Henriksen[4] and Henrik Madsen[1]

Running title: Secretion Model for IVGTT and OGTT

From [1]Informatics and Mathematical Modelling, Technical University of Denmark; [2]Novo Nordisk A/S, Måløv, Denmark; [3]Dept. of Pharmaceutical Biosciences, Uppsala University, Sweden; [4]The Diabetes Research Centre, Department of Endocrinology M, Odense University Hospital, Denmark.

Address correspondence and reprint requests to Rune V. Overgaard: rvo@imm.dtu.dk. tel: +45 30 24 78 76; fax: +45 45 88 26 73

Abstract

Evaluation of beta cell function is conducted by a variety of glucose tolerance tests and evaluated by a number of different models with less than perfect consistency among results obtained from different tests. We formulated a new approximation of the distributed threshold model for insulin secretion in order to approach a model for quantifying beta cell function, not only for one, but for several different experiments. Data was obtained from 40 subjects that had both an oral glucose tolerance test (OGTT) and an intravenous tolerance test (IVGTT) performed. Parameter estimates from the two experimental protocols demonstrate similarity, reproducibility, and indications of prognostic relevance. Useful first phase indexes comprise the steady state amount of ready releasable insulin A_0 and the rate of redistribution k_{rd}, where both yield a considerable correlation (both r=0.67) between IVGTT and OGTT estimates. For the IVGTT, A_0 correlates well (r=0.96) with the 10 min area under the curve of insulin above baseline, whereas k_{rd} represents a new and possibly more fundamental first phase index. For the useful second phase index γ, a correlation of 0.75 was found between IVGTT and OGTT estimates.

Keywords: Parameter estimation; Pancreatic beta cell; Mixed-effects; Physiological models

Abbreviations: AUC, area under the curve; BG, baseline glucose; BOV, between occasion variability; BSV, between subject variability; CV, coefficient of variation; FDR, first degree relatives to patients with diabetes; HGC hyperglycaemic clamp; IVGTT, intravenous tolerance test; MTT, meal tolerance test; OGTT, oral glucose tolerance test; RRI, ready releasable insulin; RRP, ready releasable pool; SE, standard error.

INTRODUCTION

Type 2 diabetes is a heterogeneous disorder characterized by a combination of impaired insulin secretion and insulin resistance[1], in which either factor can be dominant. Of these interrelated subjects, the present work deals with the assessment of beta cell function, which relative to insulin resistance must be impaired for development of type 2 diabetes, and may even represent the primary factor predisposing individuals to type 2 diabetes[2]. Insulin secretion in response to an abrupt increase in plasma glucose is known to be biphasic with a rapid peak at 2-4 min (first-phase), decrease to nadir at 10-15 min, and then gradually increase within the next couple of hours (second-phase). Early insulin release after glucose ingestion is a key determining factor for the subsequent glucose concentration[3], indicating that a reduced first-phase may be responsible for the development of impaired glucose tolerance[4].

Evidently, diagnostic tests for the assessment of insulin secretion as well as insulin resistance have great value for epidemiological and clinical studies. The most common oral administration tests are the oral glucose tolerance test (OGTT) and the meal tolerance test (MTT), whereas the most common intravenous (IV) tests are the intravenous glucose tolerance test (IVGTT) and the hyperglycemic clamp (HGC). Several descriptive mathematical models and model based methods have been proposed to calculate indexes for characterization of beta cell function from the various tests[5-8]. Although useful for the analysis of a specific experiment type, the models can rarely be used across different tests, and similar indexes obtained from different experiments are not necessarily in agreement, leading to the conclusion that further work is needed for these indexes to be routinely used in clinical and epidemiological studies[9].

Besides descriptive models for characterization, more comprehensive mathematical models[10-12] have been used to communicate and increase the understanding of the physiological mechanisms behind insulin secretion[13]. Of these, the distributed threshold hypothesis[11] has been used to argue and derive many of the descriptive models[14, 15]. However, to our knowledge, descriptive insulin secretion models up until now all fail to incorporate the fundamental mechanisms that have enabled the distributed threshold hypothesis to describe insulin secretion in response to a long series of glucose challenges, and hereby increase understanding of the beta cell function. In the present work we formulate a model that includes threshold distribution, redistribution, and incretin effects, and investigate the applicability of this model to data from the IVGTT and the OGTT. At a longer perspective, the present work is a step towards a model for characterizing beta cell function, not only for one, but for many of the glucose tolerance tests; with parameters that are closer related to the physiology than those of more empirical models.

Model development and evaluation was performed on data from 40 individuals[16, 17], where each subject had both an IVGTT and an OGTT performed. Indexes obtained from the OGTT were compared to those from the IVGTT in order to demonstrate parameter reproducibility and similarity, giving credit to the applicability of indexes, e.g. in epidemiological studies. Indication of prognostic relevance was demonstrated by the extreme parameter values found for 4 subjects that subsequent to the study have developed type 2 diabetes, also other such parameters exist[18].

RESEARCH DESIGN AND METHODS

A total of 40 healthy normoglycemic subjects had both an IVGTT and an OGTT performed; 20 subjects with no family history of diabetes and 20 first degree relatives (FDR) to patients with type 2 diabetes of which four subjects have developed type 2 diabetes themselves within 10 years of the initial investigation. The protocols were approved by the local Ethics Committee and informed written consents were obtained from all participants before testing both at the initial testing and at 10 years follow up. Clinical characteristics of the study populations are given in Table 1.

The OGTT was performed by ingestion of 75 g glucose in a liquid solution. Blood samples were obtained in the fasting state (three samples) and for a total of 3 h following the glucose load (15 samples). The IVGTT was performed, with an infusion of a 25% solution of glucose (300 mg of glucose per kg body weight (max 25 g)) being given over 1 minute, immediately followed by a saline flush (50 ml). Time zero was taken as the start of the glucose bolus and samples were collected at -30, -20, -10, -1, 2, 3, 4, 5, 6, 8, 10, 12, 14, 16, 19, 22, 25, 30, 40, 50, 60, 70, 80, 90, 100, 110, 120, 140, 160 and 180 minutes, for determination of plasma glucose and insulin. Plasma glucose concentration was measured at the bedside by the glucose oxidase method with a Glucose Analyzer (Beckman Instruments, Inc., Fullerton, Calif., USA). Blood samples for plasma insulin were immediately centrifuged at 4 °C at the time of study and stored at -20 °C until analysis and concentrations measured by a double antibody radioimmunoassay in duplicate (Kabi Pharmacia Diagnostics AB, Uppsala, Sweden)

Model description

Background. The distributed threshold hypothesis[11] successfully explains the dose dependent first phase insulin release following IV glucose administration with a pool of insulin stored in packets. According to this hypothesis, different packets have different thresholds, secreting insulin only when glucose concentration has exceeded this threshold. Changes in plasma glucose concentration will alter the distribution of insulin in the packets, while provision of new insulin and redistribution of insulin among packets ensures convergence toward steady state when glucose concentration is constant. In principle, each packet corresponds to a compartment, yielding a complicated numerical problem with a large number of coupled differential equations. The present simplification lump all active packets together and all passive packets together to a two-compartment system. A mathematical analysis of the differences and approximation between the present model and the distributed threshold model is given in Appendix A, whereas the following list summarizes the main differences:

1. Steady state provision was modeled with a sigmoid Emax function instead of the more complicated parametric function used in[11].
2. Incretin effects during the OGTT were implemented for provision and packet activation.
3. The flow of insulin between passive and active packets is modeled to be unidirectional, i.e. all ready releasable insulin is released from an active packet before it is deactivated.
4. Redistribution was modeled to involve random activation rather than random change of threshold, see Appendix A.
5. All passive packets were approximated to contain the same amount of insulin.

The central approximation is that all passive packets contain the same amount of insulin. This will not be influential during simple glucose challenge tests, where glucose is single peaked. But for

multiple glucose peaks, e.g. for glucose oscillations, the response of the threshold distribution hypothesis will be different from that of the present model.

Model Equations. As illustrated in Figure 1, the model can be divided into four components, 1) provision of new insulin, 2) a pool of ready releasable insulin (RRI), i.e. insulin in passive packets available for quick release as a consequence of abruptly increasing glucose concentrations, 3) a pool of insulin in active packets, which is quickly being released, and 4) a plasma compartment that represents insulin pharmacokinetics.

The provision, P of new insulin is typically written as,

$$\frac{d}{dt} P = -\alpha (P - P(G, \infty))$$

$P(G, \infty)$ is the glucose dependent steady state provision, described below. Glucose (G) is implemented as the linear interpolation between measured concentrations of plasma glucose, except during the time interval between -1 and 1 min, where the baseline glucose (BG) value was used to ensure that the interpolated glucose does not rise prior to glucose administration at time zero[15]. When the system is not at steady state, e.g. due to rapid changes in glucose, P(t) will be different from P(G, ∞). Whereas changes in P(G, ∞) are immediate, the changes in P will be delayed with time constant α, leading to smooth changes. Note that this delay is not the only contributing factor to the delay in the second phase insulin response, see Appendix B.

Oral ingestion of nutrients is known to enhance insulin secretion, the incretin effect, leading to higher insulin secretion during an OGTT than from an experiment with matched glucose concentrations obtained by IV infusion of glucose[19]. The incretin effect is mediated by insulinotropic intestinal hormones, as e.g. glucagon-like peptide-1, which enhances both first and second phase release, see e.g. the experiments by Fritsche et al.[20], and consequently also the provision. We have

$$P(G, \infty) = \frac{E_{max} G^h}{EC_{50}^h + G^h} + E_{OGTT} \frac{[G - BG]^+}{AUC_{G-BG}}$$

where the last term is the incretin effect, modeled with glucose above BG as a surrogate for incretin hormones, which are rarely measured in the OGTT. $[G\text{-}BG]^+$ is the maximum of zero and $(G\text{-}BG)$, and $AUC_{G\text{-}BG}$ is the area under the curve (AUC) of $[G\text{-}BG]^+$. EC_{50} is calculated via the initialization given below. E_{OGTT} is the effect parameter for the incretin effect in an OGTT, which is zero for an IVGTT.

The two-compartment model for the passive and active pool, as derived in appendix A, can be written:

$$\frac{d}{dt}I_{passive} = (1 - f(G))P - k_{rd}I_{passive} - Ph_1$$

$$\frac{d}{dt}I_{active} = f(G)P + k_{rd}I_{passive} + Ph_1 - mI_{active}$$

$$SR = mI_{active}$$

$$f(G) = G^{h_2}/(G^{h_2} + FC_{50}^{h_2})$$

$$FC_{50} = BG(^{1-F_{BG}}\!/\!_{F_{BG}})^{1/h_2}$$

where $I_{passive}$ is the total amount of insulin in packets with thresholds above G, and I_{active} is the amount in the active packets contributing to the total secretion rate SR. $f(G)$ is the threshold distribution function, i.e. the fraction of active packets at a certain glucose concentration. FC_{50} is the glucose concentration that activates 50% of the packets, F_{BG} is the fraction of packets activated at baseline, and h_2 is the hill coefficient. The phase 1 component, Ph_1, is the rate of insulin removal from the passive to the active packets caused by packet activation due to rising glucose concentration. The assumption that all passive packets contain the same amount of insulin allow us to calculate Ph_1 as the amount of insulin per passive packet $I_{passive}/N(1\text{-}f(G))$ times the rate of packet activation $N \cdot df(G)/dt$, where N is the total number of packets. Ph_1 is:

$$Ph_1 = \begin{cases} I_{passive}\dfrac{f'(G)\frac{d}{dt}G}{1 - f(G)} & \text{for } (\tfrac{d}{dt}G > 0) \\ 0 & \text{for } (\tfrac{d}{dt}G \le 0) \end{cases}$$

Ph_1 is seen to be sensitive to glucose changes, giving us a first phase insulin release when glucose concentration increases abruptly. Incretin effects on the first phase release are explained by increased packet activation with oral glucose administration, which is implemented through two different values of h_2 in the OGTT and the IVGTT, h_{OGTT} and h_{IVGTT}.

Plasma insulin concentration is computed assuming first order elimination,

$$\frac{d}{dt}I_{plasma} = SR/V - k_I I_{plasma}$$

where I_{plasma} is the plasma concentration of insulin. V is the apparent volume of distribution for insulin, and k_I is the elimination rate constant. Since V and E_{max} (and E_{OGTT}) can be shown not to be simultaneous identifiable, V was fixed to the plasma volume (3l), which is slightly higher than typical estimates of the central volume of distribution[21].

Model implementation. The model was implemented as a non-linear mixed-effects model in NONMEM V with FOCE[22].

Parameters to be estimated: k_I, α, E_{max}, h, E_{OGTT}, k_{rd}, m, F_{BG}, h_{IVGTT}, and h_{OGTT}, are described in Table 2. E_{max}, k_{rd}, and E_{OGTT} exhibit between subject variability (BSV) by the proportional model, $\theta\exp(\eta)$, and F_{BG} exhibit BSV via the logistic function, $FBG = \exp(\theta + \eta)/(1 + \exp(\theta + \eta))$ to ensure values between zero and one, where θ is the fixed effect and η is a Gaussian random effect that varies between individuals. Data from the OGTT and the IVGTT were treated as if it was from different individuals, such that no false correlation is introduced in the parameter estimates from the two trials.

Observed (y) and predicted insulin plasma concentrations (I_{plasma}) were log-transformed for the residuals ε to be Normal distributed, i.e.

$$\log(y) = \log(I_{plasma}) + \varepsilon$$

Initialization. The model is initiated in steady state, under the assumption that BG has produced a steady state provision corresponding to the baseline insulin concentration I_0, where BG/I_0 is calculated as the average of measured glucose/insulin concentrations prior to glucose administration. Initialization in steady state allow us to utilize the steady state equation to calculate EC_{50},

$$EC_{50} = BG\left(\frac{E_{max}}{I_0 Vk_I} - 1\right)^{1/h}$$

Indexes. The amount of RRI in the ready releasable pool (RRP) is known to change according to the history of glucose concentration[13], whereas the size of the pool at fasting, i.e. the initial amount of insulin in the passive compartment A_0 is suggested as a first phase index. In the presented model, A_0 is not estimated directly, but derived using the following equation,

$$A_0 = I_0 Vk_I \frac{1 - F_{BG}}{k_{rd}}$$

It proved useful also to present a derived second phase index γ, which is the slope of the incretin independent part of the steady state provision with respect to glucose at BG, similar to indexes of other insulin secretion models[5, 6]. γ is computed by,

$$\gamma = \frac{E_{max} hBG^{h-1} EC_{50}^h}{(BG^h + EC_{50}^h)^2}$$

Model development. Different models were discriminated based on, robustness, likelihood function value, ability to capture individual insulin profiles, reproducibility, bias of parameter estimates compared to known physiological values, bias in the predictions made by the typical set of parameters, and whether the implementation seemed physiologically reasonable.

Based on the listed criteria for model selection, a number of incretin effects on the first phase in the OGTT were attempted and discarded. These attempts include: 1) no first phase incretin effect, 2) some packets were activated during the OGTT only, 3) the Ph_1 input to passive packets was elevated compared to removal from passive packets, corresponding to recruitment of insulin from packets not contributing to steady state secretion, 4) glucose above baseline or transit compartment functions was used to elevate packets activation.

The described implementation of incretin effects for the second phase was chosen above the following list of discarded attempts. 1) transit compartments were used to model an incretin profile, 2) proportional rather than additive incretin effects, 3) incretin effects directly on the provision

rather than on the steady state provision, 4) separate levels of E_{max} and/or hill coefficient h were used for the IVGTT and OGTT.

Besides investigations of different structural models, several combinations of between-subject variation were tested. BSV on the hill coefficients were judged to run unstable, whereas BSV on α and k_I worsened the correlation between IVGTT estimates and OGTT estimates, possibly because individual values of α and k_I cannot be estimated robustly from the OGTT.

Results

The estimated typical parameter values for the study population are presented in Table 3, along with the standard error (SE) of the estimate and the coefficient of variation (CV) between subjects in the study.

Model predictions. Two kinds of model predictions are calculated for this model, 1) individual predictions are based on the individually estimated parameter values, and 2) population predictions utilize the typical parameter values to compute a typical insulin concentration profile for a given glucose profile. The geometric mean of the individual- and the population- predictions are compared to data in Figure 2, demonstrating ability of the model to capture differences between insulin response in the OGTT and the IVGTT.

Reproducibility and similarity of parameters. Parameter estimates obtained from the IVGTT are plotted against those obtained from the OGTT in Figure 3, and the correlation coefficients between estimates are presented (for parameters plotted on a log-scale the correlation coefficient for the log-transformed parameters are presented). γ, A_0, k_{rd}, exhibit a clear correlation between experiments (correlation coefficient around 0.7), whereas FC_{50}, F_{BG}, and E_{max} demonstrate an intermediate correlation (correlation coefficient around 0.5). The high degree of correlation demonstrates parameter reproducibility, in the sense that subjects characterized with high values in one experiment are most likely associated with high values in the other experiment. All parameters except FC_{50} are close to the line of unity, demonstrating similarity of the parameter values, giving a hint to a similar physiological origin of parameters from the different experiments. The bias in FC_{50} is due to the implemented incretin effect, where a higher hill coefficient results in a higher fraction of packet activation when glucose starts to rise, resulting in a decrease in the level of glucose necessary to activate 50% of the packets.

Prognostic indexes. The four subjects that subsequent to the study have developed type 2 diabetes are associated with a low A_0, a low F_{BG}, a high FC_{50}, and a high k_{rd}, especially k_{rd} for which all exhibited a high value. For the second phase, a low E_{max} seems to indicate diabetes for the OGTT, but not for the IVGTT, whereas γ and EC_{50} does not appear to be particularly predictive. As expected, also more descriptive indices, such as high BG and high AUC for glucose above BG, appear to implicate higher risk for development of type 2 diabetes. Of the four subjects in a pre-diabetic state, the one with lowest BG was found to have the lowest A_0 among the total study population, see Figure 4, indicating that the first phase indexes (A_0, k_{rd}, and F_{BG}) carry separate prognostic information to that of BG.

Discussion

We have suggested a new approximation of the distributed threshold hypothesis for parameter estimation that conserves fundamental mechanisms of threshold distribution, active and passive packets, and redistribution among packets. Effects of incretin hormones were included on packet activation and provision of insulin, to allow quantification of beta cell function, both for the IVGTT and the OGTT. The parameter estimates exhibited similarity and reproducibility, and several parameters are promising candidates for an early diagnostic for development of type 2 diabetes. However, in spite of the usefulness, the reproducibility was less than perfect, which deserves some discussion.

Reproducibility. Three factors can be named to cause reduced correlation, as that observed between some of the parameter estimates in Figure 3.

1) Between-occasion variability (BOV). For example, the less then perfect correlation of BG (r=0.70) and I_0 (r=0.76), must be caused by BOV.

2) Suboptimal design, e.g. timing of measurements and chosen glucose administration. Compared to the IVGTT, the OGTT exhibit some technical design problems: a) inevitably, incretin and plasma glucose effects occur over the same time period, making them difficult to separate. b) Glucose rises slowly, making separation of first and second phase difficult. c) Glucose elevation is lower, making estimation of E_{max} difficult.

3) Lacking physiological precision, in the sense that parameters in the OGTT and the IVGTT have separate physiological meanings. However, the similarity in parameter values obtained from the OGTT and IVGTT indicates that this last point is not a dominant issue.

Sampling design. In analogy with other models[7], the robustness of the individual parameter estimates in the OGTT were investigated for different sampling designs, and similar conclusions were obtained, i.e. the accuracy of the first phase parameter estimates drops significantly when fewer measurements are included around times 0-50 min. The original design includes sampling at (0, 5, 10, 15, 20, 30, 40, and 50 min). When sustaining the (0, 10, 20, and 30 min) samples, the first phase indexes (A_0 and k_{rd}) are robust, with high correlation to the original estimates (r~0.95). This correlation is reduced to (r~0.86), when using only the (0, 20, and 40 min) samples, and to (r~0.77) when using only the (0 and 30 min) samples. Also the estimates of E_{OGTT} and E_{max} were sensitive to reduced sampling design.

Second phase indexes. γ and E_{max} were highly correlated for the IVGTT (r=0.85), but less correlated in the OGTT (r=0.52). Whereas E_{max} was estimated, the introduction of γ was motivated by 1) γ is theoretically similar to previous successful second phase indexes[5, 6], 2) a simulation study verified that γ is more robustly estimated than E_{max} in the OGTT, which is also seen as a higher correlation in Figure 3. Both parameters were well estimated from the IVGTT, indicating design problems with the OGTT. 3) A clear relationship exists between parameter estimates of E_{max} and E_{OGTT}, but not between γ and E_{OGTT}.

Incretin effect. For the OGTT, glucose above baseline exhibit similar dynamics as incretin hormones, see e.g. experiments by Rask et al.[23], and was found the best available surrogate for their effect. However, the implementation leads to suspicion concerning the physiological origin (glucose or incretin hormones) of E_{OGTT}. Three observations indicate successful estimation of the incretin effects: 1) the similarity of E_{max} and γ estimates obtained in the IVGTT and the OGTT. 2) No correlation was found between E_{OGTT} and AUC_{G-GB}, which would be expected if glucose alone was causing what was estimated as incretin effects. 3) A simulation study confirmed that γ and E_{OGTT} can be estimated simultaneously from the OGTT, with a correlation between simulated and estimated values of (r=0.9) for γ and (r=0.95) for E_{OGTT}.

First phase indexes. The AUC of insulin above I_0 during the first 10 minutes after glucose administration has been used as an index for first phase secretion[24]. This index correlated with A_0 (r=0.96), k_{rd} (r=-0.63), and F_{BG} (r=-0.30), demonstrating a clear difference between the three indexes, where A_0 clearly represents the more traditional first phase index.

Insulin response to glucose in the OGTT has previously been successfully described by a static and a dynamic index ϕ_D[7], where ϕ_D depend on the derivative of glucose, which is similar to Ph_1 in the present model. An insulin based calculation of ϕ_D demonstrated that ϕ_D and A_0 obtained from the OGTT correlates equally well to the 10 min AUC of insulin above baseline for the IVGTT (r=0.65) and (r=0.67). However, compared to previous models, the present model brings new and potentially important indexes to describe beta cell function.

Does redistribution represent a fundamental factor for beta cell dysfunction? Under the assumption that packets represent beta cells, as eluded to in other work[25], redistribution would be the activity of passive cells, e.g. by random activation, so that fast redistribution will represent a high frequency of cells releasing their content. Note that the precise formulation of redistribution has changed slightly compared to the distributed threshold model, see appendix A, and that redistribution has not yet been understood in a cell biological framework. In the whole body system, glucose is known to have potentiating effects on the first phase release[11], and redistribution is a likely mechanism for the normalization of an elevated RRP, making k_{rd} a determining factor for the steady state RRP. Since provision of insulin to the RRP is necessary, steady state provision is another likely determining factor for the steady state RRP. For subjects 1-4 in Figure 3, k_{rd} is large and A_0 is small, but k_{rd} is more pronounced than A_0, which could indicate that redistribution is the more fundamental factor for beta cell dysfunction. This makes sense, since A_0 depend upon baseline provision, which is known to increase during development of insulin resistance. Hence, A_0 may be a composite index, influenced in opposite directions by beta cell dysfunction and insulin resistance, whereas k_{rd} may be a more fundamental factor for beta cell dysfunction.

Provision. The provision of insulin to the RRP is a simple function of glucose that lump a number of intracellular processes together, such as the glucokinase, up regulation of proinsulin, and increased formation of new insulin granules. This clear approximation of reality means that the rate constant α and E_{max}, may not be valid for other experiments on longer time horizons.

Threshold Distribution. In the light that some[25-27] believe heterogeneity in beta cells activation threshold to cause the biphasic insulin release, this heterogeneity should relate to the estimated threshold distribution. In fact, under the assumption that the potential size of the RRP in each beta cell is identical, the estimated distribution of thresholds and the measured distribution of activated beta cells should be identical. Some experiments have found that 53% of beta cells secreted

detectable amounts of insulin at 5.6 mM glucose[28], which is in the high end of the range of individual estimates of F_{BG} between 0.1 and 0.6. Two concerns for this comparison are that 1) redistribution from passive cells could also lead to insulin secretion, allowing some passive cells to be estimated as active, 2) oscillations of insulin secretion could interfere with the estimated activity frequency, which is not accounted for in the model.

It is worth noting that redistribution was estimated more robustly than F_{BG}, and also that the inclusion of BSV on redistribution was more important than for F_{BG}, to explain variations in the first phase response, possibly indicating a higher degree of uncertainty in the estimated values for F_{BG}.

Individual secretion profiles. In Figure 5, individual and population predictions are compared to data for a few selected individuals. For subject 1 to 3, a small RRP was estimated for both experiments, corresponding to a lower than typical first phase for the IVGTT, and a lower than typical quick increase in plasma insulin concentration for the OGTT. Both subject 1 to 3 have developed type 2 diabetes post study, which is in agreement with the common understanding that a low first phase secretion is an early diagnostic marker for type 2 diabetes. Also subject 4 has developed type 2 diabetes, but for this individual the first phase response appears normal, and A_0 is among the highest 50%. Interestingly, this individual was associated with a relatively low F_{BG} (among the lowest 30%) and a relatively high k_{rd} (among the highest 30%), which should indicate a low first phase. The apparent slightly above normal first phase originates from the provision of new insulin at baseline glucose, for which the subject 4 had the largest value among the 40 subjects. Subject 5 and 6 exhibit an above average amount of RRI, and as expected none of these have developed diabetes. Subject 6 has an E_{max} around average in both experiments and E_{OGTT} was the second largest in the study, explaining why insulin concentrations during the later stage of the IVGTT are close to typical, while they are far above the population predictions in the OGTT.

Using insulin vs. C-peptide for assessment of beta cell function. Beta cells release an equimolar mixture of insulin and C-peptide, but C-peptide is cleared slower from plasma and does not suffer the same first pass effect of the liver, hence C-peptide has been used in many models and model based methods to asses beta cell function[6]. In the absence of C-peptide data, the present analysis was performed using insulin data, so the obtained secretion rate reflects a post hepatic secretion. One advantage of the higher elimination rate of insulin is that changes in secretion lead to more pronounced changes in plasma concentration, which we believe to produce high estimation accuracy.

Limitations and potential future implementations. The presented method uses data from the IVGTT and the OGTT simultaneously to find all parameters. In order to use the model for estimation in a single experiment, it may be necessary to use Bayesian techniques or to fix some parameters. In our analysis, we modeled the OGTT alone by fixing some parameters to the values found by the simultaneous analysis, while estimating only parameters with BSV.

The present model is developed from oral and intravenous administration of glucose, using data within 3 hours of glucose administration. If one wish to model longer experiments or use other combinations of nutrients, then the limitations of the model in its present formulation has been exceeded. Compared to more empirical beta cell models, one advantage of the present more mechanistic model is that it can more naturally be extended and adjusted to account for new situations. Fruitful model extensions and adjustments could possibly include: 1) a description of

other experiments such as the HGC, to include new features at sustained high glucose challenges 2) model extensions to include simultaneous models of the MTT and the OGTT could possibly describe the incretin effects from various compositions and amounts of nutrients, and possibly link the incretin effect to measured incretin hormones, 3) model extensions that include a triple meal test could investigate whether the potentiating effects of insulin release[29] is caused by the RRP, or possibly another pool, 4) modeling of the modified IVGTT, to test whether the large tolbutamide driven insulin release can be related to the RRP included in the model, 5) extensions to include covariates for characterization of differences between patient populations, and 6) during development of drugs that target beta cells, description, understanding, and predictions of results in future trial designs could be aided by the presented model.

Conclusion. A new approximation of the distributed threshold hypothesis has been formulated, and it was verified that it can be used for parameter estimation of the IVGTT and the OGTT. With this initiative, we approach a population model for quantification of beta cell function that can be used for several of the different tolerance tests available. The present work focused on similarity, reproducibility, and prognostic relevance of individual parameters estimated from an IVGTT and an OGTT, for which validation further included comparison to other indexes, simulation studies, and prediction of individual profiles. First phase indexes comprise the steady state amount of ready releasable insulin, similar to traditional first phase indexes, and the rate of redistribution, which represents a new and possibly more fundamental first phase index. The most useful second phase index γ is theoretically similar to the second phase index of other models, and it is precisely estimated for the IVGTT, and to some extend believed separable from the incretin effects of the OGTT. Lack of perfect correlation between parameters estimates from the two experiments is likely caused by between-occasion variability, and by the design of the OGTT, which yield more imprecise parameter estimates, but enables estimation also of the incretin effect.

Appendix A

In the present appendix we use the original threshold distribution hypothesis[11] to derive the equations for the active and passive amounts of insulin presented in the main text. This derivation involves three approximations/alterations to the original model that can be applied in arbitrary order, for instance as described below.

The fundamental hypothesis in the original distributed threshold model is that the readily releasable insulin is stored in small packets, where the different packets have different thresholds, secreting insulin into the plasma only when the glucose concentration has exceeded this threshold. The amount of readily releasable insulin in packets with threshold between θ and $\theta+d\theta$ is given by $\xi(\theta,t)d\theta$, so the threshold density distribution function can be used to model the total secretion into plasma. The original distributed threshold model[11], can be written as,

$$\frac{d\xi(\theta,t)}{dt} = -m\xi(\theta,t)H(G-\theta) + f'(\theta)P(G,t) - k_{rd}\xi(\theta,t) + k_{rd}f'(\theta)\int_0^\infty \xi(\theta',t)d\theta'$$

$$SR = m\int_0^G \xi(\theta',t)d\theta'$$

The secretion of insulin into the plasma is realized through the first term, where $H(\cdot)$ is the Heaviside function. The second term is the provision of new insulin, and the last two terms are named redistribution terms corresponding a random change of thresholds of the different packets. Note that $f'(\theta)=d/d\theta\ f(\theta)$, is the distribution density function. In the original analysis glucose started at zero, so that $f'(\theta)$ gives the initial insulin distribution density function $\xi(\theta,0)$.

$I_{passive}$ and I_{active} can be written as,

$$I_{passive} = \int_{G}^{\infty} \xi(\theta',t)d\theta' \quad ; \quad I_{active} = \int_{0}^{G} \xi(\theta',t)d\theta'$$

The differential equations for $I_{passive}$ and I_{active} can be derived analytically,

$$\frac{d}{dt}I_{passive} = (1-f(G))P - k_{rd}(1-f(G))I_{passive} + k_{rd}f(G)I_{active} - \xi(G,t)\frac{dG}{dt}$$

$$\frac{d}{dt}I_{active} = -mI_{active} + f(G)P + k_{rd}(1-f(G))I_{passive} - k_{rd}f(G)I_{active} + \xi(G,t)\frac{dG}{dt}$$

The first suggested alteration to the distributed threshold involves unidirectional flow of insulin from passive packets to active packets. Note that the beta cell action potential will either spike or not, where a spike will lead to exocytosis. It is not possible to stop the spike by a decrease in glucose and thereby stopping exocytosis of insulin that is currently being released, motivating a unidirectional flow. Whereas this change does simplify the model structure, the rate constant m is so large that it does not alter the results. We get,

$$\frac{d}{dt}I_{passive} = (1-f(G))P - k_{rd}(1-f(G))I_{passive} - \xi(G,t)\frac{dG}{dt}H(\frac{dG}{dt})$$

$$\frac{d}{dt}I_{active} = -mI_{active} + f(G)P + k_{rd}(1-f(G))I_{passive} + \xi(G,t)\frac{dG}{dt}H(\frac{dG}{dt})$$

In the distributed threshold model, redistribution can be understood as a random change in the sensitivity to glucose, where passive packets may change threshold but still be passive. This formulation is slightly changed. In the present model, redistribution involves random activation of packets, in the sense that a passive packet may by a random mechanism release all insulin in its ready releasable pool, and then return to the passive state. By this mechanism, redistribution will not decrease to zero when all packets are passive. The equations become,

$$\frac{d}{dt}I_{passive} = (1-f(G))P - k_{rd}I_{passive} - \xi(G,t)\frac{dG}{dt}H(\frac{dG}{dt})$$

$$\frac{d}{dt}I_{active} = -mI_{active} + f(G)P + k_{rd}I_{passive} + \xi(G,t)\frac{dG}{dt}H(\frac{dG}{dt})$$

The two alternative models for redistribution were compared during model development, and the chosen formulation produced superior correlations between OGTT and IVGTT parameter estimates,

superior objective function value, and was numerically more robust when changing initial estimates in the estimation.

The central approximation in the present approach is that all passive packets contain the same amount of insulin, so that $\xi(G,t) = I_{passive}f(G)/(1-f(G))$. This approximation will not be influential during simple glucose challenge tests, where glucose is single peaked. But if a second and identical peak is seen immediately after the first peak, the threshold distribution hypothesis will predict the second peak to give no first phase, because the passive packets involved are empty, whereas the present approximation will predict a nonzero first phase, since all passive packets contain the same amount of insulin. This difference may be of particular relevance for predictions of insulin response to rapid oscillations in glucose. Following this approximation we get the equations for the amount of insulin in the passive and active packets that were presented in the main text,

$$\frac{d}{dt}I_{passive} = (1-f(G))P - k_{rd}I_{passive} - \frac{I_{passive}f(G)}{1-f(G)}\frac{dG}{dt}H(\frac{dG}{dt})$$

$$\frac{d}{dt}I_{active} = -mI_{active} + f(G)P + k_{rd}I_{passive} + \frac{I_{passive}f(G)}{1-f(G)}\frac{dG}{dt}H(\frac{dG}{dt})$$

Appendix B

The present appendix provides the exact solution to the amount of insulin in the passive and active packets following a step increase in glucose from G_1 to G_2, at time t = 0. Starting at the steady state solution:

$$P(0^-) = P(G_1,\infty)$$

$$I_{passive}(0^-) = \frac{P(G_1,\infty)(1-f(G_1))}{k_{rd}}$$

$$I_{active}(0^-) = \frac{P(G_1,\infty)}{m}$$

For a step increase in glucose, the Ph_1 contribution can be computed via a Dirac delta-function,

$$Ph_1 = \frac{P(G_1,\infty)(f(G_2)-f(G_1))}{k_{rd}}\delta(t)$$

The amount of insulin in the passive packets can be computed as

$$I_{passive}(t) = \frac{(1-f(G_2))P(G_1,\infty)}{k_{rd}} + D(t) \qquad ; \qquad t > 0$$

$$D(t) = (1-f(G_2))(P(G_2,\infty) - P(G_1,\infty))\frac{\alpha(1-e^{-k_{rd}t}) - k_{rd}(1-e^{-\alpha t})}{k_{rd}(\alpha - k_{rd})}$$

where the first term reflects the immediate removal of insulin due to packet activation, corresponding to the first phase release. The second term $D(t)$ represents the elevation in the amount

of insulin in the passive packets coming from an elevated provision, i.e. the second phase contribution to the passive packets. α and k_{rd} constitute the two timescales for the second phase contribution. Since α is more than a factor 10 larger than k_{rd}, the main contribution of the delayed increase of the second phase comes from k_{rd}.

The amount of insulin in the active packets can be computed as,

$$I_{active} = \frac{P(G_1,\infty)}{m} + \frac{P(G_1,\infty)(f(G_2)-f(G_1))}{k_{rd}}e^{-mt} + D_2(t) \quad ; \quad t > 0$$

$$D_2(t) = e^{-mt}\int_0^t e^{mt}(f(G_2)(P(G_2,\infty)-P(G_1,\infty))(1-e^{-\alpha x})+k_{rd}D(x))dx$$

where the first term in I_{active} corresponds to the initial amount, the second term is the first phase contribution, and the third term D_2 gives the second phase contribution. Since m leads to a rather fast decay compared to the remaining time scales, it is reasonable to approximate $D_2(t)$ as,

$$D_2(t) \approx \frac{(P(G_2,\infty)-P(G_1,\infty))}{m}\left((f(G_2)(1-e^{-\alpha t})+(1-f(G_2))\frac{\alpha(1-e^{-k_{rd}t})-k_{rd}(1-e^{-\alpha t})}{k_{rd}(\alpha-k_{rd})}\right)$$

One part originates from the immediate increase in provision and another part originates from the steady increase in passive packets.

Reference List

1. expert committee. Report of the expert committee on the diagnosis and classification of diabetes mellitus. *Diabetes Care* 2003; **26 Suppl 1**:S5-20.

2. Gerich JE. Is reduced first-phase insulin release the earliest detectable abnormality in individuals destined to develop type 2 diabetes? *Diabetes* 2002; **51 Suppl 1**:S117-S121.

3. Bruce DG, Chisholm DJ, Storlien LH, Kraegen EW. Physiological importance of deficiency in early prandial insulin secretion in non-insulin-dependent diabetes. *Diabetes* 1988; **37**(6):736-744.

4. Del Prato S, Marchetti P, Bonadonna RC. Phasic insulin release and metabolic regulation in type 2 diabetes. *Diabetes* 2002; **51 Suppl 1**:S109-S116.

5. Toffolo G, Bergman RN, Finegood DT, Bowden CR, Cobelli C. Quantitative estimation of beta cell sensitivity to glucose in the intact organism: a minimal model of insulin kinetics in the dog. *Diabetes* 1980; **29**(12):979-990.

6. Toffolo G, De Grandi F, Cobelli C. Estimation of beta-cell sensitivity from intravenous glucose tolerance test C-peptide data. Knowledge of the kinetics avoids errors in modeling the secretion. *Diabetes* 1995; **44**(7):845-854.

7. Breda E, Cavaghan MK, Toffolo G, Polonsky KS, Cobelli C. Oral glucose tolerance test minimal model indexes of beta-cell function and insulin sensitivity. *Diabetes* 2001; **50**(1):150-158.

8. Mari A, Schmitz O, Gastaldelli A, Oestergaard T, Nyholm B, Ferrannini E. Meal and oral glucose tests for assessment of beta -cell function: modeling analysis in normal subjects. *Am.J.Physiol Endocrinol.Metab* 2002; **283**(6):E1159-E1166.

9. Steil GM, Hwu CM, Janowski R, Hariri F, Jinagouda S, Darwin C, Tadros S, Rebrin K, Saad MF. Evaluation of insulin sensitivity and beta-cell function indexes obtained from minimal model analysis of a meal tolerance test. *Diabetes* 2004; **53**(5):1201-1207.

10. Cerasi E. An analogue computer model for the insulin response to glucose infusion. *Acta Endocrinol.(Copenh)* 1967; **55**(1):163-183.

11. Grodsky GM. A threshold distribution hypothesis for packet storage of insulin and its mathematical modeling. *J.Clin.Invest* 1972; **51**(8):2047-2059.

12. O'Connor MD, Landahl H, Grodsky GM. Comparison of storage- and signal-limited models of pancreatic insulin secretion. *Am.J.Physiol* 1980; **238**(5):R378-R389.

13. Nesher R, Cerasi E. Modeling phasic insulin release: immediate and time-dependent effects of glucose. *Diabetes* 2002; **51 Suppl 1**:S53-S59.

14. Licko V, Silvers A. Open-loop glucose-insulin control with threshold secretory mechanism: analysis of intravenous glucose tolerance tests in man. *Math.Biosci.* 1975; **27**:319-332.

15. Overgaard RV, Henriksen JE, Madsen H. Insights to the minimal model of insulin secretion through a mean-field beta cell model. *J.Theor.Biol.* 2005.

16. Henriksen JE, Alford F, Handberg A, Vaag A, Ward GM, Kalfas A, Beck-Nielsen H. Increased glucose effectiveness in normoglycemic but insulin-resistant relatives of patients with non-insulin-dependent diabetes mellitus. A novel compensatory mechanism. *J.Clin.Invest* 1994; **94**(3):1196-1204.

17. Henriksen JE, Alford F, Ward GM, Beck-Nielsen H. Risk and mechanism of dexamethasone-induced deterioration of glucose tolerance in non-diabetic first-degree relatives of NIDDM patients. *Diabetologia* 1997; **40**(12):1439-1448.

18. Henriksen JE, Durck TT, Rasmussen M, Levin K, Beck Nielsen H. Dexametazone induced glucose intolerance predicts the development of diabetes in relatives of Type 2 diabetic patients 10 years later. *Diabetologia* 2004; **47 [Suppl 1] A403**.

19. Karpe F, Fielding BA, Ardilouze JL, Ilic V, Macdonald IA, Frayn KN. Effects of insulin on adipose tissue blood flow in man. *J.Physiol* 2002; **540**(Pt 3):1087-1093.

20. Fritsche A, Stefan N, Hardt E, Haring H, Stumvoll M. Characterisation of beta-cell dysfunction of impaired glucose tolerance: evidence for impairment of incretin-induced insulin secretion. *Diabetologia* 2000; **43**(7):852-858.

21. Dea MK, Hamilton-Wessler M, Ader M, Moore D, Schaffer L, Loftager M, Volund A, Bergman RN. Albumin binding of acylated insulin (NN304) does not deter action to stimulate glucose uptake. *Diabetes* 2002; **51**(3):762-769.

22. Beal SL, Sheiner LB. NONMEM User's Guides. *NONMEM Project Group, University of California, San Francisco* 1994.

23. Rask E, Olsson T, Soderberg S, Holst JJ, Tura A, Pacini G, Ahren B. Insulin secretion and incretin hormones after oral glucose in non-obese subjects with impaired glucose tolerance. *Metabolism* 2004; **53**(5):624-631.

24. Stumvoll M, Mitrakou A, Pimenta W, Jenssen T, Yki-Jarvinen H, Van HT, Renn W, Gerich J. Use of the oral glucose tolerance test to assess insulin release and insulin sensitivity. *Diabetes Care* 2000; **23**(3):295-301.

25. Pipeleers D, Kiekens R, Ling Z, Wilikens A, Schuit F. Physiologic relevance of heterogeneity in the pancreatic beta-cell population. *Diabetologia* 1994; **37 Suppl 2**:S57-S64.

26. Pipeleers DG. Heterogeneity in pancreatic beta-cell population. *Diabetes* 1992; **41**(7):777-781.

27. Van Schravendijk CF, Kiekens R, Pipeleers DG. Pancreatic beta cell heterogeneity in glucose-induced insulin secretion. *J.Biol.Chem.* 1992; **267**(30):21344-21348.

28. Hiriart M, Ramirez-Medeles MC. Functional subpopulations of individual pancreatic B-cells in culture. *Endocrinology* 1991; **128**(6):3193-3198.

29. Mari A, Tura A, Gastaldelli A, Ferrannini E. Assessing insulin secretion by modeling in multiple-meal tests: role of potentiation. *Diabetes* 2002; **51 Suppl 1**:S221-S226.

Table 1 Physical characteristics of the study subjects at initial examination

	Relatives	Control subjects
N (F/M)	20 (8/12)	20 (8/12)
Age (yr)	6.17 ± 0.13	6.12 ± 0.08
HbA1c (%)	6.17 ± 0.13	6.12 ± 0.08
BMI (kg/m^2)	25.1 ± 1.0	25.1 ± 0.9
Weight (kg)	76.6 ± 3.3	78.8 ± 4.0
Fasting glucose (mM)	5.41 ± 0.08	5.16 ± 0.08
Fasting insulin (pmol/l)	45.6 ± 3.0	41.4 ± 3.0

Values are mean ± SE. HbA1c: glycated haemoglobin (normal range: 5.4 - 7.4 %); BMI: body mass index;

Table 2 Description of parameters to be estimated

k_I	The elimination rate of insulin.
α	The rate constant for provision to reach steady state.
E_{max}	Maximum value of the incretin independent part of the steady state provision rate.
h	Hill coefficient for the incretin independent part of the steady state provision rate.
E_{OGTT}	Effect parameter for the incretin effect in an OGTT, which is zero for an IVGTT.
k_{rd}	Redistribution rate constant from passive to active packets.
m	The rate of insulin release from active packets.
F_{BG}	The fraction of packets activated at the initial steady state glucose concentration.
h_{IVGTT}	Hill coefficient for the threshold distribution function of the IVGTT.
h_{OGTT}	Hill coefficient for the threshold distribution function of the OGTT.

Table 3 Population Parameter Estimates

Parameter	Unit	Estimate	SE of Estimate	CV of parameter
k_I	1/min	0.161	0.03	-
α	1/min	0.111	0.045	-
E_{max}	pM/min	103	15	49%
h	1	6.43	0.89	-
E_{OGTT}	nmol	8.86	1.78	55%
k_{rd}	1/min	0.00869	0.00124	58%
m	1/min	1.47	0.206	-
F_{BG}	%	27.4	11	90%
h_{IVGTT}	1	1.96	0.45	-
h_{OGTT}	1	5.14	1.76	-
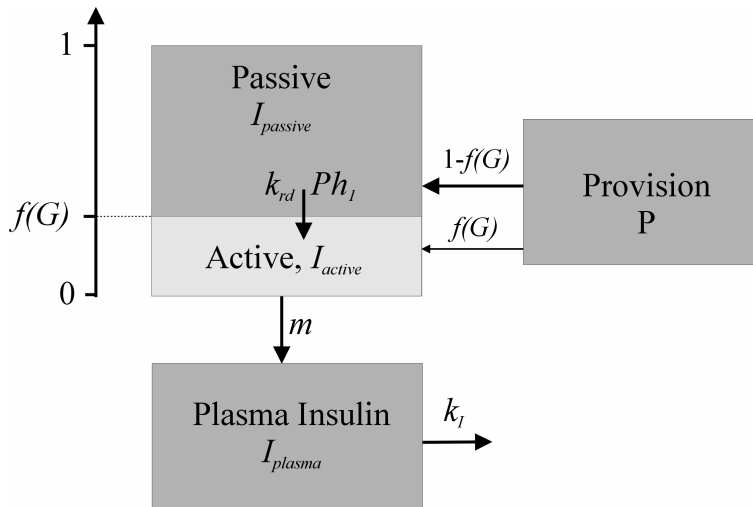
Figure 1 Model for observed insulin concentration in glucose tolerance tests. The model includes a one compartment model for insulin pharmacokinetics, two compartments to describe ready releasable insulin in the active and passive packets, and one differential equation to describe the relationship between glucose and the provision of new insulin. The provision is divided into the active and passive packets according to the fraction of active packets f(G), which is a function of the glucose concentration.
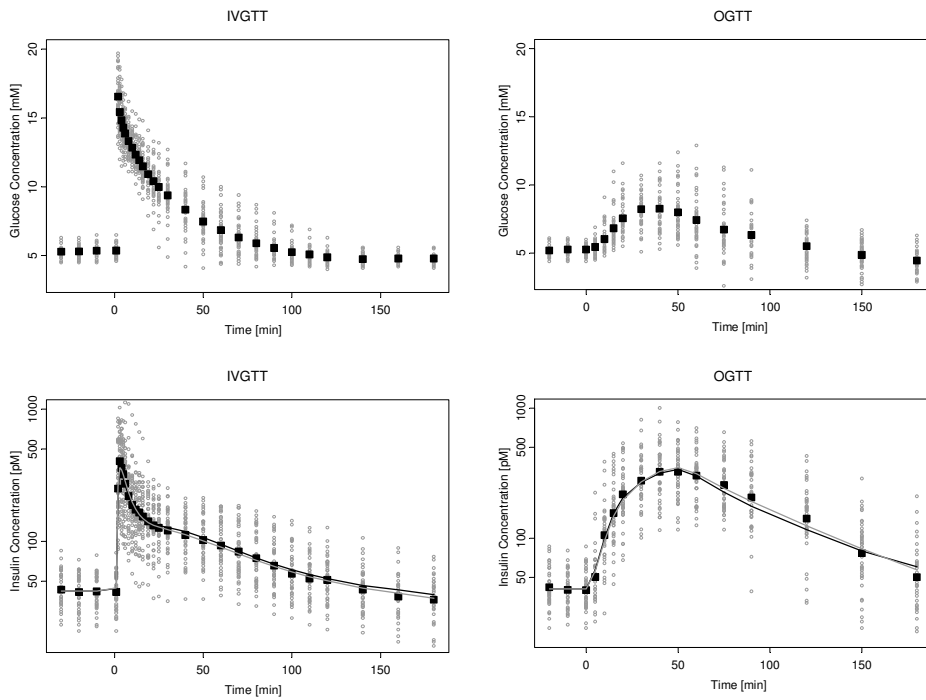
Figure 2 All observed glucose (top) and insulin (bottom) concentrations (small light colored circles), geometric mean of insulin and mean of glucose (large black squares), geometric mean of individual predictions (light colored line), and geometric mean of population predictions (black line), are presented for the IVGTT (left), and the OGTT (right).
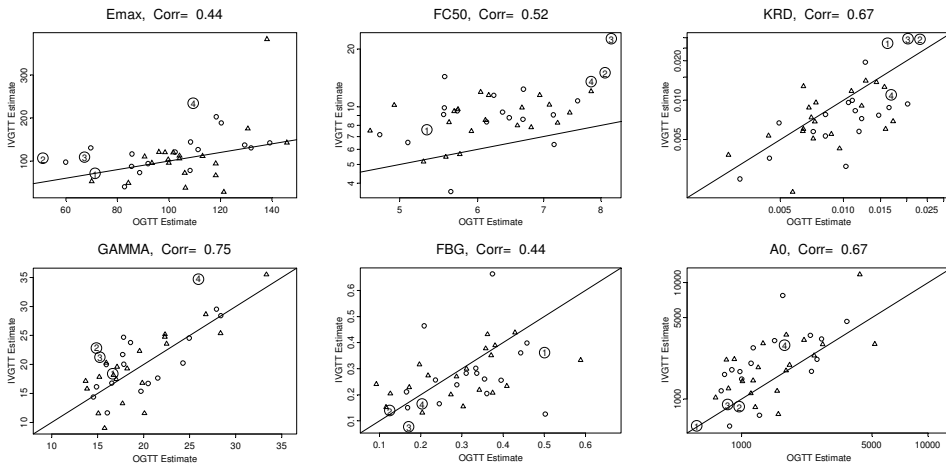
Figure 3 Individual parameter values obtained from the IVGTT are compared to those obtained from the
OGTT. Triangles signify control subjects, circles signify first degree relatives of diabetics, and numbers 1-4
signify the four first degree relatives of diabetics that have developed type 2 diabetes within the 10 years since
study completion. The correlation coefficient presented above each plot is calculated for the log transformed
parameter for k_{rd}, FC_{50}, and A_0.
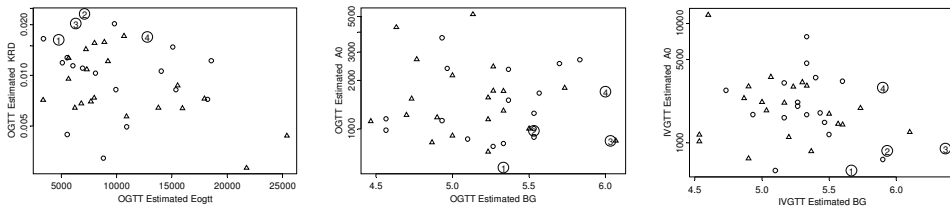
Figure 4 Individual parameter values are compared to illustrate separate prognostic relevance. Triangles signify control subjects, circles signify first degree relatives of diabetics, and the numbers 1-4 signify the four subjects that have developed type 2 diabetes within the 10 years since study completion. k_{rd} is compared to E_{OGTT} for the OGTT(left), A_0 is compared to BG for the OGTT(middle), and A_0 is compared to BG for the IVGTT(right).
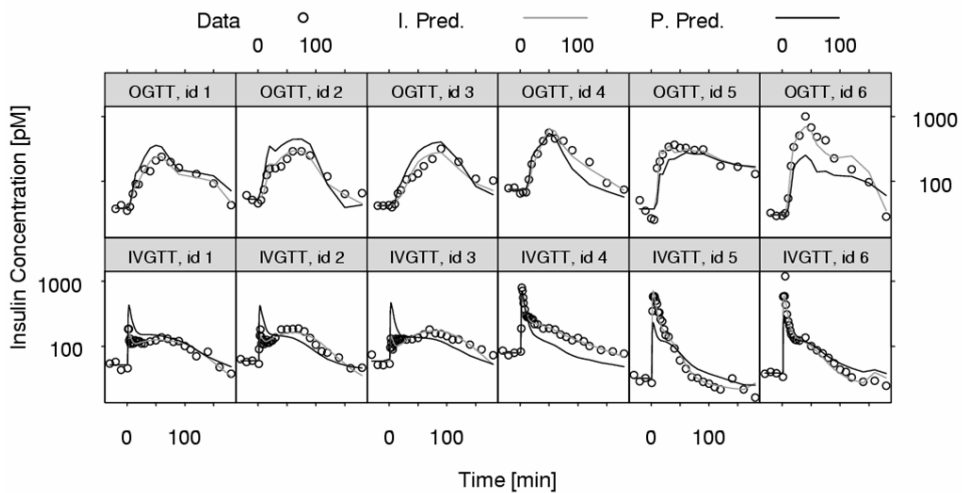
Figure 5 Observed insulin concentrations (circles), are presented together with individual predictions (light colored line) and population predictions (black line) for selected individuals. All 6 individuals were healthy at the time of the study, but individuals with id 1 to 4 have subsequently developed type 2 diabetes, whereas individuals with id 5 and 6 have remained healthy.

Paper D

Pharmacodynamic model of Interleukin-21 effects on Red Blood Cells in cynomolgus monkeys

Pharmacodynamic model of Interleukin-21 effects on Red Blood Cells in cynomolgus monkeys

Rune V. Overgaard[1,2,3*], Mats Karlsson[2], and Steen H. Ingwersen[3]

[1] Informatics and Mathematical Modelling, Technical University of Denmark, Lyngby
[2] Dept. of Pharmaceutical Biosciences, Uppsala University, Sweden
[3] Biomodelling, Novo Nordisk A/S, Bagsvaerd, Denmark
* To whom correspondence should be addressed.

Abstract

Interleukin-21 (IL-21) is a novel cytokine that is currently under clinical investigations as a potential anti-cancer agent. Like many other anti-cancer agents, including other interleukins, IL-21 is seen to produce a broad range of biological effects that may be related to both efficacy and safety of treatment. The present analysis investigates the observed pharmacodynamics effects on red blood cells following various treatment schedules of human IL-21 administrated to cynomolgus monkeys. These effects are described by a novel non-linear mixed-effects model that enabled separation of drug effects and sampling effects, the latter believed to be due partly to blood loss and partly to stress induced haemolysis in connection with blood sampling. Two different studies with a total of 9 different treatment groups of cynomolgus monkeys were used for model development and for the subsequent model validation consisting of both a cross validation and a biological test of the predicted rise in reticulocytes. In conclusion, the model consistently describes the IL-21 induced drop in red blood cells to be 1) caused by removal rather than suppression of production, and 2) considerably delayed compared to dosing, i.e. not related to the drop in red blood cells observed immediately post dose. It is believed that the structural model presented here can be used for other types of drug induced loss of red blood cells, whereas the mechanism for sampling related blood loss is relevant for investigations of anaemia in all pharmacological studies with smaller animals.

Keywords

mechanistic; PK/PD model; haemoglobin; anaemia

Abbreviations

C_{RBC}, RBC count; C_{ret}, Conversion rate of reticulocytes to mature erythrocytes; $(Drop_{RBC})$, drop in RBC; ED_{50}, steady state amount of IL-21 in the delayed compartment, giving rise to half maximum effect; E_{max}, maximal relative disappearance rate of RBCs; EPO, erythropoietin; IL, interleukin; IL-21, interleukin-21; IV, intravenous; PD, pharmacodynamic(s); PK, pharmacokinetic(s); P_{RBC}, fraction of the deficit RBC produced pr hour; RBC, red blood cell; RSE, relative standard error; SD, standard deviation; T_{IL-21}, transit time for IL-21 effects; T_{RBC}, transit time for newly synthesized RBCs; V_{blood}, estimated effective blood volume; V_{BWT}, body weight covariate on the blood volume; V_{sample}, volume of the blood sample.

Introduction

Interleukin-21 (IL-21) is a novel cytokine (1) that is produced by activated CD4^{+} T-cells and demonstrates an ability to activate CD8^{+} killer T-cells, natural killer, and B-cells (2). These immunomodulatory functions lead to the hypothesis of IL-21 as a potential anti-cancer immunotherapeutic drug, which is presently under investigation in clinical studies. Pre-clinical studies suggest that the side effects of IL-21 may be less severe than what has been observed for similar immunotherapeutic drugs, e.g. IL-2 (3), giving hope that a larger, longer, and more effective boost of the immune system is tolerable with IL-21 treatment. However, a consistent and dose dependent loss of red blood cells has been observed in monkey studies, constituting the main focus of the present work.

Drug induced anaemia is an increasing complication to therapeutic intervention (4) leading to decreased quality of life (5) and in some cases even death. This may be particularly important for cancer treatment, where both cancer and treatment are frequently reported to induce anaemia (6). Drug induced anaemia is seen both for many chemotherapeutic drugs (7) and also, which is more relevant in the present context, for many immunotherapeutic cytokines where anaemia is induced by a variety of mechanisms. A reproducible anaemia (possibly autoimmune haemolytic anaemia (8) is among the toxic effects reported for IL-2 (3). Haemolytic anaemia has also been reported for IL-12 (9), while other interleukins (IL-6 and IL-11) lead to anaemia as a consequence of increased blood volume (10, 11). The mechanism for IL-21 induced anaemia in monkeys is not known, but is associated with reticulocytosis and hyperbilirubinaemia. Erythrophagocytosis, which is a rare complication reported also for IL-3 (12), has been observed for IL-21, but it is presently not believed to be the primary cause of the observed loss of red blood cells. Also rouleaux formation and clumping of erythrocytes have been observed.

Pharmacokinetic (PK) and pharmacodynamic (PD) modelling can guide drug development by a concise and unequivocal summary of data, by making predictions, and by improving the understanding of the modelled system (13). Especially in oncology, PK/PD modelling could be useful as anticancer agents tend to have a narrow therapeutic index (14). Detailed mathematical models have been developed to describe the biology of stem cell proliferation and erythropoiesis (15-17), and several PK/PD models make use of these mechanisms to describe the effects of erythropoietin (EPO) to treat anaemia, see e.g. (18-22), whereas most published PK/PD models of drug induced anaemia (23, 24) are empirical in nature describing anaemia only at a certain time point e.g. at steady state. In the present work, we advocate the more mechanistic models that enable a description of the complete time course of drug induced anaemia and significantly improve the models ability to assist in dose regimen selection for optimal therapeutic outcome. However, we find that the most important mechanisms to describe data are different than those applied in PK/PD models of EPO, and do not include baseline production and lifespan of red blood cells.

The present analysis is based on studies of human IL-21 in monkeys subject to various treatment regimens of intra venous (IV) bolus administration. Several endpoints were addressed by these studies to investigate the complex and fascinating biology of IL-21, whereas the present analysis dealt only with the effect on the red blood cell (RBC) count. The objective was to establish the underlying relationship between drug administration schedule and the time course of RBC count that could guide the selection of treatment regimen and aid the design of future studies. A mathematical model was composed of frequently used pharmacodynamic model components (25), using an E_{max} model to describe saturation in effect, and transit compartments both to empirically

describe the delayed effect of IL21 and more mechanistically to mimic the blood cell maturation in the bone marrow. This base structure was integrated with a model of the experimental influence on the RBC count, i.e. that blood sampling reduces the RBC count in the monkey. The proposed base structure of drug action and physiologic recovery may be relevant and applicable for modelling other drug induced loss of RBC in clinical as well as preclinical settings, whereas the mechanism for sampling related blood loss is relevant for investigations of anaemia in all pharmacological studies with smaller animals.

Materials and Methods

Two different studies were used for the following analysis. The study plan for Study 1 was reviewed and approved by the Novo Nordisk non human primate task force. The animal unit was animal welfare monitored and found to be in compliance with the Novo Nordisk Principles for the use of animals as well as national legislation, including the Declaration of Helsinki. Study 2 was sponsored by ZymoGenetics, carried out at Sierra Biomedical (SBI). Treatment of the animals follows the SBI principles that adheres to the regulations outlined in the USDA Animal Welfare Act (9 CFR, Parts 1, 2 and 3) and the conditions specified in the Guide for the Care and Use of Laboratory Animals (ILAR publication, 1996, National Academy Press). The study protocol was approved by SBI's Institutional Animal Care and Use Committee prior to dose administration.

Animals

A total of 30 male and female purpose bred cynomolgus monkeys were tested in the two independent studies of the pharmacodynamic effect of IL-21, 24 monkeys in Study 1 and 6 in Study 2. Body weight prior to the first dose was between 1.8-3.8 kg in Study 1 and 3.4-4.7 kg in Study 2. Animals were acclimatized at least 6 weeks (Study 1) and 20 days (Study 2) prior to first dose. In both studies, the animals were housed individually during study days. The rooms were illuminated in a 12 hour light-dark cycle, and there were a minimum of 10 air changes per hour. Temperature was kept at 19-25°C (Study 1) and 18-29°C (Study 2).

Treatment

The animals were dosed by intravenous bolus injection according to the design described in Table I (Study 1) and Table II (Study 2).

Table I Design of study 1

Treatment group	Number of Animals Males	Females	Dose level (mg/kg/day)	Dosing Days	Haematology sampling days (+ denotes 4 hours post dose)
1	2	2	0	0, 3, 7, 10, 14	-5, 0, 0+, 3, 3+, 7, 7+, 14, 14+, 18, 22
2	2	2	1.0	0, 7,14	-5, 0, 0+, 7, 7+, 14, 14+, 18, 22
3	2	2	3.0	0, 7,14	-5, 0, 0+, 7, 7+, 14, 14+, 18, 22
4	2	2	0.2	0, 3, 7, 10, 14	-5, 0, 0+, 3, 3+, 7, 7+, 14, 14+, 18, 22
5	2	2	0.5	0, 3, 7, 10, 14	-5, 0, 0+, 3, 3+, 7, 7+, 14, 14+, 18, 22
6	2	2	0.2	10, 11, 12, 13, 14	-5, 4, 10, 10+, 14, 14+, 18, 22

Table II Design of study 2

Treatment group	Number of Animals		Dose level (mg/kg/day)	Dosing Days	Haematology sampling days (+ denotes 6 hours post dose)
	Males	Females			
1	1	1	0	1-5 and 9-14	1, 1+, 3, 5, 11, 15, 15+, 17, 19, 22, 25, 33
2	1	1	0.5	1-5 and 9-14	1, 1+, 3, 5, 11, 15, 15+, 17, 19, 22, 25, 33
3	1	1	1.5	1-5 and 9-14	1, 1+, 3, 5, 11, 15, 15+, 17, 19, 22, 25, 33

Sampling

Haematology samples were drawn at different time points in the different treatment groups as described in Table I and Table II. Other blood samples were drawn to ensure measurements of the pharmacokinetics and various parameters within serum chemistry, coagulation, and also concentrations of various blood cell lineages using flow cytometry. The extensive sampling schedules necessary to optimize the amount of information from each study was within the ethical limits for blood sampling in animal studies. The time points and approximate volume of all blood samples (not shown) were incorporated in the computational data file as exemplified in Appendix B.

Pharmacodynamic RBC Model

The model was based on differential equations, given in Appendix A, and all of these equations are represented by compartments in Figure 1.
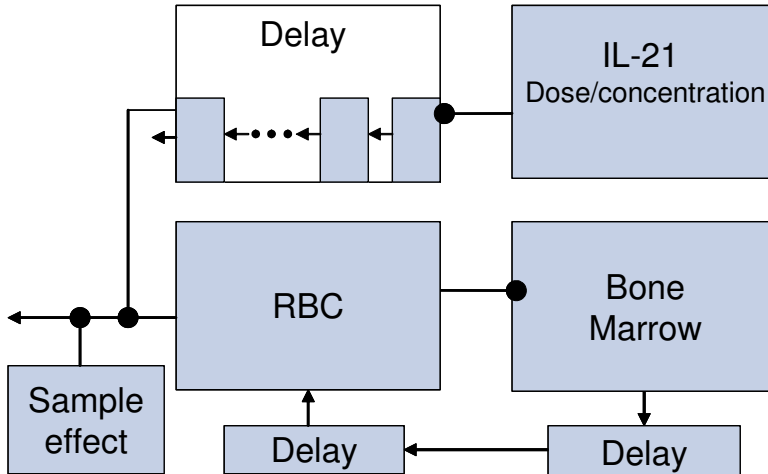
Figure 1 Compartment model for the IL-21 induced effects on red blood cells. The arrows represent a flow from one compartment to the next, whereas a bullet represents some interaction. Either dose or plasma concentration can be used as input in the first compartment. This illustrates that the model can be used as a pure PD model or as a PK/PD model where the units and values of the parameters are slightly changed.

The model consists of three fundamental parts: 1) a sampling effect, 2) an IL-21 induced effect, and 3) a model for blood recovery to steady state value.

1) Following a blood sample, interstitial fluid will enter the blood stream to keep the total blood volume constant. The fluid will dilute the blood slightly, leading to a drop in the RBC count. This mechanism was implemented in the model to explain the observed IL-21 independent drops in RBC from the predose to the postdose samples. The model hypothesis was that the total blood volume was constant during the entire experiment, so the drop in RBC ($Drop_{RBC}$) could be calculated from the estimated total blood volume (V_{blood}) of the monkeys and the volume of the blood samples (V_{sample}). Since blood samples are small compared to the total blood volume, the hypothesis of constant blood volumes leads to a drop in RBC count for each sample that is essentially identical to the drop calculated as:

$$Drop_{RBC} = C_{RBC} \, {V_{sample}} \big/ {V_{blood}}$$

V_{blood} is an effective blood volume and not the actual blood volume, since both sampling effect and stress related haemolysis of the blood may influence this volume estimate. The body weight was implemented as a reasonable covariate of the blood volume of the monkey.

2) The pharmacodynamic effect of IL-21 on RBC was modelled by a saturable model (an E_{max} model) proportional to the baseline RBC count, where the effect was delayed through transit compartments. Nine transit compartments were used, since nine gave a significantly better fit compared to three or six. The present text describes the model as a pure PD model, but one can also use plasma concentration as the input to the first compartment, making it a PK/PD model. The latter will essentially only change the units and values for the amounts in the transit compartments and the parameters in the Emax model, but inter-individual variability in PK may lead to further changes, as discussed later.

3) Recovery of the RBC count was modelled via a production in the bone marrow, which at all times was proportional to the deficit of RBCs in blood relative to the baseline value. This baseline RBC count was fixed to the value obtained from the first blood sample for each individual monkey, and it was used as an initial condition for the RBC count in the model. Newly synthesized RBCs enter into the blood stream after a delay, which was modelled by three transit compartments mimicking the maturation chain in the bone marrow. No significant improvement was gained by including more delay compartments, but the delayed entry approach was significantly better than implementing the production directly into the blood, corresponding to an indirect response model.

The structural parameters of the final model are described in Table III.

**Table III** Description of structural parameters in the PD model for IL-21 induced anaemia in cynomolgus monkeys.

Parameter	Unit	Description
V_{Blood}	ml	Effective blood volume (for a 3 kg monkey)
V_{BWT}	ml/kg	Body weight covariate on the blood volume
E_{max}	1/h	Maximal relative disappearance rate of RBCs. (Relative to baseline RBC value)
ED_{50}	mg/kg	Steady state amount of IL-21 in the delayed compartment, giving rise to half maximum effect.
T_{IL-21}	h	Mean transit time for the total delay between IL-21 dosing and effect
P_{RBC}	1/h	Fraction of the deficit RBC produced pr hour
T_{RBC}	h	Mean transit time for the synthesis of new RBCs

Inter-individual variation was included for:
1) V_{Blood} (Effective blood volume)
2) E_{max} (Maximal drug effect)

Extended Reticulocyte model

The RBC model was extended to include reticulocytes, as depicted in Figure 2, to investigate whether the predicted blood production was consistent with the observed reticulocyte levels. This extension was based on two main hypotheses. First, during anaemia the production of new RBCs is so rapid that a large part of the reticulocytes are pushed out into the blood before they are mature. A further model assumption was that the number of erythrocytes matured in the bone marrow was insignificant during this highly anaemic state, such that all newly synthesized RBCs originate from the reticulocyte compartment. Second, reticulocytes were assumed to be removed from the blood compartment, either by maturation to erythrocytes or by blood sampling, where the fractional drop for reticulocytes was identical to the one estimated for RBCs. The number of reticulocytes maturing in a given time interval was modelled to be proportional to the total number of reticulocytes.
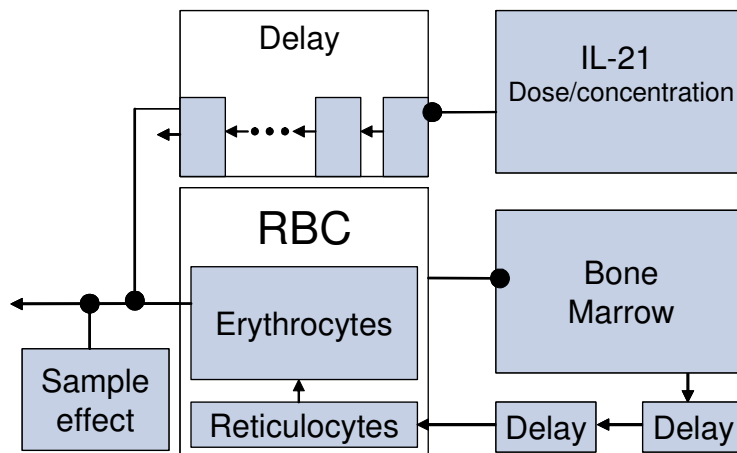
Figure 2   Compartment model for RBC and reticulocytes simultaneously. The arrows represent a flow from one compartment to the next, whereas a bullet represents some interaction.

It was chosen to use the structural parameter estimates from the RBC model above, to predict the production of reticulocytes, so only one extra structural parameter was needed to explain the observed reticulocyte counts, namely the conversion rate (C_{ret}) from reticulocytes to mature RBCs. Inter-individual variation was added to the conversion rate, such that inter-individual variation was included for three parameters (effective blood volume, proportional drug effect and reticulocyte conversion rate).

Both proportional and additive error was included in the intra-individual error model, such that the increasing variations for high reticulocyte levels were taken into account.

Computations

NONMEM version V level 1.1 (26) was used to fit the models to data, while Splus was used for graphical presentation of the results and to generate the appropriate NONMEM data file. This data file included dosing information as well as volume and timing information about all blood samples as described in the protocol. Model and data file are described in greater details in Appendix A and B, respectively.

Results

Pharmacodynamics

The effects on the RBC count during various IL-21 treatment schedules were well described by the model, as seen in Figure 3. In terms of the R^2 statistics, the fraction of variation explained by the predictions is 95.7% for the individual predictions and 89.4% for the population predictions.
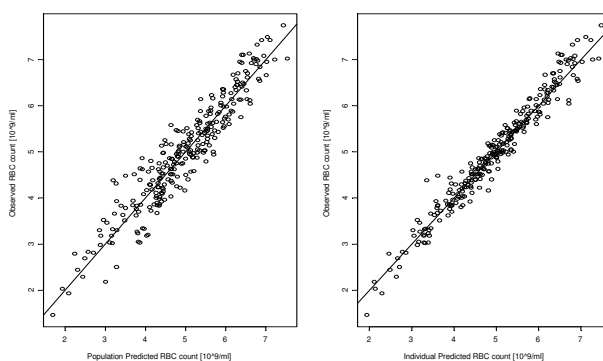
Figure 3   Observations versus population predictions of the RBC model
                 with data from two independent cynomolgus monkey studies, study 1 and study 2.

Figure 4 gives the average population predictions of the RBC count, which is compared to the average observed RBC count at the different time points in each treatment group of Study 1 and Study 2. We see marked dose independent drops in RBC count from pre- to post- dose measurements, eventually leading to significantly reduced counts, even for the vehicle group. These drops in RBC count did appear to be larger in Study 1 than in Study 2, which in the model was explained by the smaller sample volumes and larger body weights of monkeys in study 2.

Large differences were seen in the time evolution of the RBC count for the different treatment groups. This included a high level of anaemia in the treatment group with a low (0.2 mg/kg) dosing for 5 consecutive days (Days 10-14), compared to a lower level of anaemia in a treatment group with relatively high dose (1 mg/kg) administered 3 times (Days 0, 7, and 14). Figure 4 demonstrates that the model was able to describe all these between-treatment groups and between-study differences, by including a description of the sampling effect, the RBC recovery and the effect of IL-21.
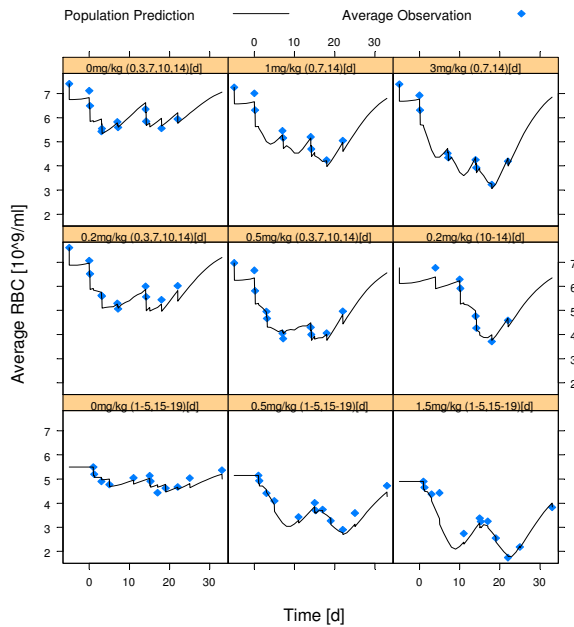
Figure 4   Average population predictions (line) and the average RBC count (dots) in various IL-21 treatment groups of cynomolgus monkeys. The top 6 dosing groups are from Study 1, while the bottom 3 dosing groups are from Study 2.

The parameter estimates are summarized in Table IV. As seen, the fixed effects were estimated with reasonably good precision, the largest relative standard error (that of ED_{50}) being 39.3%

Table IV   Parameter estimates from the pharmacodynamic model of IL-21 induced effects on red blood cells

Parameter	Unit	Parameter Estimate	RSE[1]	95 % Confidence Intervals	
				Lower	Upper
V_{Blood}	ml	106	7.34%	90.8	121
V_{BWT}	ml/kg	24.3	29.9%	10.1	38.5
E_{max}	1/h	0.00435	20.3%	0.00262	0.00608
ED_{50}	mg/kg	0.107	39.3%	0.0247	0.189
$T_{IL\text{-}21}$	h	57.3	9.97%	46.1	68.5
P_{RBC}	1/h	0.00388	5.28%	0.00348	0.00428
T_{RBC}	h	140	28.9%	60.8	219
Inter-Individual Variation					
V_{Blood}	CV = 18.3%		44.2%		
E_{max}	CV = 28.9%		32.2%		
Intra-Individual Variation					
e_{RBC}	10^9/ml	SD = 0.256	17.0%		

[1] Relative Standard Error

Cross Validation

A cross validation was performed to evaluate the robustness of the parameter estimates and the predictability of the model. The data from Study 1 and 2 was split into two, such that an equal number of monkeys from each treatment group were found in each data set. This particular splitting was judged to be necessary, since the model could easily be over parameterized if all data from one or two treatment groups were missing. In practice the data set was split into those with even and those with odd identification numbers, and hereafter the parameters were estimated using the entire data set and each of the partial data sets. Table V compares the structural parameter estimates and their confidence intervals, which do indeed seem to be reasonable robust. Note that during cross validation it was chosen to parameterize the Emax model with $p_1=1/ED_{50}$ and $p_2=E_{max}/ED_{50}$, as suggested by (27). The predictions obtained from the cross validation explained 89.2% of the variation, which is only slightly lower than the fraction of explanation obtained when using the entire dataset for estimation (where $R^2 = 89.4\%$). This similarity, illustrates the good predictive properties of the model that was also seen for the graphical presentation of the predictions obtained during cross validation, which was practically indistinguishable from the previously presented plots using predictions based on the entire dataset.

Table V   Cross validation of parameter estimates from the pharmacodynamic model of IL-21 induced loss of red blood cells (Model 1). Parameter estimates were based on two different studies with cynomolgus monkeys (Study 1 and Study 2). Note that during cross validation it was chosen to parameterize the E_{max} model with E_{max}/ED_{50} and $1/ED_{50}$.

| Parameter	Unit	Study 1 and 2		Odd IDs		Even IDs	
		Estimate	95% Conf. I.	Estimate	95% Conf. I.	Estimate	95% Conf. I.
V_{Blood}	ml	106	[90.7, 121]	108	[82.9, 133]	108	[85.7, 130]
V_{BWT}	ml/kg	24.2	[10.3, 38.1]	23.2	[2.03, 44.4]	31.4	[5.72, 57.1]
E_{max}/ED_{50}	kg/(mg*h)	0.0381	[0.0181, 0.0581]	0.0411	[0.0017, 0.081]	0.0363	[0.0165, 0.0561]
$1/ED_{50}$	kg/mg	8.57	[1.71, 15.4]	11.0	[-4.39, 26.4]	6.74	[0.919, 12.6]
T_{IL-21}	h	57.4	[45.7, 69.1]	59.7	[47.0, 72.4]	53.3	[28.0, 78.6]
P_{RBC}	1/h	0.00389	[0.0035, 0.0043]	0.00391	[0.0037,0.0046]	0.00385	[0.0034, 0.0043]
T_{RBC}	h	140	[62.8, 217]	146	[38.4, 254]	140	[27.9, 252]

The parameter estimates obtained from the monkeys with even IDs were used to give population predictions of the RBC counts for the monkeys with odd IDs, and vice verse. This gave us predictions, where the observed RBC count had not been used directly in the estimation. However, the first observation of the RBC count for each monkey does enter directly into the model as a baseline parameter, and was thereby used to calculate predictions for the remaining observations.

Biological test of the Model

The reticulocyte extension of the RBC model was included as a biological test of the model. This model included only one extra structural parameter, namely the conversion rate from reticulocytes to mature erythrocytes. The estimated value for the conversion rate was 3.2% per hour with an inter-individual variation with CV= 23.2%. Proportional as well as additive error was used for the reticulocyte count, which was estimated to, CV= 39.7% and SD= 0.0453 10^9/ml respectively.

Figure 5 shows the average population predictions of the reticulocyte counts, which are compared to the average of the observed reticulocyte counts at the different time points in each treatment group of Study 1 and Study 2. As seen, the production of RBCs implemented in the model adequately described the between-group variations in reticulocyte levels, supporting the sufficiency

of the simple linear relationship between production of new RBCs and the deficit in RBCs. This also supports the fundamental structural hypothesis of the model, i.e. that the anaemia is due to removal of red blood cells, and not due to suppression of RBC production in the bone marrow.
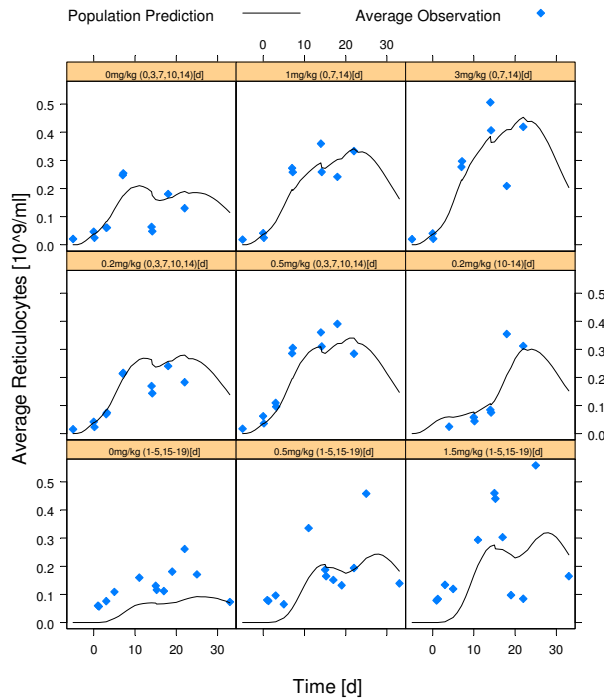
Figure 5   Average population predictions (line) and the average reticulocyte count (dots) in various IL-21 treatment groups of cynomolgus monkeys. The top 6 dosing groups are from Study 1, while the bottom 3 dosing groups are from Study 2.

Discussion

The presented results demonstrated a successful model with high predictive power, for the effect of IL-21 on RBCs. One reason for the apparent success was the extensive use of transit compartments, to empirically describe the delay of drug effect. Data confirmed that IL-21 had a delayed effect on RBC elimination, and that nine transit compartments gave a better description of this delay compared to three or six delay compartments. A good description of the delay may be essential for any system containing delays as well as saturation, because the effect may saturate both for a large single dose and when many smaller doses are given close together. At least two causes may have contributed to the identification of the empirical description of this delay in the present model: First, the interplay between delay and saturation might be the critical factor enabling a description of the different effects in the different treatment groups. Second, for a small number of delays a significant fraction of the effect will occur between the pre- and post- dose measurement, which is inconsistent with data. For other system, the saturation due to frequent administration could be simply related to

the dose response saturation via accumulation of plasma concentration, but that is not the case for the present analysis since IL-21 was essentially cleared within 24 hours, which was the shortest dosing interval.

According to the model presented here, a feedback loop ensures that a drop in RBC count stimulates a production of new red blood cells at a rate proportional to the deficit in the RBC count. However, other mechanisms may account for the return to the RBC baseline. Thus, cell lifespan models (28) could facilitate a recovery due to the natural turnover of blood cells. However, initial investigations revealed that the rate of recovery was faster than that from the natural turnover of cells. Other investigations attempted to include a constant production and turnover of RBCs in addition to the modelled feedback production, but this was not significant and subsequently neglected. It was proposed to model the delay of the RBC feedback by using transit compartments to mimic the maturation chain of RBCs in the bone marrow, and this was seen to be a statistically significant improvement. The chosen combination of mechanisms for the model of blood production was further supported by the observed rise in reticulocyte count, which is an observation that cannot be explained by a constant RBC production.

During model development PD and PK/PD models were compared to test whether dose, population fitted plasma concentration, individually fitted plasma concentration profiles, or individually fitted AUC estimates would be the best predictor for the effect (details not shown). These models could not be discriminated based on the available data, and subsequently it was chosen to use the pure PD model, which includes no assumptions about the link between plasma concentration and effect. The lack of superiority of the PK/PD model could origin from various reasons. First, the individual plasma concentrations were measured for the first dose only, but used in the simulation of all subsequent doses. So the lack of correlation between individual variability in PK and PD may be due to inter-occasion variability. Second, the IL-21 plasma concentration varies on a faster time scale than the effects, which may be another reason for the lack of its predictive power compared to the IL-21 doses.

Two effects were included in the PD model, one arising from IL-21 and blood sampling, both leading to a loss of red blood cells. From information about sampling, a theoretical effective blood volume was estimated. The estimates of this volume for each individual monkey are given in Figure 6, and we see that the differences of sampling effect in Study 1 and Study 2 could partially be understood through the differences in body weight of the animals. The estimated volumes were 106 ml for a 3 kg cynomolgus monkey, which is comparable to- but lower than the cynomolgus blood volumes reported in the literature (63 ml/kg) (29). This indicated that the drop in RBC was larger than it would be if it was only due to the sampling volumes. We find that the most likely explanation for the larger effect was a stress induced haemolysis caused by the blood sampling procedure, which is consistent with increased bilirubin levels in all dosing groups including the vehicle group.
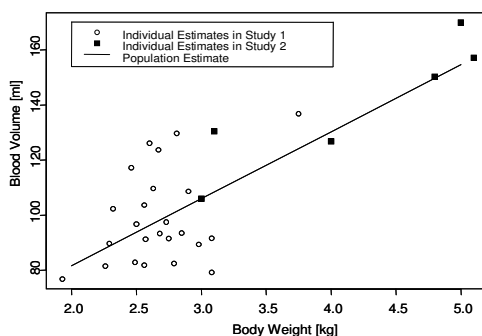
Figure 6 Estimated effective blood volume for each cynomolgus monkey in study 1 and study 2 is plotted against body weight.

Figure 5 demonstrated that the reticulocyte levels at initiation of Study 2 were elevated compared to study 1. This may indicate an elevated production of blood, which may be related to the low initial RBC counts in Study 2, see Figure 4. We have no obvious explanation for these differences between the two studies.

The population prediction of the reticulocytes explains only 60% of the variations in data, which is significantly lower than for the RBC model, and should not be viewed on its own, but only as a validation of the RBC model. Reticulocyte response to erythropoietin (EPO) and the endogenous EPO production has recently been modelled in acute anaemia, including a "paradoxal" down regulation of EPO production (19). It was judged paradoxal, since EPO does not have a negative feed-back on its own production; however a negative feed-back connected to RBC mass is not unlikely. Such a down regulation is to some extent also seen for the reticulocyte counts in Figure 5, where a drop in the reticulocyte level is seen at time points where the anaemia is still significant. It was attempted to improve the presented reticulocyte model by including both a higher baseline in Study 2 and a negative feedback mechanism. This gave a significant improvement of the reticulocyte model, but did not aid the RBC model, and the more complicated model was therefore not advocated as a better description of loss of red blood cells.

In conclusion, the present study describes the pharmacodynamics of the drop in RBC count observed in response to interleukin-21 administrated intravenously in monkeys in several different treatment regimens. A novel model was constructed by combining an Emax model with transit compartments and a mechanism for sampling effect. The model consistently describes the IL-21 induced drop in red blood cells to be 1) caused by removal rather than suppression of production, and 2) significantly delayed compared to dosing, i.e. not related to the drop in red blood cells observed immediately post dose. The model description was validated through standard statistical procedures (cross-validation) as well as by a biological validation that checked for consistency with the observed increase in reticulocyte count. Other cases of drug induced loss of RBC in clinical as well as preclinical settings may be investigated using the same structural model, while the mechanism for sampling related blood loss is relevant for investigations of anaemia in all pharmacological studies with smaller animals.

Appendix A

Using the parameters given in Table III, the model can be described by the following equations:

Parameters to be estimated
V_{Blood}, V_{BWT}, E_{max}, ED_{50}, T_{IL-21}, P_{RBC}, and T_{RBC}

Supplementary Parameters:
$K_T = 9/(T_{IL-21})$
$K_{TB} = 4/(T_{RBC})$
$E = E_{max} exp(\eta_1)$
$V = (V_{blood} + (BWGT-3)V_{BWT}) \, exp(\eta_2)$
Where η_1 and η_2 are random effects describing the inter-individual variation.
CHK is the volume of the blood sample. It is given directly in the data file, where it is turned on immediately after a blood sample and turned off 1hour later.
RBC0 is the first measured RBC count, which is given directly in the data file.

Differential Equations:
DADT(1)=$-K_T$ *A(1)   # IV dosing enters into this compartment
DADT(2)= K_T *A(1)- K_T *A(2)
DADT(3)= K_T *A(2)- K_T *A(3)
DADT(4)= K_T *A(3)- K_T *A(4)
DADT(5)= K_T *A(4)- K_T *A(5)
DADT(6)= K_T *A(5)- K_T *A(6)
DADT(7)= K_T *A(6)- K_T *A(7)
DADT(8)= K_T *A(7)- K_T *A(8)
DADT(9)= K_T *A(8)- K_T *A(9)
DADT(10)= K_{TB} *A(13)-CHK*(1+A(10))/V - E *A(9)/(ED_{50}+A(9))
DADT(11)=- P_{RBC} *A(10)- K_{TB} *A(11)
DADT(12)= K_{TB} *A(11)- K_{TB} *A(12)
DADT(13)= K_{TB} *A(12)- K_{TB} *A(13)

Predictions:
IPRE=RBC0*(1+A(10))
PRED=RBC0*(1+A(10)) (for $\eta_1=\eta_2=0$)

Appendix B

A representative section of the NONMEM data file that includes dosing as well as sampling information is given below:

C		Data Desc: Updated Individual data from NN and ZGI									
	C	TIME	ID	GRP	RBC	RBC2	SEX	BWGT	EVID	DOSE	CHK	RBC0
	1	360	2201	1 .		7.97	1	3.75	2 .		0	7.97
	2	360	2201	1 .	.		1	3.75	2 .		0	7.97
	3	361	2201	1 .	.		1	3.75	2 .		9.8	7.97
	4	384	2201	1 .	.		1	3.75	2 .		0	7.97
	5	408	2201	1 .	.		1	3.75	2 .		0	7.97
	6	432	2201	1 .	.		1	3.75	2 .		0	7.97
	7	456	2201	1 .	.		1	3.75	2 .		0	7.97
	8	480	2201	1	7.74	7.74	1	3.75	0 .		0	7.97
	9	480	2201	1 .	.		1	3.75	1	0.0001	0	7.97
	10	480	2201	1 .	.		1	3.75	2 .		0	7.97
	11	481	2201	1 .	.		1	3.75	2 .		7	7.97
	12	484	2201	1	7.49	7.49	1	3.75	0 .		0	7.97
	13	484	2201	1 .	.		1	3.75	2 .		0	7.97
	14	485	2201	1 .	.		1	3.75	2 .		9.8	7.97
	15	504	2201	1 .	.		1	3.75	2 .		0	7.97

'C' is the row number, 'TIME' is the time in hours, starting with 0 at day -20, 'ID' is the id number of the monkey, 'GRP' is the treatment group of the monkey, 'RBC' is the dependent variable for the RBC count [10^9/ml], 'RBC2' gives all the measured RBC counts also the baseline measurement. 'SEX' is 1 for male and 2 for female, 'BWGT' is the body weight, 'EVID' is the standard NONMEM event identifier, 'DOSE' gives the dosing amount, 'CHK' gives the blood volume [ml] drawn at a specific sampling time, 'RBC0' gives the baseline RBC count fixed to the first measurement

References

1. J. Parrish-Novak, S. R. Dillon, A. Nelson, A. Hammond, C. Sprecher, J. A. Gross, J. Johnston, K. Madden, W. Xu, J. West, S. Schrader, S. Burkhead, M. Heipel, C. Brandt, J. L. Kuijper, J. Kramer, D. Conklin, S. R. Presnell, J. Berry, F. Shiota, S. Bort, K. Hambly, S. Mudri, C. Clegg, M. Moore, F. J. Grant, C. Lofton-Day, T. Gilbert, F. Rayond, A. Ching, L. Yao, D. Smith, P. Webster, T. Whitmore, M. Maurer, K. Kaushansky, R. D. Holly, and D. Foster. Interleukin 21 and its receptor are involved in NK cell expansion and regulation of lymphocyte function, *Nature.* **408:57-63 (2000).**

2. T. Habib, A. Nelson, and K. Kaushansky. IL-21: a novel IL-2-family lymphokine that modulates B, T, and natural killer cell responses, *J Allergy Clin Immunol.* **112:1033-1045 (2003).**

3. D. R. Parkinson. Interleukin-2 in cancer therapy, *Semin Oncol.* **15:10-26 (1988).**

4. M. S. Wright. Drug-induced hemolytic anemias: increasing complications to therapeutic interventions, *Clin Lab Sci.* **12:115-118 (1999).**

5. D. Cella. Factors influencing quality of life in cancer patients: anemia and fatigue, *Semin Oncol.* **25:43-46 (1998).**

6. S. Mercadante, V. Gebbia, A. Marrazzo, and S. Filosto. Anaemia in cancer: pathophysiology and treatment, *Cancer Treat Rev.* **26:303-311 (2000).**

7. J. E. Groopman and L. M. Itri. Chemotherapy-induced anemia in adults: incidence and treatment, *J Natl Cancer Inst.* **91:1616-1634 (1999).**

8. P. J. Schlegel, W. E. Samlowski, and J. H. Ward. Autoimmune hemolytic anemia in a patient with chronic lymphocytic leukemia and renal cell carcinoma after treatment with high-dose intravenous bolus interleukin-2, *J Immunother.* **23:507-508 (2000).**

9. J. A. Gollob, K. G. Veenstra, J. W. Mier, and M. B. Atkins. Agranulocytosis and hemolytic anemia in patients with renal cell cancer treated with interleukin-12, *J Immunother.* **24:91-98 (2001).**

10. M. B. Atkins, K. Kappler, J. W. Mier, R. E. Isaacs, and E. M. Berkman. Interleukin-6-associated anemia: determination of the underlying mechanism, *Blood.* **86:1288-1291 (1995).**

11. K. H. Dykstra, H. Rogge, A. Stone, J. Loewy, J. C. Keith, Jr., and U. S. Schwertschlag. Mechanism and amelioration of recombinant human interleukin-11 (rhIL-11)-induced anemia in healthy subjects, *J Clin Pharmacol.* **40:880-888 (2000).**

12. N. Hurwitz, A. Probst, G. Zufferey, A. Tichelli, M. Pless, L. Kappos, B. Speck, and A. Gratwohl. Fatal vascular leak syndrome with extensive hemorrhage, peripheral neuropathy and reactive erythrophagocytosis: an unusual complication of recombinant IL-3 therapy, *Leuk Lymphoma.* **20:337-340 (1996).**

13. R. Gieschke and J. L. Steimer. Pharmacometrics: modelling and simulation tools to improve decision making in clinical drug development, *Eur J Drug Metab Pharmacokinet.* 25:49-58 (2000).

14. C. van Kesteren, R. A. Mathot, J. H. Beijnen, and J. H. Schellens. Pharmacokinetic-pharmacodynamic guided trial design in oncology, *Invest New Drugs.* 21:225-241 (2003).

15. M. Loeffler and H. E. Wichmann. A comprehensive mathematical model of stem cell proliferation which reproduces most of the published experimental results, *Cell Tissue Kinet.* 13:543-561 (1980).

16. V. G. Tyazhelova. Regulation of recovery in the erythroid lineage: model studies, *Cell Tissue Kinet.* 20:435-445 (1987).

17. H. E. Wichmann, M. Loeffler, and S. Schmitz. A concept of hemopoietic regulation and its biomathematical realization, *Blood Cells.* 14:411-429 (1988).

18. N. H. Al-Huniti, J. A. Widness, R. L. Schmidt, and P. Veng-Pedersen. Pharmacokinetic/pharmacodynamic analysis of paradoxal regulation of erythropoietin production in acute anemia, *J Pharmacol Exp Ther.* 310:202-208 (2004).

19. S. H. Chapel, P. Veng-Pedersen, R. L. Schmidt, and J. A. Widness. A pharmacodynamic analysis of erythropoietin-stimulated reticulocyte response in phlebotomized sheep, *J Pharmacol Exp Ther.* 295:346-351 (2000).

20. W. Krzyzanski, W. J. Jusko, M. C. Wacholtz, N. Minton, and W. K. Cheung. Pharmacokinetic and pharmacodynamic modeling of recombinant human erythropoietin after multiple subcutaneous doses in healthy subjects, *Eur J Pharm Sci.* 26:295-306 (2005).

21. R. Ramakrishnan, W. K. Cheung, F. Farrell, L. Joffee, and W. J. Jusko. Pharmacokinetic and pharmacodynamic modeling of recombinant human erythropoietin after intravenous and subcutaneous dose administration in cynomolgus monkeys, *J Pharmacol Exp Ther.* 306:324-331 (2003).

22. P. Veng-Pedersen, S. Chapel, R. L. Schmidt, N. H. Al-Huniti, R. T. Cook, and J. A. Widness. An integrated pharmacodynamic analysis of erythropoietin, reticulocyte, and hemoglobin responses in acute anemia, *Pharm Res.* 19:1630-1635 (2002).

23. D. Ganes, S. Bansal, D. Johnson, M. Leal, G. Nicolau, and A. Yacobi. Population pharmacodynamic modeling of drug-induced anemia, *J Pharm Sci.* 82:546-549 (1993).

24. J. Jen, M. Laughlin, C. Chung, S. Heft, M. B. Affrime, S. K. Gupta, P. Glue, and G. Hajian. Ribavirin dosing in chronic hepatitis C: application of population pharmacokinetic-pharmacodynamic models, *Clin Pharmacol Ther.* 72:349-361 (2002).

25. D. E. Mager, E. Wyska, and W. J. Jusko. Diversity of mechanism-based pharmacodynamic models, *Drug Metab Dispos.* 31:510-518 (2003).

26.   S.L.Beal and L.B.Sheiner. *NONMEM User's Guides*, NONMEM Project Group, University of California, San Francisco'', 1994.

27.   R. C. Schoemaker, J. M. van Gerven, and A. F. Cohen. Estimating potency for the Emax-model without attaining maximal effects, *J Pharmacokinet Biopharm.* 26:581-593 (1998).

28.   W. Krzyzanski and W. J. Jusko. Multiple-pool cell lifespan model of hematologic effects of anticancer agents, *J Pharmacokinet Pharmacodyn.* 29:311-337 (2002).

29.   K. H. Diehl, R. Hull, D. Morton, R. Pfister, Y. Rabemampianina, D. Smith, J. M. Vidal, and d. van, V. A good practice guide to the administration of substances and removal of blood, including routes and volumes, *J Appl Toxicol.* 21:15-23 (2001).

Paper E

PKPD Model of Interleukin-21 Effects on Thermoregulation in Monkeys - Application and Evaluation of Stochastic Differential Equations

Research Paper

PKPD Model of Interleukin-21 Effects on Thermoregulation in Monkeys — Application and Evaluation of Stochastic Differential Equations

Rune Viig Overgaard,[1,2,3,5] Nick Holford,[4] Klaus A. Rytved,[2] and Henrik Madsen[1]

Purpose. To describe the pharmacodynamic effects of recombinant human interleukin-21 (IL-21) on core body temperature in cynomolgus monkeys using basic mechanisms of heat regulation. A major effort was devoted to compare the use of ordinary differential equations (ODEs) with stochastic differential equations (SDEs) in pharmacokinetic pharmacodynamic (PKPD) modelling.
Methods. A temperature model was formulated including circadian rhythm, metabolism, heat loss, and a thermoregulatory set-point. This model was formulated as a mixed-effects model based on SDEs using NONMEM.
Results. The effects of IL-21 were on the set-point and the circadian rhythm of metabolism. The model was able to describe a complex set of IL-21 induced phenomena, including 1) disappearance of the circadian rhythm, 2) no effect after first dose, and 3) high variability after second dose. SDEs provided a more realistic description with improved simulation properties, and further changed the model into one that could not be falsified by the autocorrelation function.
Conclusions. The IL-21 induced effects on thermoregulation in cynomolgus monkeys are explained by a biologically plausible model. The quality of the model was improved by the use of SDEs.

KEY WORDS: autocorrelation; immunomodulation; PKPD model; SDE; statistical model; thermoregulation.

INTRODUCTION

Interleukin-21 (IL-21) is a novel cytokine (1) that is produced by activated $CD4^+$ T-cells and demonstrates an ability to activate $CD8^+$ killer T-cells, natural killer, and B-cells (2). These immunomodulatory functions lead to the hypothesis of IL-21 as a potential anti-cancer immunotherapeutic drug, which is presently under investigation in clinical studies. Like many other anti-cancer agents, including other interleukins, IL-21 is seen to produce a broad range of biological effects that may be related to both efficacy and safety of treatment. The present work focuses on the effects of human recombinant IL-21

on thermoregulation in monkeys where IL-21 is observed to cause an increased core body temperature.

Drugs may modify the regulation of body temperature, either by changing heat production i.e., increasing metabolism, by changing heat loss e.g., by cutaneous vasoconstriction, or indirectly by changing the regulation process i.e., by increasing the set-point temperature (3) that may be associated with lowering the signalling of temperature sensitive neurons in the hypothalamus. In technical terms, fever has been defined as a state of elevated body temperature caused by an elevated thermoregulatory set-point (4). However, this definition is still under debate (5), and we shall use the term fever in the broader meaning of the word that includes any kind of hyperthermia, and refer to the specific mechanistic causes when necessary. Drug-induced fever is observed following treatment with a wide variety of drugs (3) e.g., halothane causes a hypermetabolic state called malignant hyperpyrexia, phenothiazines cause an increase in the set-point temperature, and anticholinergic drugs increase temperature by decreasing sweat production. Fever is a characteristic effect of pyrogenic cytokines, for which elevation of the set-point is a likely, but possibly not the only mechanism. Most often, fever is associated with fatigue and nausea and can significantly reduce the quality of life, while the more extreme drug induced hyperthermia can be fatal. Fever caused by an elevated set-point can be treated with antipyretic drugs, e.g., the NSAIDs, whereas hyperthermia caused by a hypermet-

[1] Informatics and Mathematical Modelling, Technical University of Denmark, Richard Petersens Plads, Building 321, Room 015, Kongens Lyngby 2800, Denmark.
[2] Novo Nordisk A/S, Copenhagen, Denmark.
[3] Department of Pharmaceutical Biosciences, Uppsala University, Uppsala, Sweden.
[4] Department of Pharmacology & Clinical Pharmacology, University of Auckland, Auckland, New Zealand.
[5] To whom correspondence should be addressed. (e-mail: ruvo@novonordisk.com)

ABBREVIATIONS: ACF, autocorrelation function; IL-21, interleukin21; IOV, inter-occasion variability; ODE(s), ordinary differential equation(s); PKPD, pharmacokinetic pharmacodynamic; PGE_2, prostaglandin E_2; QQ, quantile-quantile; SDE(s), stochastic differential equation(s); UR, unbound receptor.

abolic state is generally unaffected by the antipyretics and more difficult to treat.

The present work proposes to quantify interleukin-21 (IL-21) induced elevation of core body temperature in cynomolgus monkeys with a pharmacokinetic pharmacodynamic (PKPD) model. The mechanism for IL-21 induced fever are currently unknown, but they are believed to include elevated thermoregulatory set-point, consistent with the clinical finding that IL-21 induced fever can be brought down by administration of paracetamol, and with findings of other cytokines. PKPD modelling of drug induced changes in body temperature can provide a summary description of the observed effects, enable predictions for other administration schemes, and increase understanding of the underlying mechanisms. For a general system, one could imagine that modelling of temperature could forecast dangerous hyperthermia, or guide administration of antipyretic drugs given in combination with fever inducing drugs.

Modelling of the regulation and variation of body temperature are well established problems that have been challenged with many types of mathematical models. Some models incorporate a vast amount of physiological and physical details about heat regulation that enables fruitful simulation models, e.g., (6). Other more statistical models aim to precisely describe and help to identify the circadian rhythm of body temperature, e.g., see (7) and (8). PKPD models of temperature regulation are typically formulated via a system of ordinary differential equations (ODEs) incorporated in a mixed-effects model to account for inter-individual differences, e.g., see (9–11). Among these, the set-point model involves a complex systems feedback mechanism that has proven useful for several studies (10,11). Whereas these efforts have been productive, we find that previous PKPD models of temperature regulation fail to integrate many of the elements in the physiological simulation models as well as the methodology applied in more statistical models. The present model aim to comply with these two points, as discussed below.

Aspects of more physiological models has been included by extending a model with a set-point to include also metabolism and heat loss; all merged in accordance with the basic, but evidently not all theory of heat regulation and experimental findings in monkeys. This allows the pharmacodynamic effect to be described as direct effects on the metabolism, the set-point, and/or the heat conduction with a natural inclusion of the basic counter regulatory mechanisms of the body, which may improve predictions of new experimental situations. Note that this type of model aim to include the most basic mechanisms to explain the most basic phenomena of heat regulation, but we do not aim to produce a model that can explain all phenomena of this complicated system.

The methodology of more statistical temperature models is incorporated by extending the set of ODEs to a set of stochastic differential equations (SDEs), using a mixed-effects model based on SDEs (12). The use of SDEs is a novel technique in PKPD modelling that has been presented both as a diagnostic tool that can facilitate systematic model development (13,14), and also as a means to facilitate a more realistic description of the variations in the system (15,16). The present work focuses on the implementation of SDEs to provide a more realistic description of the variations, and

among other things, we aim to demonstrate that implementation of SDEs may improve the predictions of the model by producing more realistic probabilities for a given animal to get fever. Since SDEs is a new technique of PKPD modelling, it will be emphasized how the results using SDEs differ from the corresponding results based on ODEs.

MATERIALS AND METHODS

The study plan was reviewed and approved by a Novo Nordisk ethical committee. The animal unit was animal welfare monitored and found to be in compliance with the Novo Nordisk Principles for the use of animals as well as national legislation and the NIH "Guide for the Care and Use of Laboratory Animals."

Animals

Sixteen purpose bred adolescent male cynomolgus primates (*Macaca fascicularis*) obtained from Guangxi, China, were used in the study. Prior to the study each primate was examined by veterinary surgeon and confirmed fit for the study.

The animals were implanted with telemetry transducers, type TL11M2-D70-PCT (Data Sciences International), for measurement of core body temperature. The animals were group-housed in a primate unit in gang cages. The room was illuminated by fluorescent lights timed to give a 12 h light–dark cycle. The temperature range was 21–26°C and the relative humidity range was 41–86%. The animals were aged 3.6 to 4.75 years and weighed 3.1–4.8 kg at the initiation of the study. The primates were fed a diet of MP(E) SQC (Special Diets Services, Witham, UK) with a supplementary diet of fruit, vegetables, and nuts. Tap water was available *ad libitum*.

The animals were acclimatized in general three weeks prior to the study and in the measuring cage on three occasions before the initiation of the study. A number of environmental enrichments were available: swings, stubs, swimming pool, puzzle feeders, toys etc.

Data Acquisition

During data acquisition the animals were in isolation cages within the animal house. Each telemetered cage was equipped with Data Sciences receivers. A Data Sciences telemetry recording system was used for continuous recording of the physiological data. The acquisition and analysis were made using Notocord HEM data acquisition and analysis software (version 3.2). For each dose, data collection commenced at least 1 h before dosing and ended approximately 24 h after dosing with 500 Hz sampling. Pretreatment of data prior to modelling involved, assessment of average temperature for each 10 min interval, keeping only the first average temperature of each hour.

Study Design

Four dosing groups consisting of four animals each were treated with 0, 0.03, 0.5 or 3 mg/kg IL-21. The animals were

dosed by intravenous bolus injection. The dose volume for the 0.5 and 3.0 mg/kg IL-21 administrations was 3.0 ml/kg and 1.0 ml/kg for the 0.03 mg/kg IL-21 administrations. The animals received a dose on days one, three and five of the study. Following each dose body temperature was recorded continuously for 24 h.

The study was conducted in accordance with the OECD Principles of GLP.

MODEL OF TEMPERATURE REGULATION

The PKPD model of temperature regulation can be divided into two parts. First, a baseline model that aims to reflect physiological mechanisms of temperature regulation, including the effects induced by a circadian rhythm, changes in ambient temperature, and/or forced changes in metabolic rate, e.g., induced by exercise. This part is presumably generally applicable for other drugs, since various pharmacological mechanisms can be implemented. The second part of the model includes a specific proposal for the pharmacodynamic effect of IL-21 on thermoregulation. For a brief overview of the structural model, see Fig. 2. The description of the inter- and intra-individual variability models are of special interest for the present analysis, and shall be described separately after presentation of the structural model.

Baseline Model

Body temperature is ultimately regulated by the balance of heat production and heat loss, where the primary mechanism of regulation is based on control of heat loss, whereas increased metabolism, e.g., by shivering is used in more extreme situations, see (17). In this setting, heat production is understood as an independent variable that drives the system, i.e., metabolism varies in order to meet the energy demand of daily living, causing changes first in temperature and subsequently in heat loss. One could imagine two ways of regulating heat loss after an increased heat production, see Fig. 1. First, the heat loss may increase to approach the metabolic rate and thus obtain heat balance, where the delay between the increase in

heat production and increase in heat loss will lead to heat balance at an elevated temperature. Second, the heat loss may exceed heat production so that heat balance will not be reached until the temperature has decreased to its original baseline value.

The physiology of heat regulation reviewed in (17) indicates that heat loss is controlled to obtain balance between heat production and heat loss, rather than to defend a specific temperature. We note that temperature sensing is probably the most important mechanism to detect discrepancies between heat production and loss in order to control this balance. Experimental results lead to the understanding that the typical nocturnal decrease of body temperature is a consequence of the delay between a rapid decrease in metabolic rate e.g., due to inactivity, and the subsequent decrease in heat loss until temperature returns to a new steady state. The present model adheres to this concept by letting metabolic rate drive the circadian rhythm, and further by letting body temperature control conduction of heat. An increased heat production or equivalently an increase in external temperature will increase the body temperature, and subsequently the regulatory mechanism will increase heat conductance and thereby also heat loss, which ultimately drives the system towards steady state at a higher temperature. The equations can be written,

$$
\begin{aligned}
M_c(t) &= \begin{cases} M_{day} & \text{for } t \in \{[0, t_{night}], [t_{day}, t_{night} + 24h], \ldots\} \\ M_{night} & \text{for } t \in \{[t_{night}, t_{day}], [t_{night} + 24h, t_{day} + 24h], \ldots\} \end{cases} \\
dM/dt &= -k_m(M - M_c(t)) \quad\quad ; \quad M(0) = M_{day} \\
dT/dt &= c^{-1}(M - k(T - T_a)) \quad ; \quad T(0) = T_{day} \\
k &= k_b + k_{inc}(T - T_b)
\end{aligned}
$$

$$(1)$$

M is the metabolic rate, which decays with a rate constant k_m towards the metabolism dictated by the circadian rhythm $M_c(t)$, which under normal physiological conditions varies around a baseline value M_b with a day time M_{day} and a night time value M_{night}, where t_{day} and t_{night} are the times where the day and night periods start. The mechanisms causing diurnal variation in $M_c(t)$ are not included in the present model. c
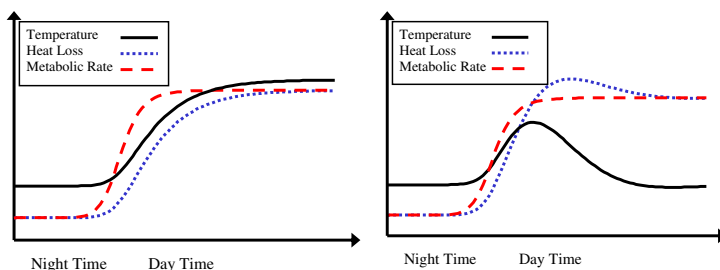
Fig. 1. Two possible ways of regulating heat loss after an increased heat production. First (*left*), the heat loss may increase to approach the metabolic rate and thus obtain heat balance, where the delay between the increase in heat production and increase in heat loss will lead to heat balance at an elevated temperature. Second (*right*), the heat loss may exceed heat production so that heat balance will not be reached until the temperature has decreased to its original baseline value.
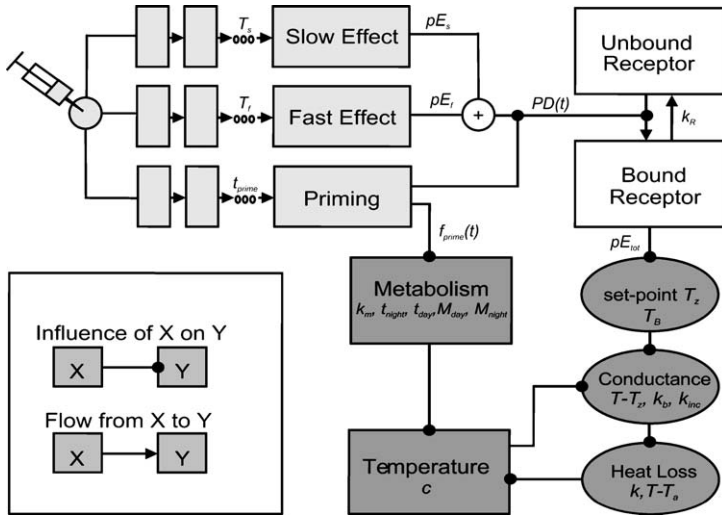
Fig. 2. Model for IL-21 induced regulation of core body temperature in cynomolgus monkeys. The model includes a part that describes the general mechanisms for temperature regulation (*dark*), a part that describes how IL-21 is believed to regulate the set-point through prostaglandin E_2 (*white*), and a part that empirically explains the relationship between administration of IL-21 and the effects (*light*). Each square box represents a compartment, i.e., a differential equation or the solution thereof, whereas each oval box represents an algebraic expression. A physical flow from one compartment to the next is depicted with an arrow, while a bullet is used to signify an influence of one model entity on another.

is the specific heat constant, T_a is the ambient temperature, k is the conductance of heat, which has the baseline value k_b when the temperature is at baseline T_b, and k_{inc} gives the increment in conductance per degree when the temperature rises. The model explains heat loss, only through terms proportional to the difference between body temperature and ambient temperature $(T - T_a)$, as appropriate for conduction. Radiation causes a heat loss proportional to $(T^4 - T_a^4)$ and evaporation is typically understood as temperature independent. Conductance ceases to explain heat loss for example when T_a approaches body temperature, and the model should be extended if it is needed to include e.g., high ambient temperatures.

The structural parameters to be estimated for the baseline model were chosen as: T_b, k_{inc}, k_m, t_{day}, t_{night}, and ΔT, where ΔT is the difference between day and night time steady state temperature, T_{day} and T_{night}. $T_{day} = T_b + \Delta T/2$, and $T_{night} = T_b - \Delta T/2$.

Neither the specific heat nor the baseline metabolic rate are identifiable when only temperature data is available, and consequently c was fixed to values obtained in humans, $c = 3.47$ kJ/(kg C), and M_b was fixed to 3 W/kg. This value was derived using squirrel monkey baseline metabolic rate of approximately 4 W/kg (18), and allometric scaling (19). Likewise, the ambient temperature was fixed to 21°C, as suggested by the experimental conditions, and except for k_{inc}, the model was not sensitive to changes in the ambient temperature. The baseline conductance and the night and

day time metabolic rate can now be calculated from the steady state conditions:

$$
\begin{aligned}
k_b &= M_b/(T_b - T_a) \\
M_{day} &= \left(k_b + k_{inc}\left(T_{day} - T_b\right)\right)\left(T_{day} - T_a\right) \\
M_{night} &= \left(k_b + k_{inc}\left(T_{night} - T_b\right)\right)\left(T_{night} - T_a\right)
\end{aligned}
\tag{2}
$$

Pharmacodynamic Model

The baseline variations of temperature regulation can be altered e.g., by disease, or by the introduction of exogenous compounds. Drugs are seen to modify thermoregulation either by directly affecting the metabolic rate, by direct effects on the heat loss, e.g., via vasodilatation, or indirectly by affecting the set-point temperature. Physiologically, the set-point is modulated through the temperature sensing neurons in the hypothalamus. If these neurons emit signals that correspond to a temperature lower than the set-point, the conductance is decreased and the temperature increases towards a higher steady state. For the baseline model described above, there is no single temperature that the body regulates towards, rather the level of the steady state temperature depend upon the metabolic rate. Consequently, it is necessary to define the set-point temperature relative to some metabolic rate. In the present work, the set-point is defined as the temperature the

body regulates itself towards at M_b, i.e., T_b if no drug has been introduced. The introduction of drugs can be understood to change the baseline model by,

$$
dM/dt = -k_m(M - f_1(M_c(t), Drug, t))
$$
$$
dT/dt = c^{-1}(M - k(T - T_a)) \qquad (3)
$$
$$
k = k_b + k_{inc}(T - T_b(1 + f_3(Drug, t))) + f_2(Drug, t)
$$

where f_1, f_2, and f_3, are some functions of time and drug intervention, as typically modelled via plasma concentration. f_1 allows drug modulated steady state metabolism, f_2 describes a drug effect on heat conduction, whereas f_3 involves drug modulation of the set-point to a new value $T_z = T_b(1 + f_3(Drug, t))$. Whereas this model structure can be used to describe the effects of a given drug, it is unlikely that it can be used to discriminate between e.g., effects on set-point and direct effects on conductance, when based exclusively on temperature data without precise knowledge of the function of drug effect.

The IL-21 induced rise of body temperature in cynomolgus monkeys is a rather complex set of phenomena (see data presented in Fig. 5 in the following section):

1) The effect of IL-21 seems to be absent following the first dose. This phenomenon confirms previous findings, indicating the existence of some regulating mechanism that must be switched on before any IL-21 induced effects on temperature can occur. For the 3 mg/kg treatment group, the temperature seems to be unaffected within 24 h of the first dose, but an increase is seen 48 h later at the time of the second dose. For the 0.5 mg/kg group, most monkeys exhibit only a partial response to the second dose, and a full response to the third dose.

2) The nocturnal decrease in temperature seems to vanish for the two highest treatment groups during the period where IL-21 has an effect. Note that the monkeys were unable to sleep in these periods.

3) IL-21 induces fast as well as slow temperature elevations. A quick peak is seen to last about 24 h, whereas a slower mechanism leads to persistent elevated temperature 48 h after the second dose of 3 mg/kg.

4) The fast peak is considerably lower in magnitude when temperature is already elevated; compare e.g., the effect following third dose in the 0.5 and the 3 mg/kg treatment groups.

The delayed onset of the pharmacodynamic effects (phenomenon 1) was modelled with an empirical function that starts at 0 indicating no effect, and when the time since the first dose increases, the function smoothly goes towards one, indicating full effect. We assume that a certain dose level is necessary for this priming to take place, but the available data did not allow a reasonable estimate of this value. For practical reasons, priming was implemented only for the high dosing groups, where an effect on temperature was seen in the animals. The following priming function was used,

$$
f_{prime}(t) = \delta_{high\_dose}\left(1 - \exp\left(-\alpha\left(t - t_{dose1} - t_{prime}\right)\right)\right)^{-1} \quad (4)
$$

where δ_{high_dose} is 0 for the low dose levels and 1 for the high dose levels, t_{dose1} is the time of administration of dose 1, t_{prime}

is the characteristic time of priming, and α gives the shape of the priming function. The priming function for the onset of the pharmacodynamic effect was also used to model the disappearance of the nocturnal decrease in the metabolic rate (phenomenon 2). This effect on metabolism, perhaps by preventing sleep and rest at night, was consistent with simultaneous observations of heart rate that maintain a day time high value during nights when IL-21 affects temperature, but exhibit a nocturnal decrease when no effect is seen on temperature. The steady-state day and night time metabolic rates were modelled to be changed by the drug as

$$
M^*_{day} = f_1(Drug, t)_{day} = M_{day}
$$
$$
M^*_{night} = f_1(Drug, t)_{night} = \left(1 - f_{prime}\right)M_{night} + f_{prime}\,M_{day}
$$
$$(5)$$

where M^*_{day} and M^*_{night} are the drug modulated day and night time metabolic rates. At the present time, we were not able to formulate a reasonable model for "un-priming" of the system, e.g., the return to a normal circadian rhythm. It may be appropriate to develop more realistic and mechanistic dose-response relationships for the priming and the "un-priming," but at present we use the function given above.

The fast and slow effects following dosing with IL-21 (phenomenon 3) are modelled to elevate the thermoregulatory set-point as described below. Both effects are described by gamma distribution functions giving the solution to a system of transit compartments that could represent the chain of events between dosing and effect. The gamma distribution function can be written as

$$
g_{N,T}(t) = \exp(-tN/T)(t)^{N-1}(N/T)^N(N-1)! \text{ for } t
$$
$$
> 0 ; g_{N,T}(t) = 0 \text{ for } t \leq 0 \qquad (6)
$$

where g_{NT} is the gamma function, yielding the value in the Nth transit compartment, and T is the mean total transit time to compartment N. In the model, the slow effect is dose proportional, whereas the fast effect is a dose independent fixed response. Such dose independence could reflect that the maximum effect has been reached, or that a predetermined acute phase response is induced. The total effect is modelled as the sum of the slow and the fast effect, and proportional to the priming function, which ensures that the effect is seen only when the priming has occurred. The equations describing these rather empirical effects are,

$$
E_{slow} = pE_s \sum_{doses} AMT_{doses}g_{Ns,Ts}(t - t_{dose})
$$
$$
E_{fast} = pE_f \sum_{doses} g_{Nf,Tf}(t - t_{dose}) \qquad (7)
$$
$$
PD(t) = f_{prime}(t)\left(E_{slow} + E_{fast}\right)
$$

where AMT_{dose}. is the amount of IL-21 administered by a given dose at time t_{dose}. The mean total delay for the slow and the fast effect is parameterized by T_s and T_f, whereas pE_f and pE_s gives the level of the fast and the slow effect. N_f and N_s are the number of transit compartments used in the two effects, both fixed to four in order to produce a standard third order delay between the dose and the effect compart-

ment. It was judged reasonable to combine the fast and the slow effect, assuming that they act through the same mechanism, as motivated by the observed saturation of the combined effect (phenomenon 4). The combined pharmacodynamic effect PD(t) is modelled to affect the thermoregulatory set-point. Although not completely understood, this effect is likely mediated by prostaglandin E_2 (PGE_2), which is believed to mediate cytokine induced fever (20–22) by lowering the signalling of temperature sensitive neurons in the hypothalamus. Many possible mechanisms can be proposed to describe the link between drug effect, PGE_2 release, and the subsequent increase in set-point temperature. A simple E_{max} model could describe the set-point temperature as a saturable function of PD(t). In general the E_{max} relationship can be motivated by the classical receptor occupancy theory under the assumption of equilibrium, e.g., see (23). However, for the present analysis, this receptor occupancy was modelled explicitly, without the assumption of steady state. The rate of increase in the number of bound receptors is proportional to the pharmacodynamic effect and the fraction of unbound receptors. When no pharmacodynamic effect is present, the bound receptors will decay to unbound receptors. This can give rise to phenomenon four—saturation in effect, because for an elevated temperature, only few unbound receptors will be available, so a subsequent response will produce only a few more bound receptors. We get,

$$dBR/dt = PD(t)\,(1 - BR) - k_R BR \quad ; BR(0) = 0$$
$$f_3(Drug,\, t) = pE_{tot}BR \quad ; \; T_z = (1 + pE_{tot}BR)T_b \tag{8}$$

BR is the fraction of bound receptors, and k_R is the off rate. Empirically, k_R give us one extra parameter to describe the shape of the delayed fast and slow effects, and further for the SDE model k_R is also involved in the correlation structure for the residuals, to be discussed below. The actual effect on the set-point is proportional to the fraction of bound receptors with the coefficient being the effect parameter pE_{tot}. Whereas, pE_f and pE_s parameterize the effect on the receptors, i.e., they control the induced level of saturation. The complete set of structural parameters to be estimated for the pharmacodynamic model was chosen as: (pE_{tot}, k_R, t_{prime}, T_s, T_f, pE_f, pE_s, and α).

The complete model of the mechanistic baseline system, the mechanistic effect model, and the empirical drug interaction are presented in Fig. 2, while simulations of the different model entities are presented in Fig. 3. Following the first administration of IL-21, the system will become primed according to Eq. (4), which will affect the metabolic rate to maintain a day time value Eq. (5). Subsequent administrations of IL-21 will exhibit a reduced or a full response Eq. (7), where the fast effect is of a fixed size, whereas the slow effect is proportional to the dose level. The effect will convert unbound receptors to bound receptors Eq. (8), which raises the thermoregulatory set-point Eq. (8), so that the normal physiological regulatory system will raise the body temperature according to the change in set-point and metabolic rate, see Eq. (3) or Eq. (9).

Variability Model

The present analysis utilize a new technique for variability in PKPD models, where system noise is added to a set

of ordinary differential equations to account for model mis-specification and true random fluctuations, producing a set of stochastic differential equations. The SDEs are embedded into a typical mixed effects setting with uncorrelated measurement noise and inter-individual and/or inter-occasion variability in the parameters. In summary, the intra-individual statistical model can be written as,

$$dM = -k_m(M - f_1(Drug,\, t))dt + \sigma_M dW_M \quad ; M(0) = M_{day}$$
$$dT = c^{-1}(M - k(T - T_a))dt \quad ; \; T(0) = T_{day}$$
$$dBR = (PD(t)(1 - BR) - k_R BR)dt + \sigma_{BR}dW_{BR} \quad ; BR(0) = 0$$
$$k = k_b + k_{inc}(T - T_z) \text{ and } T_z = (1 + pE_{tot}BR)T_b$$
$$T_{obs} = T + e \quad ; \; e \in N(0, \sigma_e^2) \tag{9}$$

The SDEs given by the first three equations correspond to the ODEs previously defined, now with system noise added to the metabolism and the receptor compartment. T_{obs} gives the observed temperature, modelled with additive uncorrelated measurement noise e, which is normally distributed with standard deviation σ_e. $\sigma_M dW_M$ and $\sigma_{BR}dW_{BR}$ give system noise in the metabolism and the receptor compartment, respectively. Where W_M and W_{BR} are independent standard Wiener processes, e.g., see (24). System noise produces fluctuations directly into the structural model, and will therefore depend upon the structural parameters. Specifically, the metabolism fluctuates and the correlation between the metabolic rate at time t_1 and t_2 will be $\exp(-k_m|t_1 - t_2|)$. Similarly, the correlation of BR will be $\exp(-k_R|t_1 - t_2|)$ when no drug is included. These fluctuations will thus give two time scales for the correlations in the model.

From data presented in Fig. 5, variability is seen to be higher after second dose than after third dose. This effect can be understood as inter-individual variability in the time point where the effects are switched on t_{prime}, so that the system can be more or less turned on during the second dosing day, whereas it is completely turned on for the third dose. A proportional inter-individual model was implemented as,

$$t_{prime} = \theta \exp(\eta)\,; \; \eta \in N(0, \Omega) \tag{10}$$

where θ is the typical value of t_{prime}, and η is a normally distributed random effect with variance Ω. Several other inter-individual and inter-occasion models were investigated during model development.

MODEL DEVELOPMENT

Different models were discriminated based on, robustness, likelihood function value, reasonable physiological values of the parameter estimates, and performance of the simple predictive check described in the results.

A number of different baseline models have been investigated and rejected in favour of the chosen model. These include, square wave metabolism, sine wave metabolism, modelling temperature directly as a sine wave, and modelling heat loss to approach metabolism exponentially
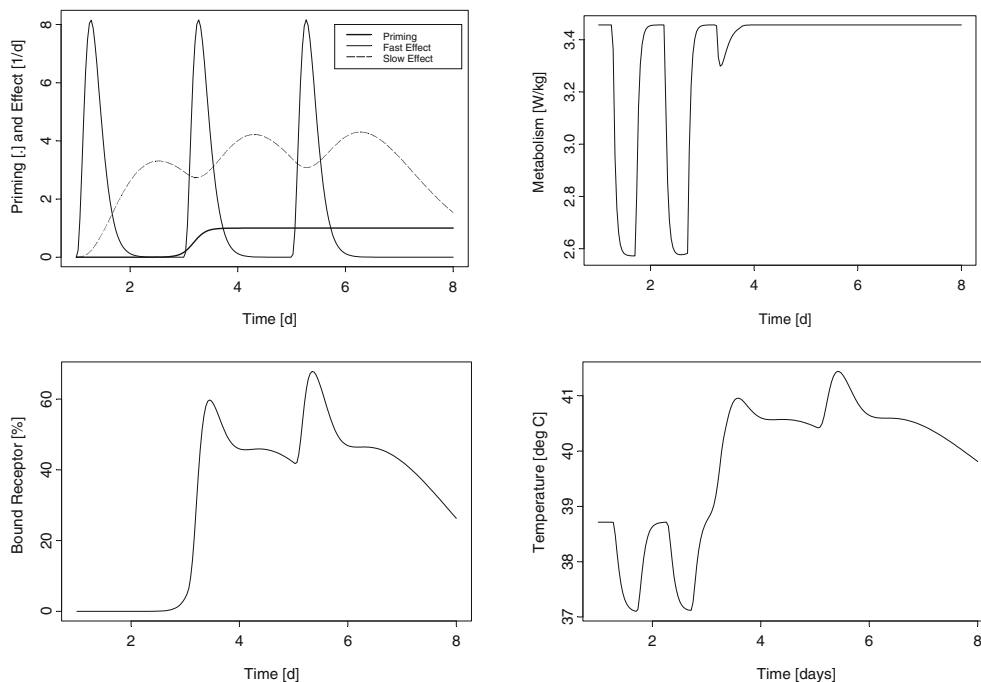
Fig. 3. Simulations of the different components in the pharmacodynamic model for IL-21 induced regulation of core body temperature in cynomolgus monkeys. These simulations illustrate the dynamics of the structural model following administration of 3 mg/kg IL-21 at days one, three, and five. The fast, the slow, and the priming effect are seen in the top left plot. After the system is primed, the metabolic rate maintains a daytime high (*top right*), and the sum of the fast and the slow effect initiates the conversion of unbound to bound receptors (*bottom left*). The bound receptors elevate the set-point, giving rise to an elevated temperature (*bottom right*).

instead of the chosen model where change in conductance gives the change in heat loss. It was not tested whether a more complicated oscillator model, as e.g., described in (25), could explain the circadian rhythm.

During development of the pharmacodynamic model, it was investigated whether simulated pharmacokinetic profiles could be used instead of dosing to drive the pharmacodynamics, but using dose directly turned out to be more productive. It was further investigated whether the slow and fast effects could be joined into one effect, and also whether the effect on metabolism could be explained as a function of the slow effect.

Inter-individual variability was tested for all parameters. Whereas many of these parameters were significant based on objective function value, only inter-individual variation for t_{prime} gave a large improvement, and was crucial for the performance of the simple predictive check.

Stochastic Model Development

Investigation of system noise may be motivated by the significantly autocorrelated residuals of the ODE model, as demonstrated in Fig. 4. If the system noise parameters σ_M and σ_{BR} in the SDE model are set to zero, then we get our original ODE model. In other words, the ODE and SDE models are nested, making it appropriate to test the inclusion of system noise with the likelihood ratio test. The inclusion of system noise was highly significant with $\Delta \log(L) > 1,000$.

System noise was investigated for temperature, metabolism, and receptor compartments, testing also a term proportional to $PD(t)$ in the receptor compartment. The following considerations contributed to the chosen implementation:

Stochastic fluctuations in metabolism were motivated by the natural variations in movement and exercise patterns. A simulation test confirmed that the level of fluctuations in metabolism were reasonable compared to those observed in squirrel monkeys (18). The simulations of metabolism were far from zero, and subsequently it was judged unnecessary to investigate a numerically more complicated proportional model that would ensure metabolism to be strictly positive.

System noise for the temperature compartment could to a large extent compensate for variations in metabolism, but
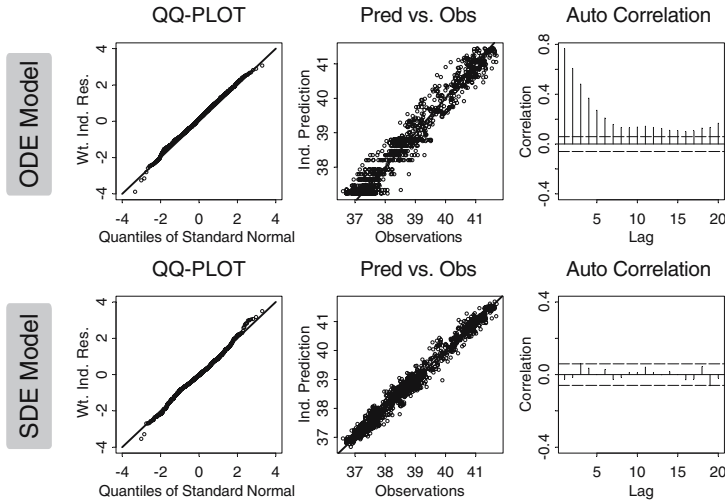
Fig. 4. Diagnostic plots for the ODE and SDE model for IL-21 induced regulation of core body temperature in cynomolgus monkeys. QQ-plots (*left*) provide a visual test for weighted individual residuals being standard normal distributed. Predicted *versus* observed plots (*middle*) are based on individual one-step predictions, which are identical to the usual individual predictions for the ODE model. The autocorrelation functions (*right*) of the weighted residuals are plotted with the 95% confidence intervals for the null hypothesis that these are uncorrelated.

including both effects gave only modest improvement to the objective function value. System noise on metabolism was selected instead of direct effects on temperature because of an improved objective function value, more realistic simulations of metabolism, and since it enabled estimation of the rate constant k_m.

System noise was also introduced for the receptor compartment, which could reasonably account for slow fluctuations and were significant in a likelihood ratio test. The chosen stochastic implementation ensures that the total number of bound and unbound receptors remain constant. A term with system noise proportional to the pharmacodynamic effect was tested and rejected.

COMPUTATIONS

Parameter estimation was performed using NONMEM (26), where stochastic differential equations were implemented in NONMEM version VI beta as explained in (14). The model was processed at the cluster of the PKPD group at Uppsala University, which is a heterogenic cluster of 20 computers with dual processors running Redhat 9 (http://www.redhat.com), kernel version 2.4.26 with the openmosix cluster patch version 2.4.26-1 (http://www.openmosix.org). To save computational time, it was chosen to estimate parameters by the following two stage procedure. First, we estimate the parameters in the baseline model, using data from the vehicle group and the 0.03 mg/kg group where no effect is seen. Second, the complete dataset is used to

estimate the pharmacodynamic parameters, including all variability parameters, while keeping baseline parameters fixed to the previously estimated values. For both steps, estimation of standard errors (SE) was obtained by bootstrapping, i.e., from the estimation results of 100 randomly generated datasets. New datasets were generated by replacing each monkey in the dataset with a randomly selected monkey, while allowing for duplicates. For bootstrapping of the pharmacodynamic model, new datasets were constrained to contain four monkeys from all of the four treatment groups.

RESULTS

Parameter estimates and their relative standard errors for the pharmacodynamic model of IL-21 induced effects on temperature regulation are presented in Table I. SDE model parameter estimates are compared to the corresponding estimates obtained with ODEs. We note that the ODE model estimate of k_m was very unstable, as indicated by a large relative standard error. During estimation of the remaining parameters, the ODE model k_m was fixed to the value obtained in the SDE model, allowing a more reasonable comparison of the two sets of estimates. For most parameters, the estimates are very similar, while some estimates clearly differ in the two estimation procedures. The most characteristic changes are that the SDE model produces estimates with lower inter-individual variability and measurement noise compared to the ODE model.

Table I. Parameter Estimates and Their Relative Standard Errors From the Model of IL-21 Induced Regulation of Core Body Temperature in Cynomolgus Monkeys

Parameter	Unit	SDE parameter estimate	ODE parameter estimate	% Difference of ODE estimate
Baseline parameters				
t_{night}	h	6.64 (1.9%)	6.73 (1.7%)	1.4
t_{day}	h	17.3 (0.8%)	17.5 (1.4%)	1.1
k_m	1/d	27.3 (17%)	*591 (140%)	2064
k_{inc}	W/(kg°C²)	0.0169 (19%)	0.0258 (10%)	52
ΔT	°C	1.66 (3.2%)	1.57 (3.3%)	−5.4
T_B	°C	37.9 (0.15%)	38 (0.15%)	0.26
Pharmacodynamic parameters				
T_s	d	2.15 (21%)	2.45 (12%)	14.0
T_f	d	0.303 (8.4%)	0.368 (7.4%)	21.5
pE_s	kg/(d mg)	2.97 (19%)	3.57 (48%)	20.2
pE_f	1/d	2.16 (22%)	2.43 (40%)	12.5
pE_{tot}	1	0.16 (9.4%)	0.144 (10%)	−10.0
k_R	1/d	4.1 (20%)	5.35 (36%)	30.5
t_{prime}	d	2.12 (9.3%)	1.88 (16%)	−11.3
α	–	11.2 (37%)	5.35 (47%)	−52.2
Inter-individual variability				
$CV(t_{prime})\ \eta$	%	14.9 (46.5%)	37.5 (37%)	152
Measurement noise				
σ_e	°C	0.102 (8.2%)	0.31 (3.9%)	224
System noise				
σ_m	W/(kgd$^{1/2}$)	1.46 (22%)	–	–
σ_R	1/d$^{1/2}$	0.179 (34%)	–	–

*For the ODE model, k_m could not be estimated reliably, and was subsequently fixed to the value estimated in the SDE model, allowing a more reasonable comparison of the remaining estimates.
The parameter estimates are compared to the corresponding model based on ordinary differential equations.
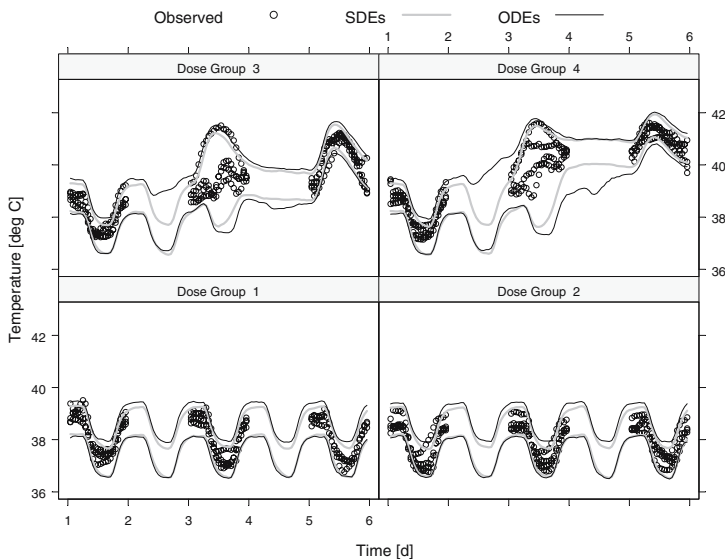
Fig. 5. 90% prediction intervals from the ODE (*thin dark*) and SDE model (*fat light*) are compared to the observed temperature (*black circles*) in four different treatment groups. Each group include four cynomolgus monkeys receiving an IV bolus administration of IL-21 at day one, day three, and day five, at a dose level of, 0 mg/kg in Group one, 0.03 mg/kg in Group two, 0.5 mg/kg in Group three, and 3 mg/kg in Group four.

A representative set of diagnostic plots are presented in Fig. 4. Similarly to the QQ-plot and the predicted *versus* observed, the autocorrelation function for individual weighted residuals was computed from the vector containing data from all individuals, as given by the NONMEM output file.

A simple predictive performance check was performed by simulating the model 500 times and calculating the 90% prediction interval. These prediction intervals were calculated both for the ODE and the SDE model and compared to the observed temperatures for each of the four treatment groups in Fig. 5. The ODE and SDE intervals are reasonably similar, with the same strengths and weaknesses. Both models capture the particularly high variability following second dose, as well as the four phenomena of the structural model: 1) absent effect after first dose, 2) effects on temperature circadian rhythm, 3) fast and slow effects, and 4) saturation of effect. The 90% prediction intervals seem to include more than 90% of data, which indicates a slightly overestimated variation, more so for the ODE model than the SDE model.

Figure 6 compares simulated individual profiles from the SDE model and the ODE model of the observed temperatures following third administration of IL-21 at a dose level of 3 mg/kg, which is the most critical time for the present study. Simulations based on SDEs vary continuously, similarly to the observed temperatures, whereas ODE simulations are seen to jump up and down erratically.

DISCUSSION

The thermoregulatory effects of IL-21 in cynomolgus monkeys were described by a PKPD model based on stochastic differential equations. Whereas temperature modelling is well established in the literature, the present model and results do include a series of features that justify further discussion.

Priming The mechanism behind an absent effect on temperature after first dose is presently not understood. This priming effect was described by an empirical function that switches on sometime after the first dose, and inter-individual variation in the time of onset could describe an increased variation after second dose. However, the model does not satisfactorily describe how the system returns to normal. During model development it was attempted to model priming as a function of the slow effect, but various attempts were discarded because of poor simulation properties.

Receptor model The standard E_{max} model was extended to explicitly include a receptor compartment, extending the model with an off rate for the receptors k_R. Empirically, this off rate is related to the shape of the response, and to the correlation structure in the SDE model. The estimated value for k_R corresponds to a half-life of 4 h, and it is presently not known whether this off rate relate to that of any physiological receptor involved in the response. In particular, intracerebral injections of PGE_2 in rat leads to elevated temperatures lasting for only tens of minutes (22), indicating a much faster half life of response.

Metabolism model Whereas the metabolism was unobserved in the present study, the circadian rhythm of thermoregulation has been investigated in detail for squirrel monkeys (18). These calorimetric experiments showed that the metabolic rate begin to decrease around the time of lights-off, and reach a stable level within 1.5–2.5 h. This is in reasonable agreement with the estimated value of k_m, corresponding to a half life of 0.7 h for cynomolgus monkeys. Since the correlation structure in data contributed significantly to the estimation of k_m, this result constitutes a test, both for the structural model and for the implemented system noise.

For the squirrel monkeys, it was also found experimentally that the metabolic rate varies approximately between 3 W/kg at night and 5 W/kg at day (18). Cynomolgus monkeys are approximately three times larger than squirrel monkeys, so allometric scaling yield a night and day time metabolic rate, of 2.57 and 3.45 W/kg in cynomolgus monkeys. In the present analysis, we used a fixed baseline metabolic rate M_b in cynomolgus monkeys of 3 W/kg. From the fixed value of M_b and the estimated parameter values of k_{inc}, T_b, and ΔT, we can calculate or simulate model predictions for the night and day time metabolic rate in cynomolgus monkeys. The model prediction yield night and day time values at 2.63 and 3.40 W/kg which is in perfect agreement with the values found by allometric scaling.

Model Diagnostics A series of diagnostic plots were presented in Fig. 4 to compare the ODE model with the SDE model. Models based on ODEs typically assume independence of the individual prediction errors, whereas SDE models assume independence of the individual one-step prediction errors, i.e., prediction errors based on predictions that include information of all previous data to predict the next observation. So the individual residuals refer to the one-step prediction errors, which reduce to the usual prediction errors when
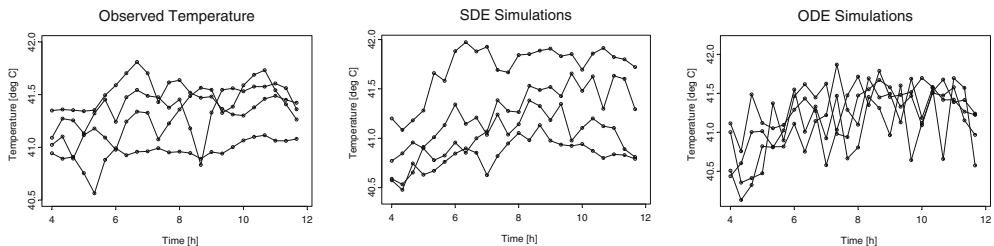
Fig. 6. Core body temperature for cynomolgus monkeys 4 h to 12 h post third administration of IL-21 at a dose level of 3 mg/kg. The three plots compare the actual observed temperatures for the four monkeys (*left*) to simulations of four monkeys based on the SDE model (*middle*) and the ODE model (*right*).

ODEs are used. Diagnostic plots of predictions *versus* observations demonstrate that SDE model predictions are closer to the observations than ODE model predictions, illustrating that one-step predictions are based on all previous data for SDEs, but not for ODEs. The autocorrelation function presented in Fig. 4 clearly demonstrates significantly correlated individual residuals for the ODE model, which falsifies the statistical model assumption. The SDE model on the other hand, successfully passes this statistical test. Diagnostic Quantile–Quantile (QQ) plots presented in Fig. 4 illustrate that the weighted individual residuals are close to being normal distributed for the SDE model as well as for the ODE model. This is one of the fundamental assumptions for both models, and particularly for the Extended Kalman Filter approximation to the individual SDE likelihood function (12). Failure to produce Gaussian residuals may indicate that the Extended Kalman Filter is inadequate, possibly motivating the pursuit of higher order filters or other estimation methods (24).

Do SDEs represent true fluctuations? Investigation of system noise may be motivated by the significantly autocorrelated residuals of the ODE model, as demonstrated in Fig. 4. Such correlations may be due to true variations that can be modelled by SDEs, or by model misspecification that may be described but not reproduced by SDEs. If the estimated system noise in reality originates from model misspecification, one would presume that simulations with SDEs would produce large confidence bands, because unlike a model deficiency, system noise will change the model in a different direction with every simulation. Figure 5 clearly demonstrates that the SDE model reproduces data with reasonable confidence bands, leading to the conclusion that the autocorrelated residuals reflect true fluctuations in data, and Fig. 6 confirms that the simulations look reasonable compared to data.

System noise and inter-occasion variability From a mixed-effects modelling perspective, the inter-occasion variability (IOV) and the residual variability are treated as separate entities. However, in some cases it may be more realistic to explain inter-occasion variability as a continuous random varying process, i.e., system noise that is high on some occasions and low on others. During model development, the likelihood ratio test indicated the significant between-day variability in the steady state day and night time temperature (T_{day} and T_{night}) for both the ODE and the SDE model. However, for the ODE model IOV was seen to give individual predictions that were visibly closer to data, while this was not the case for SDEs. For SDEs, IOV did not visibly improve individual predictions, neither for the diagnostic plots in Fig. 4, nor when comparing to observations over time. Since the implemented system noise seemed to reasonably describe the day-to-day variation of T_{day} and T_{night}, no explicit IOV was included for these parameters, which considerably reduced the computational time.

Simulation Properties The simple predictive check given in Fig. 5 provide a reasonable diagnostic for the model to capture overall differences between treatment groups, and thereby predict the overall outcome of new experimental designs. However, PKPD models are quite often used for predictions of new individuals possibly in new treatment regimens. For any drug that may elevate body temperature, one might be interested in the probability for a new individual to show three readings (at least 1 h apart) higher

than 38°C (100.4°F) or a single reading higher than 38.3°C (101°F), which is used in oncology practice as a criteria for significant fever (27). Model predictions of such probabilities require accurate simulations of the individual profiles. Figure 6 demonstrate that simulations based on SDEs vary continuously, similarly to the observed temperatures, whereas ODE simulations are seen to jump up and down erratically, possibly leading to erroneous conclusions.

Benefits of SDEs In summary, the benefits of SDEs were found to include,

1. The ODE model with uncorrelated residuals could be falsified by a simple statistical test of the autocorrelation function (ACF), whereas the SDE model was able to describe the correlation structure in the residuals. The ACF can be seen as a general model diagnostic, where an erroneous ACF will falsify the model, but the ACF may also be a more direct quality mark for model simulations. In particular, simulated data could be used to assess precision of parameter estimates for different sampling schedules. It is to be expected that the results would change if simulations are made with a model that produce a completely different ACF for the residual errors.

2. The introduction of SDEs allows us to quantify and propose a mechanism for the fluctuations in temperature, i.e., random fluctuations in metabolic rate and in the fraction of bound receptors that affect the thermoregulatory set-point.

3. The high measurement error estimated in the ODE model caused simulations to jump up and down erratically and unrealistically compared to simulations based on SDEs that realistically resembled the variations seen in data. This could become important, e.g., if one wish to predict the probability that treatment of a given individual cause temperature elevation above a certain level.

4. IIV was reduced by the inclusion of system noise, and the simple predictive check demonstrated that the SDE model led to narrower confidence intervals, as is often seen with more accurate variability models.

5. SDEs allowed us to simplify the model for inter-occasion variability on day and night time steady state temperature, which significantly improved the model speed.

Other statistical techniques, such as the autoregressive (AR) process that has previously been incorporated in NONMEM (28) or the more general autoregressive moving average (ARMA) process, would also enable quite general inclusion of correlated residuals. The present approach favours SDEs, because they incorporate random fluctuations directly on the different mechanisms or entities of the model, which gives us an understanding of the origin of the correlation structure found in data.

Model Limitations and potential future applications First of all, the model includes only the most basic mechanisms of heat control, and it fail to explain what happens e.g., if the ambient temperature is changed far from 21°C.

As previously mentioned the empirical effects on priming have not been implemented to return to normal. This poses serious problems for the model to simulate longer dosing intervals, long term treatment, and termination of treatment. We should note that previous unpublished experiments have demonstrated qualitatively similar patterns of IL-21 induced effects on temperature regulation for a series of different

dosing regiments. However, the empirical parts of the model must be extended if it is to give a complete understanding of the effects of IL-21 on thermoregulation.

On the other hand, a mechanistic framework of thermoregulation has been put forward. It is hoped that this framework can be used to improve the descriptions and predictions not only for IL-21, but also for other pharmaceutical and biological compounds. In particular it is hoped that the mechanistic aspects of the thermoregulation model can improve predictions of the overall outcome of new dosing regimens, whereas the inclusion of SDEs can provide better predictions of the variations seen in temperature for individual animals.

CONCLUSION

A new baseline PKPD model for thermoregulation has been formulated to include potential effects on the circadian rhythm, metabolism, heat loss, and a thermoregulatory setpoint. The baseline model quantitatively reproduces basic physiological findings of the circadian regulation of heat production and heat loss in monkeys. It further qualitatively reflects some basic effects of thermoregulation following exercise and changed ambient temperatures, while clearly not explaining all phenomena in this complicated system.

The proposed mechanisms of IL-21 were incorporated into the baseline model via effects on the circadian rhythm of metabolism, and on the thermoregulatory set-point, which could describe a complex set of IL-21 induced phenomena. These phenomena include 1) absent effect after first dose, 2) disappearance of the circadian rhythm, 3) fast and slow effects, and 4) saturation of effect. Further more, inter-individual variability in the onset of effect could explain increased variability after second dose.

System noise was implemented in the metabolism and the receptor compartment, converting the ODE model into an SDE model. SDEs provided a more realistic description of the variability that improved individual simulation/predictive properties, accelerated model speed by simplifying inter-occasion variability, and finally changed the model into one that could not be falsified by the autocorrelation function.

REFERENCES

1. J. Parrish-Novak, S. R. Dillon, A. Nelson, A. Hammond, C. Sprecher, J. A. Gross, J. Johnston, K. Madden, W. Xu, J. West, S. Schrader, S. Burkhead, M. Heipel, C. Brandt, J. L. Kuijper, J. Kramer, D. Conklin, S. R. Presnell, J. Berry, F. Shiota, S. Bort, K. Hambly, S. Mudri, C. Clegg, M. Moore, F. J. Grant, C. Lofton-Day, T. Gilbert, F. Rayond, A. Ching, L. Yao, D. Smith, P. Webster, T. Whitmore, M. Maurer, K. Kaushansky, R. D. Holly, and D. Foster. Interleukin 21 and its receptor are involved in NK cell expansion and regulation of lymphocyte function. *Nature* **408**:57–63 (2000).
2. T. Habib, A. Nelson, and K. Kaushansky. IL-21: A novel IL-2-family lymphokine that modulates B, T, and natural killer cell responses. *J. Allergy Clin. Immunol.* **112**:1033–1045 (2003).
3. P. A. Mackowiak. Drug induced fever: In fever. *Basic Mechanisms and Management*. Raven Pr. 1997.
4. T. C. Chan, S. D. Evans, and R. F. Clark. Drug-induced hyperthermia. *Crit. Care Clin.* **13**:785–808 (1997).
5. A. A. Romanovsky. Do fever and anapyrexia exist? Analysis of set point-based definitions. *Am. J. Physiol. Lung Cell. Mol. Physiol.* **287**:R992–R995 (2004).
6. G. Havenith. Individualized model of human thermoregulation for the simulation of heat stress response. *J. Appl. Physiol.* **90**:1943–1954 (2001).
7. E. N. Brown, Y. Choe, H. Luithardt, and C. A. Czeisler. A statistical model of the human core-temperature circadian rhythm. *Am. J. Physiol. Endocrinol. Metab.* **279**:E669–E683 (2000).
8. R. A. Irizarry, C. Tankersley, R. Frank, and S. Flanders. Assessing homeostasis through circadian patterns. *Biometrics* **57**:1228–1237 (2001).
9. I. F. Troconiz, S. Armenteros, M. V. Planelles, J. Benitez, R. Calvo, and R. Dominguez. Pharmacokinetic–Pharmacodynamic Modelling of the antipyretic effect of two oral formulations of ibuprofen. *Clin. Pharmacokinet.* **38**:505–518 (2000).
10. S. A. Visser, B. Sallstrom, T. Forsberg, L. A. Peletier, and J. Gabrielsson. Modeling drug- and system-related changes in body temperature: application to clomethiazole-induced hypothermia, long-lasting tolerance development, and circadian rhythm in rats. *J. Pharmacol. Exp. Ther.* (2005).
11. K. P. Zuideveld, H. J. Maas, N. Treijtel, J. Hulshof, P. H.van der Graaf, L. A. Peletier, and M. Danhof. A set-point model with oscillatory behavior predicts the time course of 8-OH-DPAT-induced hypothermia. *Am. J. Physiol. Regul. Integr. Comp. Physiol.* **281**:R2059–R2071 (2001).
12. R. V. Overgaard, N. Jonsson, C. W. Tornøe, and H. Madsen. Non-linear mixed-effects models with stochastic differential equations: implementation of an estimation algorithm. *J. Pharmacokinet. Pharmacodyn.* **32**:85–107 (2005).
13. N. R. Kristensen, H. Madsen, and S. H. Ingwersen. Using stochastic differential equations for PK/PD model development. *J. Pharmacokinet. Pharmacodyn.* **32**:109–141 (2005).
14. C. W. Tornøe, R. V. Overgaard, H. Agerso, H. A. Nielsen, H. Madsen, and E. N. Jonsson. Stochastic differential equations in NONMEM: implementation, application, and comparison with ordinary differential equations. *Pharm. Res.* **22**:1247–1258 (2005).
15. K. E. Andersen and M. Hojbjerre. A population-based Bayesian approach to the minimal model of glucose and insulin homeostasis. *Stat. Med.* **24**:2381–2400 (2005).
16. S. Ditlevsen and A. de Gaetano. Stochastic *vs.* deterministic uptake of dodecanedioic acid by isolated rat livers. *Bull. Math. Biol.* **67**:547–561 (2005).
17. P. Webb. The physiology of heat regulation. *Am. J. Physiol.* **268**:R838–R850 (1995).
18. E. L. Robinson, V. H. maria-Pesce, and C. A. Fuller. Circadian rhythms of thermoregulation in the squirrel monkey (*Saimiri sciureus*). *Am. J. Physiol.* **265**:R781–R785 (1993).
19. J. F. Gillooly, J. H. Brown, G. B. West, V. M. Savage, and E. L. Charnov. Effects of size and temperature on metabolic rate. *Science* **293**:2248–2251 (2001).
20. C. M. Blatteis. Prostaglandin E2: a putative fever mediator. In Mackowiak (ed.), *Fever: Basic Mechanisms and Management*, Raven Pr, 1997.
21. C. M. Blatteis and E. Sehic. Cytokines and fever. *Ann. N. Y. Acad. Sci.* **840**:608–618 (1998).
22. A. I. Ivanov and A. A. Romanovsky. Prostaglandin E2 as a mediator of fever: synthesis and catabolism. *Front. Biosci.* **9**:1977–1993 (2004).
23. D. E. Mager, E. Wyska, and W. J. Jusko. Diversity of mechanism-based pharmacodynamic models. *Drug Metab. Dispos.* **31**:510–518 (2003).
24. A. H. Jazwinski. *Stochastic Processes and Filtering Theory*. Academic, New York, 1970.
25. B. Sallstrom, S. A. Visser, T. Forsberg, L. A. Peletier, A. C. Ericson, and J. Gabrielsson. A pharmacodynamic turnover model capturing asymmetric circadian baselines of body temperature, heart rate and blood pressure in rats: challenges in terms of tolerance and animal-handling effects. *J. Pharmacokinet. Pharmacodyn.* **32**:835–859 (2005).
26. S. L. Beal and L. B. Sheiner. *NONMEM User's Guides*. NONMEM Project Group, University of California, San Francisco, 1994.
27. S. Dalai and D. S. Zhukovsky. Pathophysiology and management of fever. *J. Support Oncol.* **4**:9–16 (2006).
28. M. O. Karlsson, S. L. Beal, and L. B. Sheiner. Three new residual error models for population PK/PD analyses. *J. Pharmacokinet. Biopharm.* **23**:651–672 (1995).